ORIGINAL PAPER



A Review of Variational Multiscale Methods for the Simulation of Turbulent Incompressible Flows

Naveed Ahmed¹ · Tomás Chacón Rebollo² · Volker John^{1,3} · Samuele Rubino^{2,4}

Received: 7 December 2015/Accepted: 9 December 2015/Published online: 21 December 2015 © CIMNE, Barcelona, Spain 2015

Abstract Various realizations of variational multiscale (VMS) methods for simulating turbulent incompressible flows have been proposed in the past fifteen years. All of these realizations obey the basic principles of VMS methods: they are based on the variational formulation of the incompressible Navier-Stokes equations and the scale separation is defined by projections. However, apart from these common basic features, the various VMS methods look quite different. In this review, the derivation of the different VMS methods is presented in some detail and their relation among each other and also to other discretizations is discussed. Another emphasis consists in giving an overview about known results from the numerical analysis of the VMS methods. A few results are presented in detail to highlight the used mathematical tools. Furthermore, the literature presenting numerical studies with the VMS methods is surveyed and the obtained results are summarized.

1 Introduction

The accurate numerical simulation of turbulence is one of the more challenging scientific problems, with wide classical applications such as engineering, weather, and climate forecasting, for instance, besides more recent applications in medicine, astrophysics, or oceanography, among others. Fluid mechanics establishes that the motion of a viscous fluid is governed by the Navier–Stokes equations, which constitute the basic model to perform numerical simulations of turbulent flows: Let $\Omega \in \mathbb{R}^d$, $d \in \{2,3\}$, be a bounded domain with Lipschitz boundary Γ and (0,T) be a bounded time interval, then these equations are given by: Find a velocity field $\boldsymbol{u}:(0,T)\times\Omega\to\mathbb{R}^d$ and a pressure field $\boldsymbol{p}:(0,T)\times\Omega\to\mathbb{R}$ such that

$$\partial_t \mathbf{u} - 2\mathbf{v} \nabla \cdot \mathbb{D}(\mathbf{u}) + (\mathbf{u} \cdot \nabla)\mathbf{u} + \nabla \mathbf{p} = \mathbf{f} \quad \text{in } (0, T] \times \Omega,$$

$$\nabla \cdot \mathbf{u} = 0 \quad \text{in } [0, T] \times \Omega.$$
(1)

These equations have to be equipped with an initial condition u_0 at t=0 and with boundary conditions on the boundary Γ of Ω . The velocity deformation tensor is the symmetric part of the velocity gradient $\mathbb{D}(u) = (\nabla u + \nabla u^T)/2$. Given data are the dimensionless kinematic viscosity v and the body forces f. The first equation in (1) models the conservation of momentum and the second equation, the so-called continuity equation, models the conservation of mass.

Flows at Reynolds number beyond the turbulence threshold develop a wide range of space and time scales

Naveed Ahmed ahmed@wias-berlin.de

Tomás Chacón Rebollo chacon@us.es

Volker John john@wias-berlin.de

- Weierstrass Institute for Applied Analysis and Stochastics (WIAS), Mohrenstr. 39, 10117 Berlin, Germany
- Department EDAN and IMUS, University of Seville, C/Tarfia s/n., 41012 Seville, Spain
- Department of Mathematics and Computer Science, Free University of Berlin, Arnimallee 6, 14195 Berlin, Germany
- Laboratoire Jacques-Louis Lions, Sorbonne Universités, UPMC Univ. Paris 06, 75005 Paris, France



Samuele Rubino samuele@us.es

with nonlinear interactions and a seemingly random behavior. Large eddies generate smaller and smaller eddies by inertial effects, until these reach the viscous length scale, below which they are destroyed by molecular friction. The computational complexity associated to the accurate numerical simulation of such a wide range of space-time scales makes direct numerical simulations (DNS) of the Navier–Stokes equations for flows at large Reynolds numbers nowadays impossible. It is estimated that if the improvement of the computational resources continues at the same rate, an accurate computation of all scales of a turbulent flow will be possible only by the end of the XXIth century.

Meanwhile, "turbulence" models aim to simulate statistical means of turbulent flows (RANS -Reynolds Averaged Navier-Stokes- models), or rather their larger scales (LES -Large Eddy Simulation- models). The traditional models are based upon statistical theories of equilibrium turbulence at large Reynolds numbers: The generation of small eddies draws energy from the large eddies, and the total energy drawn may be estimated by statistical similarity properties, basically the Kolmogorov theory that applies to eddies located in the inertial range, in which only the convection effects are relevant. The effect of the creation of small eddies on the large ones is modeled by means of an equivalent diffusion, named the "eddy diffusion" or "eddy viscosity". The actual mathematical structure of this eddy diffusion is built by similarity arguments in such a way that the dissipated deformation energy of the resolved scales equals the estimated energy drawn by the unresolved scales. In RANS models the eddy diffusion affects all the flow scales, leading to an excessive damping of large scales. However, RANS models (in particular the most popular one, the $k-\epsilon$ model) are widely used in engineering due to their robustness and economy of computational time (see [38, Chapter 4]).

Classical (explicit) LES models are formally obtained by convolution of the Navier-Stokes equations with a smoothing kernel. The large scales are determined by a cutoff length, that should be placed within the inertial range, and the eddy viscosity acts usually directly on all resolved scales. LES models provide more accurate results than RANS models, in particular for unsteady flows, although they are much more costly and thus much less used in industrial applications. LES models (as RANS models) are systems of partial differential equations, that need to be endowed with initial and boundary conditions, and solved numerically. The convolution with the smoothing kernel destroys the no-slip boundary conditions, generating a source of errors, e.g., see [51]. The numerical discretization leads to an additional numerical diffusion, needed to reach stability. The accurate numerical simulation of LES models thus needs high-order discretizations to prevent that the numerical diffusion masks the eddy diffusion.

Variational multiscale (VMS) models propose an alternative to the "standard" turbulence modeling. VMS models are increasingly used as a promising and successful approach that seeks to simulate large scale structures in turbulent flows. However, there are fundamental differences between VMS methods and LES methods. In contrast to LES methods, VMS methods consider large scales which are defined by projection into appropriate function spaces. Moreover, VMS methods are based on the variational formulation of the model problem, while the LES methods consider the strong form of the model problem. One of the promising features of the derived variational formulation and the use of the projection for defining the scales is that the boundary conditions are incorporated into the mathematical analysis in a natural way. Thus, compared to classical LES based on filtering, the VMS approach does not face difficulties associated to inhomogeneous non-commutative filters in wall-bounded flows, and as consequence is mathematically consistent also in the presence of boundaries.

VMS models were introduced in the seminal papers [80, 83] as a general technique to model the subgrid scales in the numerical solution of partial differential equations. In parallel, in [71] was introduced an alternative technique for multiscale subgrid modeling. The application of VMS modeling to the simulation of turbulent flows was proposed in [85].

VMS methods have experienced a fast development, in particular their application to the simulation of turbulent flows that has led to well-established models. A relevant achievement of some of these models (the residual-based VMS models) is that they do not need any modeling of the subgrid scales by statistical theories of turbulence, in particular they do not include eddy viscosity. The numerical diffusion inherent to those models plays the role of the eddy diffusion.

There essentially exist two classes of VMS turbulence models, depending on the resolution levels number of the scales:

- Two-scale VMS models The large and small scales are respectively approximated by discrete spaces. A coupled set of equations for large and small scales is derived, where each of them is driven by the residual associated to the other. The small scales are either modeled or resolved, leading to
 - Residual-based VMS models The unresolved scales themselves are modeled in terms of the large scales, and their modeled expression is inserted in the resolved scale equations, leading to a single set of equations for the resolved scales, with additional



stabilizing terms modeling the action of the unresolved scales. In particular, for the orthogonal subscales (OSS) model, if all inertial interactions are kept in the modeled terms, the numerical diffusion generated by this residual-based VMS model is asymptotically equivalent, as the Reynolds number increases to infinity, to the eddy diffusion dissipated by the unresolved scales. Thus, the residual-based procedure does not make use of the statistical theory of equilibrium turbulence, and no ad-hoc eddy viscosity modeling is required. Further, it retains numerical consistency in the finite element equations. This approach, which hence rely on purely numerical artifacts without any modification of the continuous problem, was seldom followed, the MILES (Monotone Integrated LES) approach [21] being the main exception, until the (residual-based) VMS models were introduced in the seminal papers [80, 83] and subsequently proposed as implicit LES techniques (ILES) for turbulent flows in [10, 44]. It is worth emphasizing that, while ILES techniques are usually considered to be based on the addition of purely dissipative numerical terms, see [126, Sections 5.3.4], this is not the case for instance of the OSS model with dynamic subscales that allow to model backscatter similar to dynamic LES closures, as shown in [118] and discussed in Sect. 5.1.

- Three-scale VMS models: The flow is decomposed into large resolved, small resolved, and unresolved scales. A coupled set of equations for large and small resolved scales is derived. The effect of the unresolved scales on the resolved ones is modeled by means of an eddy viscosity term that only acts directly on the small resolved scales.
 - Residual-free bubble VMS models: The small scales are approximated by "bubble" finite elements which are residual-free to take into account the effect of the unresolved scales. The final model consists of a coupled system of partial differential equations for large and small resolved scales of the flow.
 - Projection-based VMS models: The large and small resolved scales are jointly discretized in a single discrete space. A projection operator into an underlying large resolved scale space is used to construct the small resolved scales that appear in the eddy viscosity term.
 - Algebraic VMS models: These models are similar to the projection-based models, but the projection operator is built at the algebraic level of the model, once the model is written as a set of nonlinear equations in \mathbb{R}^n .

This classification of VMS methods also creates a division in the family of turbulence models separating those that use eddy diffusion (in a more or less sophisticated manner) to model the effect of subgrid scales, and those (residual-based) that use a direct modeling of the subgrid scale flow by approximating the related equations.

The aim of this review consists in presenting the different VMS methods in a structured manner, comparing their derivation, numerical analysis (when available), and their ability to solve turbulent flow problems. There are already reviews of VMS methods available in [62, 89, 92]. It is intended to update these reviews, thereby putting special emphasis on the comparisons of formulations of the methods and on aspects from numerical analysis.

1.1 Nomenclature

Standard symbols will be used for Lebesgue and Sobolev spaces. To simplify notations, the domain is omitted if the space is with respect to Ω and vector-valued spaces are denoted by bold symbols, e.g., $\mathbf{L}^2 = [L^2(\Omega)]^d$

 $a(\cdot, \cdot)$ Weak form of the viscous term

 $A(\cdot;\cdot,\cdot)$ Trilinear form for the left-hand side of Navier–Stokes equations

 $b(\cdot,\cdot,\cdot)$ Weak form of the convective term

 $b_{\rm s}(\cdot,\cdot,\cdot)$ Skew-symmetric form of the convective term

 $c(\cdot;\cdot,\cdot)$ Trilinear form defining a turbulence model

f Right-hand side of Navier–Stokes equations $f(\cdot)$ Linear form for the right-hand side of Navier–

 $f(\cdot)$ Linear form for the right-hand side of Navier–Stokes equations

h Mesh width

 h_K Local mesh width for mesh cell K

K Mesh cell

M Macro element

n Outward pointing unit normal on Γ

p Continuous pressure

 \overline{p} Large scale pressure

 \hat{p} Small resolved scale pressure

 p_h Resolved scale pressure

p' Unresolved scale pressure

 P_k Finite element space of degree k on simplices

 Q_k Finite element space of degree k on

quadrilaterals or hexahedra

T Final time

 \mathcal{T}_h Triangulation

u Continuous velocity

 \overline{u} Large scale velocity

 \hat{u} Small resolved scale velocity

 u_h Resolved scale velocity

u' Unresolved scale velocity

 $\boldsymbol{U} = (\boldsymbol{u}, p)^T$



$V_h^l(\Omega)$	P_l on simplices, Q_l on quadrilaterals or
T 7	hexahedra
X	Space for continuous velocity
<u>X</u> *	Dual space of X
$\overline{X}, \overline{Y}$	Resolved scales (two-scale VMS) or large scale (three-scale VMS)
\widehat{X} , \widehat{Y}	Small resolved scales (three-scale VMS)
X', Y'	Unresolved scales
$X_{ m div}$	Space of weakly divergence-free functions
X_h	Finite element velocity space
$\boldsymbol{X}_{h, ext{div}}$	Finite element velocity space with discretely
,	divergence-free functions
Y	Space for continuous pressure
Y_h	Finite element pressure space
Z	$X \times Y$
Γ	Boundary of Ω
δ	Filter width
ν	Dimensionless viscosity
v_{T}	Turbulent viscosity
I	Identity operator
π_h, \varPi	Projection operators
$ au_{ m m}$	Stabilization parameter for velocity
τ_{c}	Stabilization parameter for pressure, grad-div
	parameter
Ω	Bounded domain
(\cdot,\cdot)	Inner product in $L^2(\Omega)$ or $L^2(\Omega)$
$(\cdot,\cdot)_{\omega}$	Inner product in $L^2(\omega)$ or $L^2(\omega)$
$\ \cdot\ _k$	Norm in $H^k(\Omega)$
$\ \cdot\ _{k,\omega}$	Norm in $H^k(\omega)$
$\ \cdot\ _{k,p}$	Norm in $W^{k,p}(\Omega)$
$ \cdot _k$	Seminorm in $H^k(\Omega)$
$ \cdot _{k,\omega}$	Seminorm in $H^k(\omega)$
$ \cdot _{k,p,\omega}$	Seminorm in $W^{k,p}(\omega)$
$\ \cdot\ _{\mathrm{F}}$	Frobenius norm of a tensor

2 Finite Element Methods for the Incompressible Navier-Stokes Equations

As already mentioned, VMS methods are based on the variational formulation of the Navier–Stokes equations (1). This section introduces this formulation and some properties are summarized. Then, the basic finite element discretization, the so-called Galerkin method, is given and important properties are stated.

2.1 The Incompressible Navier–Stokes Equations

For simplicity of presentation, the case of homogeneous Dirichlet boundary conditions

$$\boldsymbol{u} = \boldsymbol{0}$$
 in $(0, T) \times \Gamma$

will be considered. Then the appropriate function spaces for velocity and pressure are given by

$$X = \left[H_0^1(\Omega)\right]^d = \left\{ v \in \left[H^1(\Omega)\right]^d : v = 0 \text{ on } \Gamma \right\},$$

$$Y = L_0^2(\Omega) = \left\{ q \in L^2(\Omega) : \int_{\Omega} q \, dx = 0 \right\}.$$

The variational formulation of (1) is derived by multiplying the momentum equation with test functions $v \in X$, the continuity equation with test functions $q \in Y$, and with integration by parts of the viscous term and the pressure term. The resulting variational formulation reads as follows: Find $(u,p):(0,T)\to X\times Y$ such that for all $(v,q)\in X\times Y$

$$\frac{d}{dt}(\boldsymbol{u},\boldsymbol{v}) + a(\boldsymbol{u},\boldsymbol{v}) + b(\boldsymbol{u},\boldsymbol{u},\boldsymbol{v}) - (\nabla \cdot \boldsymbol{v},p) = \langle \boldsymbol{f},\boldsymbol{v} \rangle \quad \text{in } \mathcal{D}^*(0,T),$$

$$(\nabla \cdot \boldsymbol{u},q) = 0 \quad \text{in } \mathcal{D}^*(0,T),$$

$$\boldsymbol{u}(0,\boldsymbol{x}) = \boldsymbol{u}_0(\boldsymbol{x}) \quad \text{in } \Omega.$$

$$(2)$$

Here, $\langle \cdot, \cdot \rangle$ denotes the duality pairing between X and its dual $X^* = [H^{-1}(\Omega)]^d$ and $\mathcal{D}^*(0,T)$ is the space of distributions on (0,T). The forms a and b are given by

$$a(\mathbf{u}, \mathbf{v}) = 2\mathbf{v}(\mathbb{D}(\mathbf{u}), \mathbb{D}(\mathbf{v})), \quad b(\mathbf{u}, \mathbf{v}, \mathbf{w}) = ((\mathbf{u} \cdot \nabla)\mathbf{v}, \mathbf{w}),$$

 $\mathbf{u}, \mathbf{v}, \mathbf{w} \in X.$

Using that u is divergence-free, one finds that

$$2v(\mathbb{D}(\boldsymbol{u}), \mathbb{D}(\boldsymbol{v})) = v(\nabla \boldsymbol{u}, \nabla \boldsymbol{v}).$$

Applying Hölder's inequality, Sobolev imbeddings, interpolation theorems in Sobolev spaces, Poincaré's and Korn's inequality one gets the estimate

$$b(\mathbf{u}, \mathbf{v}, \mathbf{w}) \le C \|\mathbf{u}\|_0^{1/2} \|\mathbb{D}(\mathbf{u})\|_0^{1/2} \|\mathbb{D}(\mathbf{v})\|_0 \|\mathbb{D}(\mathbf{w})\|_0$$

$$\forall \mathbf{u}, \mathbf{v}, \mathbf{w} \in X.$$
(3)

For studying the existence of a velocity solution of (2), this system is usually considered in the subspace of divergence-free functions

$$X_{\mathrm{div}} = \{ \mathbf{v} \in X : (\nabla \cdot \mathbf{v}, q) = 0 \text{ for all } q \in Y \}.$$

The second equation of (2) states that $u \in X_{\text{div}}$ for almost every time. For test functions from X_{div} , the pressure term in the first equation vanishes such that only the velocity is left. Then, the velocity solution of (2) can be computed by solving the following problem: Find $u:(0,T)\to X_{\text{div}}$ such that for all $v\in X_{\text{div}}$

$$\langle \hat{o}_t \boldsymbol{u}, \boldsymbol{v} \rangle + a(\boldsymbol{u}, \boldsymbol{v}) + b(\boldsymbol{u}, \boldsymbol{u}, \boldsymbol{v}) = \langle \boldsymbol{f}, \boldsymbol{v} \rangle \quad \text{in } (0, T), \boldsymbol{u}(0, \boldsymbol{x}) = \boldsymbol{u}_0(\boldsymbol{x}) \quad \text{in } \Omega.$$
 (4)



An appropriately defined variational velocity solution satisfies [58, 134]

$$\boldsymbol{u} \in L^2(0, T; \boldsymbol{X}_{\text{div}}) \cap L^{\infty}(0, T; \mathbf{L}_{\text{div}}^2(\Omega)) \tag{5}$$

with

$$\mathbf{L}^2_{\text{div}}(\Omega) = \{ \mathbf{v} : \mathbf{v} \in \mathbf{L}^2(\Omega), \nabla \cdot \mathbf{v} = \mathbf{0}, \mathbf{v} \cdot \mathbf{n}|_{\Gamma} = \mathbf{0} \}$$

In this space, the divergence has to be understood in the sense of distributions and the boundary condition in the This section will describe the basic finite element discretization, the so-called Galerkin discretization. Analytical tools which will be needed in the finite element error analysis will be introduced.

The continuous-in-time Galerkin finite element discretization of the Navier–Stokes equations (2) reads as follows: Find $(\boldsymbol{u}_h,p_h):(0,T)\to \boldsymbol{X}_h\times Y_h$ such that for all $(\boldsymbol{v}_h,q_h)\in \boldsymbol{X}_h\times Y_h$

$$(\partial_t \boldsymbol{u}_h, \boldsymbol{v}_h) + a(\boldsymbol{u}_h, \boldsymbol{v}_h) + b_s(\boldsymbol{u}_h, \boldsymbol{u}_h, \boldsymbol{v}_h) - (\nabla \cdot \boldsymbol{v}_h, p_h) = \langle \boldsymbol{f}_h, \boldsymbol{v}_h \rangle \quad \text{in } (0, T) (\nabla \cdot \boldsymbol{u}_h, q_h) = 0 \quad \text{in } (0, T), \boldsymbol{u}_h(0, \boldsymbol{x}) = \boldsymbol{u}_{0,h}(\boldsymbol{x}) \quad \text{in } \Omega,$$

$$(6)$$

sense of traces. The initial condition also makes sense in $\mathbf{L}^2(\Omega)$ as from (5) \boldsymbol{u} is weakly continuous from [0, T] into $\mathbf{L}^2(\Omega)$.

The existence of a variational velocity solution can be proved in several ways, e.g., by considering a sequence of regularized problems [107], with the Galerkin method [78], or with the semi-group method [133]. However, the uniqueness of the weak solution is an open problem for the practical relevant three-dimensional case. Uniqueness can be proved with stronger regularity assumptions than (5), e.g., with the assumption [130]

$$\boldsymbol{u} \in L^{s}(0,T;\mathbf{L}^{q}(\Omega)) \quad \text{with } \frac{3}{q} + \frac{2}{s} \leq 1.$$

The unresolved question of the uniqueness of a variational solution possesses some impact on the numerical analysis of discretizations of turbulence models. Topics like error estimates are studied usually with the assumption of a unique solution of the variational problem. To ensure this property for the three-dimensional situation, one has to require a regularity of the solution which is stronger than in the formulation of the variational problem. But in particular for turbulent flows, it is counterintuitive to assume additional regularity of the solution.

2.2 The Galerkin Finite Element Method

The basic idea of finite element methods consists in replacing the infinite-dimensional spaces (X,Y) in the definition of the weak problem (2) with finite-dimensional spaces (X_h,Y_h) . Here, only the case of conforming finite element methods will be considered, i.e., the finite-dimensional spaces are subspaces of the infinite-dimensional spaces $X_h \subset X$ and $Y_h \subset Y$.

where $u_{0,h}(x)$ is an approximation of the initial condition in the finite element space and $b_s(u_h, u_h, v_h)$ is a skew-symmetric form of the convective term, e.g.,

$$b_{s}(\boldsymbol{u},\boldsymbol{v},\boldsymbol{w}) = \frac{1}{2}(b(\boldsymbol{u},\boldsymbol{v},\boldsymbol{w}) - b(\boldsymbol{u},\boldsymbol{w},\boldsymbol{v})). \tag{7}$$

Note that in the case $u \in X_{\text{div}}$ it holds $b(u, v, w) = b_s(u, v, w)$. From (3) one obtains directly

$$b_{s}(\boldsymbol{u}, \boldsymbol{v}, \boldsymbol{w}) \leq C \|\boldsymbol{u}\|_{0}^{1/2} \|\mathbb{D}(\boldsymbol{u})\|_{0}^{1/2} \|\mathbb{D}(\boldsymbol{v})\|_{0} \|\mathbb{D}(\boldsymbol{w})\|_{0}$$

$$\forall \boldsymbol{u}, \boldsymbol{v}, \boldsymbol{w} \in \boldsymbol{X}.$$
(8)

For problem (6) to be well posed, the finite element spaces have to satisfy the so-called discrete inf-sup condition

$$\inf_{q_h \in Y_h, q_h \neq 0} \sup_{\mathbf{v}_h \in X_h, \mathbf{v}_h \neq 0} \frac{(\nabla \cdot \mathbf{v}_h, q_h)}{\|\nabla \mathbf{v}_h\|_0 \|q_h\|_0} \ge \beta > 0, \tag{9}$$

with β constant independent of the triangulation, [8, 24].

Given a regular triangulation \mathcal{T}_h of Ω into a set $\{K\}$ of simplices, or quadrilaterals (2D)/hexahedra (3D), the diameter of a mesh cell K is denoted by h_K and $h = \max_{K \in \mathcal{T}_h} h_K$. The space of continuous functions whose restriction to each mesh cell of \mathcal{T}_h is a polynomial of degree less than or equal to k is denoted by P_k . The space Q_k consists of continuous functions whose restriction to each mesh cell is in each variable is a polynomial of degree less than or equal to k. Popular pairs of spaces that satisfy (9) on simplicial meshes are the pairs from the Taylor–Hood family P_k/P_{k-1} , $k \ge 2$ from [77] and the MINI element P_1^{bub}/P_1 from [6]. In P_1^{bub} , the space P_1 is enriched with local bubble functions (i.e., functions that vanish at the boundaries of all elements of \mathcal{T}_h). On hexahedral meshes, again the Taylor–Hood pairs Q_k/Q_{k-1} , $k \ge 2$, are popular, but also pairs with discontinuous pressure $Q_k/P_{k-1}^{\rm disc}$, $k \ge 2$.



Let $X_{h,\mathrm{div}}$ be the space of discretely divergence-free functions

$$X_{h,\text{div}} = \{ \mathbf{v}_h \in X_h : (\nabla \cdot \mathbf{v}_h, q_h) = 0 \text{ for all } q_h \in Y_h \}.$$

Note that for all pairs of finite element spaces introduced above it holds $X_{h,\mathrm{div}} \not\subset X_{\mathrm{div}}$, i.e., the discretely divergence-free finite element functions are generally not divergence-free. This issue and possible remedies are discussed comprehensively in the survey [102].

With the discrete inf-sup condition (9), the velocity finite element solution of (6) can be computed equivalently by solving: Find $u_h \in X_{h,\text{div}}$ such that for all $v_h \in X_{h,\text{div}}$

$$(\hat{o}_t \mathbf{u}_h, \mathbf{v}_h) + a(\mathbf{u}_h, \mathbf{v}_h) + b_s(\mathbf{u}_h, \mathbf{u}_h, \mathbf{v}_h) = \langle \mathbf{f}_h, \mathbf{v}_h \rangle \text{ in } (0, T)$$
(10)

and $u_h(0,x) = u_{0,h}(x)$. This formulation of the problem will be used in the finite element analysis.

Analytical tools which are often applied in the finite element error analysis comprise Young's inequality

$$ab \leq \frac{t}{p}a^p + \frac{t^{-q/p}}{q}b^q, \quad a, b, p, q, t \in \mathbb{R}, \quad \frac{1}{p} + \frac{1}{q} = 1,$$

$$p, q \in (1, \infty),$$

$$(11)$$

for t > 0, Poincaré's inequality in X

$$\|\mathbf{v}\|_0 \le C \|\nabla \mathbf{v}\|_0 \quad \forall \ \mathbf{v} \in \mathbf{X},\tag{12}$$

and Korn's inequality in X

$$\|\nabla v\|_0 \le C\|\mathbb{D}(v)\|_0 \quad \forall \ v \in X. \tag{13}$$

Since the triangulations are assumed to be regular, the following inverse inequality holds for each $v_h \in X_h$ and each mesh cell $K \in \mathcal{T}_h$, e.g., see [40, Theorem 3.2.6],

$$\|\mathbf{v}_h\|_{m,K} \le c_{\text{inv}} h_K^{l-m} \|\mathbf{v}_h\|_{l,K}, \quad 0 \le l \le m.$$
 (14)

The Stokes projection is the solution of the following problem: Find $\tilde{u}_h \in X_{h,\mathrm{div}}$ such that

$$(2v\nabla(\boldsymbol{u}(t,\cdot)-\tilde{\boldsymbol{u}}_h),\nabla \boldsymbol{v}_h)=(p(t,\cdot),\nabla \cdot \boldsymbol{v}_h) \quad \forall \ \boldsymbol{v}_h \in \boldsymbol{X}_{h,\mathrm{div}}.$$
(15)

Let $u(t,\cdot) \in (H^k(\Omega))^d$, $p(t,\cdot) \in H^{k-1}(\Omega)$, $k \ge 1$, and X_h possess a (k-1)th order approximation property, e.g., X_h is the finite element space P_{k-1} on simplicial meshes or Q_{k-1} on quadrilateral/hexahedral meshes. Then a scaling argument of [75, Lemma 5.3] gives the approximation properties of the Stokes projection

$$\|\boldsymbol{u} - \tilde{\boldsymbol{u}}_h\|_0 + h\|\nabla(\boldsymbol{u} - \tilde{\boldsymbol{u}}_h)\|_0$$

$$\leq Ch^k \left(\|\boldsymbol{u}(t,\cdot)\|_k + \frac{1}{\nu}\|p(t,\cdot)\|_{k-1}\right),$$
(16)

and

$$\|\partial_{t}(\boldsymbol{u} - \tilde{\boldsymbol{u}}_{h})\|_{0} + h\|\partial_{t}(\nabla(\boldsymbol{u} - \tilde{\boldsymbol{u}}_{h}))\|_{0}$$

$$\leq Ch^{k}\left(\|\boldsymbol{u}(t,\cdot)\|_{k} + \frac{1}{\nu}\|p(t,\cdot)\|_{k-1}\right),$$
(17)

where the constants depend only on Ω . Even for t = 0, the pressure can be well defined, e.g., see [74].

Finally, a stability estimate and an error estimate for the finite element velocity solution will be given. The presentation of the proofs will be omitted for the sake of brevity. However, the principal approach for deriving results of this kind is the same as for VMS methods, e.g., see Sect. 8.4 for a detailed presentation.

Lemma 1 Let $u_{0,h} \in X_{h,\text{div}}$ and $f \in L^2(0,t;X')$, then the finite element problem (10) has a unique solution $u_h \in X_h$ and it holds for all $t \in (0,T)$ that

$$\|\boldsymbol{u}_{h}(t)\|_{0}^{2} + v\|\nabla\boldsymbol{u}_{h}\|_{L^{2}(0,t;\boldsymbol{L}^{2})}^{2} \leq \|\boldsymbol{u}_{0,h}\|_{0}^{2} + \frac{1}{v}\|\boldsymbol{f}\|_{L^{2}(0,t;\boldsymbol{X}')}^{2}.$$
(18)

The stability bound (18) depends on the inverse of v.

Theorem 1 Let $\Omega \subset \mathbb{R}^d$, $d \in \{2,3\}$, be a bounded domain with polyhedral and Lipschitz continuous boundary, let $\mathbf{f} \in L^2(0,T;\mathbf{X}')$, $\mathbf{u}_0 \in L^2_{\mathrm{div}}(\Omega)$, and $\mathbf{u}_{0,h} \in \mathbf{X}_{h,\mathrm{div}}$. In addition, the following regularities are assumed for the solution of (2)

$$\partial_t \mathbf{u} \in L^2(0, T; \mathbf{X}'), \quad \nabla \mathbf{u} \in L^4(0, T; \mathbf{L}^2), \quad p \in L^2(0, T; \mathbf{L}^2).$$
(19)

Then the following error estimate holds for the solution \mathbf{u}_h of (10) and for all $t \in (0,T)$

$$\begin{split} &\|(\boldsymbol{u} - \boldsymbol{u}_{h})(t)\|_{0}^{2} + v\|\nabla(\boldsymbol{u} - \boldsymbol{u}_{h})\|_{L^{2}(0,t;L^{2})}^{2} \\ &\leq C \Bigg\{ \|(\boldsymbol{u} - I_{h}\boldsymbol{u})(t)\|_{0}^{2} + v\|\nabla(\boldsymbol{u} - I_{h}\boldsymbol{u})\|_{L^{2}(0,t;L^{2})}^{2} \\ &+ \exp\left(\frac{C}{v^{3}}\|\nabla\boldsymbol{u}\|_{L^{4}(0,t;L^{2})}^{4}\right) \Bigg[\|\boldsymbol{u}_{0,h} - I_{h}\boldsymbol{u}(0)\|_{0}^{2} \\ &+ v\|\nabla(\boldsymbol{u} - I_{h}\boldsymbol{u})\|_{L^{2}(0,t;L^{2})}^{2} + v^{-1} \Big(\|\partial_{t}(\boldsymbol{u} - I_{h}\boldsymbol{u})\|_{L^{2}(0,t;X')}^{2} \\ &+ \|\nabla(\boldsymbol{u} - I_{h}\boldsymbol{u})\|_{L^{4}(0,t;L^{2})}^{2} \|\nabla\boldsymbol{u}\|_{L^{4}(0,t;L^{2})}^{2} \\ &+ \inf_{q_{h} \in L^{2}(0,t;Q_{h})} \|p - q_{h}\|_{L^{2}(0,t;L^{2})}^{2} \Big) \\ &+ \frac{1}{v^{3/2}} \Big(\|\boldsymbol{u}_{0,h}\|_{0}^{2} + \frac{1}{v}\|\boldsymbol{f}\|_{L^{2}(0,t;X')}^{2} \Big) \|\nabla(\boldsymbol{u} - I_{h}\boldsymbol{u})\|_{L^{4}(0,t;L^{2})}^{2} \Big] \Bigg\}, \end{split}$$

where $I_h \mathbf{u}(t)$ is a projection of optimal order at time t, e.g., the Stokes projection, $\partial_t I_h \mathbf{u} \in L^2(0,T;\mathbf{X}')$ is assumed.

It can be seen that the error bound (20) scales like the exponential of v^{-3} .

3 Basic Concepts of VMS Methods

This section discusses basic concepts of VMS methods. Starting point of all VMS methods is the separation of the flow field into resolved and unresolved scales. It should be emphasized once more that although this approach is in principle the same as in LES, the definition of the scales is different. VMS methods which use just resolved and unresolved scales belong to the class of two-scale VMS methods. However, the VMS methodology allows further decompositions of the resolved scales. The most common approach of this kind is a decomposition of these scales into large resolved scales (or large scales) and small resolved scales, leading finally to a so-called three-scale VMS method.

The principal ideas behind two-scale and three-scale VMS methods will be discussed below. For clearness of presentation, the weak formulation (2) of the Navier–Stokes equations will be expressed in a short form as follows: Find $(\boldsymbol{u}, p) : (0, T) \to \boldsymbol{X} \times \boldsymbol{Y}$ satisfying

$$A(\mathbf{u}; (\mathbf{u}, p), (\mathbf{v}, q)) = \mathbf{f}(\mathbf{v}) \quad \forall \ (\mathbf{v}, q) \in \mathbf{X} \times \mathbf{Y}$$
 (21)

with $u(0,x) = u_0(x)$, where $A(\cdot;\cdot,\cdot)$ stands for the left-hand side of (2) and $f(\cdot)$ for the right-hand side of (2).

3.1 Two-Scale VMS Methods

A two-scale VMS method uses a decomposition of the scales in resolved scales $(\overline{u}, \overline{p})$ and unresolved scales (u', p') such that

$$\mathbf{u} = \overline{\mathbf{u}} + \mathbf{u}', \quad p = \overline{p} + p'$$
 (22)

Inserting decomposition (22) in (21), using the same decomposition for the test functions, and the linearity of the variational formulation with respect to the test functions gives

• an equation for the resolved scales

$$A(\boldsymbol{u}; (\overline{\boldsymbol{u}}, \overline{p}), (\overline{\boldsymbol{v}}, \overline{q})) + A(\boldsymbol{u}; (\boldsymbol{u}', p'), (\overline{\boldsymbol{v}}, \overline{q})) = \boldsymbol{f}(\overline{\boldsymbol{v}}),$$
(24)

• and an equation for the unresolved scales

$$A(\mathbf{u}; (\overline{\mathbf{u}}, \overline{p}), (\mathbf{v}', q')) + A(\mathbf{u}; (\mathbf{u}', p'), (\mathbf{v}', q')) = \mathbf{f}(\mathbf{v}').$$
(25)

To simplify notations, define

$$U = \begin{pmatrix} u \\ p \end{pmatrix}$$
, $V = \begin{pmatrix} v \\ q \end{pmatrix}$, and so on.

Now, the form $A(\cdot;\cdot,\cdot)$ is decomposed into its linear part and the trilinear convective term

$$A(\mathbf{u}; \mathbf{U}, \mathbf{V}) = A_{\text{lin}}(\mathbf{U}, \mathbf{V}) + b(\mathbf{u}, \mathbf{u}, \mathbf{v}).$$

Then, (25) can be written in the form

$$A_{U}(U',V') + b(u',u',v') = \langle \operatorname{Res}(\overline{U}), V' \rangle$$
 (26)

with

$$A_{U}(U', V') = A_{\text{lin}}(U', V') + b(u', \overline{u}, v') + b(\overline{u}, u', v'),$$
$$\langle \operatorname{Res}(\overline{U}), V' \rangle = f(v') - A_{\text{lin}}(\overline{U}, V') - b(\overline{u}, \overline{u}, v').$$

Using the linearity of $A_{\text{lin}}(\cdot,\cdot)$ and the trilinearity of $b(\cdot,\cdot,\cdot)$, a straightforward calculation gives that the operator $A_U(U',V')$ is the Gâteaux derivative of $A(\cdot;\cdot,\cdot)$ at U in the direction of U'

$$\begin{split} &\lim_{\varepsilon \to 0} \frac{A\big(\overline{\boldsymbol{u}} + \varepsilon \boldsymbol{u}'; \overline{\boldsymbol{U}} + \varepsilon \boldsymbol{U}', \boldsymbol{V}'\big) - A\big(\overline{\boldsymbol{u}}; \overline{\boldsymbol{U}}, \boldsymbol{V}'\big)}{\varepsilon} \\ &= \lim_{\varepsilon \to 0} \frac{A_{\mathrm{lin}}\big(\overline{\boldsymbol{U}} + \varepsilon \boldsymbol{U}', \boldsymbol{V}'\big) + b\big(\overline{\boldsymbol{u}} + \varepsilon \boldsymbol{u}', \overline{\boldsymbol{u}} + \varepsilon \boldsymbol{u}', \boldsymbol{v}') - A_{\mathrm{lin}}\big(\overline{\boldsymbol{U}}, \boldsymbol{V}'\big) - b\big(\overline{\boldsymbol{u}}, \overline{\boldsymbol{u}}, \boldsymbol{v}'\big)}{\varepsilon} \\ &= A_{\mathrm{lin}}\big(\boldsymbol{U}', \boldsymbol{V}'\big) + b\big(\boldsymbol{u}', \overline{\boldsymbol{u}}, \boldsymbol{v}'\big) + b\big(\overline{\boldsymbol{u}}, \boldsymbol{u}', \boldsymbol{v}'\big). \end{split}$$

with the underlying direct sum decomposition

$$X = \overline{X} \oplus X', \quad Y = \overline{Y} \oplus Y'.$$
 (23)

It should be emphasized once more that the decomposition of the scales and the spaces is performed with variational projections. Equation (26) provides an interpretation of the unresolved scales in terms of the resolved scales: The unresolved scales are a function of the residual of the resolved scales. Hence, there is a representation of the form

$$U' = F_U(\operatorname{Res}(\overline{U})). \tag{27}$$



Inserting this representation in (24) gives an equation for the resolved scales.

The operator F_U is generally not known. However, its knowledge is even not necessary since if the unresolved scales are modeled with this operator, then Eq. (24) has the same complexity as the Navier–Stokes equations. In this case there is no turbulence modeling. Two-scale VMS methods aim to approximate F_U . Note that the model for F_U does not need to rely on considerations from the physics of turbulent flows, it might be derived just with mathematical arguments. In Sects. 4, 5, and 6 concrete approaches will be presented.

3.2 Three-Scale VMS Methods

In a three-scale VMS method, the flow field is decomposed into large (resolved) scales, small resolved scales, and unresolved scales. Applying this scale separation to the underlying solution and test spaces and specifying a direct sum decomposition yields

$$X = \overline{X} \oplus \widehat{X} \oplus X', \quad Y = \overline{Y} \oplus \widehat{Y} \oplus Y',$$

where the three scales are denoted by, respectively, $\overline{()}$, $\overline{()}$ and ()'. Accordingly, one performs the scale decomposition of the solution

$$u = \overline{u} + \widehat{u} + u', \quad p = \overline{p} + \widehat{p} + p'$$

and likewise for the test functions $\mathbf{v} = \overline{\mathbf{v}} + \hat{\mathbf{v}} + \mathbf{v}'$, and $q = \overline{q} + \hat{q} + q'$.

In the same way as for the two-scale VMS methods, the derivation of a three-scale VMS method starts by considering the variational form (21) of the Navier–Stokes equations for the different scales of the test function, using again that the variational form is linear with respect to the test functions. This approach results in a coupled system of three equations with respect to the large scales, small resolved scales, and unresolved scales, which are defined as follows: Find $(\boldsymbol{u}, p) : (0, T) \to \boldsymbol{X} \times \boldsymbol{Y}$ satisfying for all $(\boldsymbol{v}, q) \in \boldsymbol{X} \times \boldsymbol{Y}$

the large-scale problem

$$A(\mathbf{u}; (\overline{\mathbf{u}}, \overline{p}), (\overline{\mathbf{v}}, \overline{q})) + A(\mathbf{u}; (\widehat{\mathbf{u}}, \widehat{p}), (\overline{\mathbf{v}}, \overline{q})) + A(\mathbf{u}; (\mathbf{u}', p'), (\overline{\mathbf{v}}, \overline{q})) = f(\overline{\mathbf{v}}),$$
(28)

- the small resolved scale problem

$$A(\boldsymbol{u}; (\overline{\boldsymbol{u}}, \overline{p}), (\widehat{\boldsymbol{v}}, \widehat{q})) + A(\boldsymbol{u}; (\widehat{\boldsymbol{u}}, \widehat{p}), (\widehat{\boldsymbol{v}}, \widehat{q})) + A(\boldsymbol{u}; (\boldsymbol{u}', p'), (\widehat{\boldsymbol{v}}, \widehat{q})) = \boldsymbol{f}(\widehat{\boldsymbol{v}}),$$
(29)

and the problem for the unresolved scales

$$A(\boldsymbol{u}; (\overline{\boldsymbol{u}}, \overline{p}), (\boldsymbol{v}', q')) + A(\boldsymbol{u}; (\widehat{\boldsymbol{u}}, \widehat{p}), (\boldsymbol{v}', q')) + A(\boldsymbol{u}; (\boldsymbol{u}', p'), (\boldsymbol{v}', q')) = f(\boldsymbol{v}').$$
(30)

In the modeling step of a three-scale VMS method, the following assumptions are taken into account:

- First, it is not intended to explicitly resolve any quantities which are termed "unresolved". Hence, Eq. (30) for the unresolved scales is neglected.
- It is further assumed that the direct influence of the unresolved scales on the large scales is negligible, i.e., in (28) it is set

$$A(\mathbf{u}; (\mathbf{u}', p'), (\overline{\mathbf{v}}, \overline{q})) = 0.$$

• Finally, the influence of the unresolved scales onto the small resolved scales is modeled, i.e., in (29) it is used

$$A(\mathbf{u}; (\mathbf{u}', p'), (\widehat{\mathbf{v}}, \widehat{q})) \approx c(\mathbf{u}; (\overline{\mathbf{u}}, \overline{p}), (\widehat{\mathbf{u}}, \widehat{p}), (\widehat{\mathbf{v}}, \widehat{q})).$$
(31)

The turbulence model $c(\cdot; \cdot, \cdot)$ will be discussed below.

The above assumptions lead to an abstract three-scale VMS method that reads as a coupled system of the form: Find $(\overline{\boldsymbol{u}},\overline{p})\times(\widehat{\boldsymbol{u}},\widehat{p})\in(\overline{\boldsymbol{X}},\overline{\boldsymbol{Y}})\times(\widehat{\boldsymbol{X}},\widehat{\boldsymbol{Y}})$ satisfying

$$A(\overline{u} + \widehat{u}; (\overline{u}, \overline{p}), (\overline{v}, \overline{q})) + A(\overline{u} + \widehat{u}; (\widehat{u}, \widehat{p}), (\overline{v}, \overline{q})) = f(\overline{v})$$
(32)

$$A(\overline{\boldsymbol{u}} + \widehat{\boldsymbol{u}}; (\overline{\boldsymbol{u}}, \overline{p}), (\widehat{\boldsymbol{v}}, \widehat{q})) + A(\overline{\boldsymbol{u}} + \widehat{\boldsymbol{u}}; (\widehat{\boldsymbol{u}}, \widehat{p}), (\widehat{\boldsymbol{v}}, \widehat{q})) + c(\overline{\boldsymbol{u}} + \widehat{\boldsymbol{u}}; (\overline{\boldsymbol{u}}, \overline{p}), (\widehat{\boldsymbol{u}}, \widehat{p}), (\widehat{\boldsymbol{v}}, \widehat{q})) = f(\widehat{\boldsymbol{v}})$$
(33)

for all
$$(\overline{v}, \overline{q}) \times (\widehat{v}, \widehat{q}) \in (\overline{X}, \overline{Y}) \times (\widehat{X}, \widehat{Y})$$
.

This problem may be reduced to a monolithic equations system for the unknowns $u_h = \overline{u} + \widehat{u}$, $p_h = \overline{p} + \widehat{p}$ by introducing the spaces $X_h = \overline{X} \oplus \widehat{X}$ and $Y_h = \overline{Y} \oplus \widehat{Y}$, and the restriction operators

$$\overline{\Pi}_m: X_h \mapsto \overline{X}$$
 and $\overline{\Pi}_c: Y_h \mapsto \overline{Y}$

by

$$\overline{\Pi}_m \mathbf{u}_h = \overline{\mathbf{u}}, \ \overline{\Pi}_c p_h = \overline{p} \text{ whenever } \mathbf{u}_h = \overline{\mathbf{u}} + \widehat{\mathbf{u}},$$
 and $p_h = \overline{p} + \widehat{p}.$

Summing up (32) and (33) one obtains the equivalent problem: Find $(u_h, p_h) \in (X_h, Y_h)$ satisfying

$$A(\mathbf{u}_h; (\mathbf{u}_h, p_h), (\mathbf{v}_h, q_h)) + c(\mathbf{u}_h; \overline{\Pi}(\mathbf{u}_h, p_h), (\mathbf{I} - \overline{\Pi}) \times (\mathbf{u}_h, p_h), (\mathbf{I} - \overline{\Pi})(\mathbf{v}_h, q_h)) = \mathbf{f}(\mathbf{v}_h)$$
(34)

for all $(v_h, q_h) \in (X_h, Y_h)$, where for brevity the notation $\overline{\Pi} = (\overline{\Pi}_m, \overline{\Pi}_c)$ is used, and I denote the component-wise extension of the identity operator to vector-valued functions.

A characteristic feature of a three-scale VMS method is that the turbulence model $c(\cdot;\cdot,\cdot)$ acts directly only on the small resolved scales. However, due to the coupling of the



small resolved and the large scales in (32) and (33), the model $c(\cdot;\cdot,\cdot)$ influences the large scales indirectly. In contrast to this situation, the turbulence model in a classical LES method acts directly on all resolved scales.

To specify a concrete three-scale VMS method, one has to define the spaces for the large and small resolved scales and a model $c(\cdot;\cdot,\cdot)$.

For a finite element discretization of (32)–(33), there are two principal approaches for choosing appropriate spaces:

- In the first approach, standard finite element spaces are used for the large scales $(\overline{X} \times \overline{Y})$. The finite element spaces for the small resolved scales $(\widehat{X} \times \widehat{Y})$ require a higher resolution than the spaces for the large scales since they should represent smaller scales. A proposal consists in using bubble functions on the mesh cells for the small resolved scales. A detailed description of this approach is discussed in Sect. 7.
- The second way for choosing the spaces consists in using a common standard finite element space for all resolved scales and an additional large scale space. Methods of this type will be addressed in Sects. 8 and 9.

In its turn, the discretization of (34) requires a common space $X_h \times Y_h$ for the resolved scales and a restriction operator on the large resolved scales. This operator may be defined by interpolation or projection on a coarser grid. The explicit space of large resolved scales is not needed, it is implicitly considered by means of the restriction operator. This kind of methods will be addressed in Sects. 6 and 10.

The choice of the turbulence model $c(\cdot;\cdot,\cdot)$ in (31) may be guided by physical ideas in turbulence modeling. For VMS methods, widely used turbulence models are eddy viscosity models of Smagorinsky type. Writing $c(\cdot;\cdot,\cdot)$ in the form

$$c(\boldsymbol{u}; (\overline{\boldsymbol{u}}, \overline{p}), (\widehat{\boldsymbol{u}}, \widehat{p}), (\widehat{\boldsymbol{v}}, \widehat{q})) := (v_{\mathsf{T}} \mathbb{D}(\widehat{\boldsymbol{u}}), \mathbb{D}(\widehat{\boldsymbol{v}})), \tag{35}$$

three different versions of the Smagorinsky model within VMS methods can be distinguished, where the second part of the name refers to $\mathbb{D}(\widehat{u})$ in (35):

• the 'small-small' model

$$v_{\mathrm{T}} = C_{\mathrm{S}} \delta^{2} \| \mathbb{D}(\widehat{\boldsymbol{u}}) \|_{\mathrm{F}}, \tag{36}$$

• the 'large-small' model

$$v_{\mathrm{T}} = C_{\mathrm{S}} \delta^{2} \| \mathbb{D}(\overline{\boldsymbol{u}}) \|_{\mathrm{F}}, \tag{37}$$

• the 'all-small' model

$$v_{\rm T} = C_S \delta^2 \| \mathbb{D}(\widehat{\boldsymbol{u}} + \overline{\boldsymbol{u}}) \|_{\rm F}. \tag{38}$$

Here C_S denotes a user-chosen constant, δ a scaling factor related to the mesh width, and $\|\cdot\|_{F}$ the Frobenius tensor norm.

The Smagorinsky model is also a widely used model in LES. Its advantages and drawbacks are well known. The most severe drawback is that it introduces too much viscosity. To reduce this drawback, in [60, 108] the so-called dynamic Smagorinsky model was proposed, which computes C_S a posteriori as a function in time and space, i.e., $C_S = C_S(t, x)$. The use of the dynamic Smagorinsky model is very popular in LES. Also a three-scale VMS method with Smagorinsky model (with constant C_S) can be interpreted as an approach to reduce the viscosity introduced with this model. Here, the reduction comes from the feature that the turbulence model is applied directly only to the small resolved scales and not to all resolved scales.

4 Two-Scale Residual-Based VMS Method

A two-scale VMS method which is based on modeling residuals was proposed in [10]. The resulting method can be considered as a generalization of classical stabilization methods for the Navier–Stokes equations.

4.1 Derivation

Starting point of the derivation of this method is a decomposition of the spaces of form (23). The resolved scales are defined either by the L^2 projection or the elliptic projection. Note that the decomposition of X into a direct sum induces that both the resolved and the unresolved velocity scales have homogeneous Dirichlet boundary data as the functions in X.

Next, a perturbation series for a potentially small quantity is considered. This quantity is $\varepsilon = \|\mathbf{Res}(\overline{U})\|_{(X \times Y)'}$. For this quantity to be small, $\overline{X} \times \overline{Y}$ has to be sufficiently large. In fact, it is assumed that the larger $\overline{X} \times \overline{Y}$, the better \overline{U} approximates U and the smaller is $\mathbf{Res}(\overline{U})$. The perturbation series is of the form

$$U' = \varepsilon U_1' + \varepsilon^2 U_2' + \ldots = \sum_{i=1}^{\infty} \varepsilon^i U_i'.$$
 (39)

In particular, if $\varepsilon = 0$, i.e., $\operatorname{Res}(\overline{U}) = 0$, then $U' = F_U(\operatorname{Res}(\overline{U})) = 0$.

Inserting the perturbation series (39) in the terms of Eq. (26) for the unresolved scales leads to

$$A_U \Biggl(\sum_{i=1}^{\infty} \varepsilon^i U_i', V' \Biggr) = \sum_{i=1}^{\infty} \varepsilon^i A_U \bigl(U_i', V' \bigr)$$

and



$$b\left(\sum_{i=1}^{\infty} \varepsilon^{i} \boldsymbol{u}_{i}^{\prime}, \sum_{i=1}^{\infty} \varepsilon^{i} \boldsymbol{u}_{i}^{\prime}, \boldsymbol{v}^{\prime}\right)$$

$$= \varepsilon^{2} b\left(\boldsymbol{u}_{1}^{\prime}, \boldsymbol{u}_{1}^{\prime}, \boldsymbol{v}^{\prime}\right) + \varepsilon^{3} [b\left(\boldsymbol{u}_{1}^{\prime}, \boldsymbol{u}_{2}^{\prime}, \boldsymbol{v}^{\prime}\right) + b\left(\boldsymbol{u}_{2}^{\prime}, \boldsymbol{u}_{1}^{\prime}, \boldsymbol{v}^{\prime}\right)] + \dots$$

$$= \sum_{i=2}^{\infty} \varepsilon^{i} \left(\sum_{j=1}^{i-1} b\left(\boldsymbol{u}_{j}^{\prime}, \boldsymbol{u}_{i-j}^{\prime}, \boldsymbol{v}^{\prime}\right)\right).$$

These terms can be inserted in (26) giving

$$\sum_{i=1}^{\infty} \varepsilon^{i} A_{U}(U'_{i}, V') + \sum_{i=2}^{\infty} \varepsilon^{i} \left(\sum_{j=1}^{i-1} b(u'_{j}, u'_{i-j}, v') \right)$$

$$= \varepsilon \left\langle \frac{\operatorname{Res}(\overline{U})}{\|\operatorname{Res}(\overline{U})\|_{(X \times Y)'}}, V' \right\rangle.$$

Collecting terms with respect to ε yields

$$A_{U}(U'_{1}, V') = \left\langle \frac{\operatorname{Res}(\overline{U})}{\|\operatorname{Res}(\overline{U})\|_{(X \times Y)'}}, V' \right\rangle,$$

$$A_{U}(U'_{i}, V') = -\sum_{j=1}^{i-1} b(\mathbf{u}'_{j}, \mathbf{u}'_{i-j}, \mathbf{v}') \quad i \geq 2.$$

$$(40)$$

Hence, one obtains a system of variational problems where the computation of U'_i requires the knowledge of all U'_i with j < i. All equation of this system have the same linear operator on the left-hand side.

In [10] it is proposed to truncate the series (39) after the first term, i.e.,

$$U' \approx \varepsilon U_1' = \| \operatorname{Res}(\overline{U}) \|_{(X \times Y)'} U_1'. \tag{41}$$

The function U_1' can be obtained formally by solving the linear partial differential equation (40) with the operator $A_U(U_1,V_1)$. However, solving (40) analytically is generally not possible and the unresolved scale test functions are in practice not available. From the mathematical point of view, there is a formal representation of the solution of (40) with a so-called fine-scale Green's operator

$$U_1' = G_{\overline{U}}' \left(\frac{\operatorname{Res}(\overline{U})}{\|\operatorname{Res}(\overline{U})\|_{(X \times Y)'}} \right). \tag{42}$$

In [10] it is proposed to use a linear approximation of this operator

$$U_1' pprox au rac{\mathbf{Res}(\overline{U})}{\left\|\mathbf{Res}(\overline{U})
ight\|_{(X imes Y)'}},$$

of the unresolved scales, denoted by $\tilde{m{U}}'$, becomes

$$\tilde{U}' = \varepsilon \tilde{U}'_1 = \tau \mathbf{Res}(\overline{U}).$$



Now, this approach will be applied to the Navier-Stokes equations (2). There, the approximation of the resolved scales (u_h, p_h) is computed in a standard finite element space. It is proposed in [10] that the parameter τ is a diagonal tensor-valued functions, i.e.,

$$\tau = \begin{pmatrix} \tau_{\rm m} & \mathbf{0} \\ \mathbf{0}^T & \tau_{\rm c} \end{pmatrix} = \begin{pmatrix} \tau_{\rm m} & 0 & 0 & 0 \\ 0 & \tau_{\rm m} & 0 & 0 \\ 0 & 0 & \tau_{\rm m} & 0 \\ 0 & 0 & 0 & \tau_{\rm c} \end{pmatrix}. \tag{43}$$

The model of the unresolved scales has the form

$$\tilde{U}' = \tau \operatorname{Res}\left(\begin{pmatrix} u_h \\ p_h \end{pmatrix}\right) \\
= \begin{pmatrix} \tau_{\mathrm{m}}(f - \partial_t u_h + v \Delta u_h - (u_h \cdot \nabla)u_h - \nabla p_h) \\ -\tau_{\mathrm{c}}(\nabla \cdot u_h) \end{pmatrix} (44) \\
= \begin{pmatrix} \operatorname{res}_{\mathrm{m},h} \\ \operatorname{res}_{c,h} \end{pmatrix}.$$

This model can be inserted in the large scale equation (24). In [10] it is proposed to neglect the models of the terms $(\partial_t \boldsymbol{u}', \boldsymbol{v}_h)$ and $2v(\mathbb{D}(\boldsymbol{u}'), \mathbb{D}(\boldsymbol{v}_h)).$

Defining the large scales with one of the projections mentioned at the beginning of this section, then one of these terms will vanish already in the derivation of the method, the first term if the $L^2(\Omega)$ projection is used and the second term in case of the elliptic projection. Additionally, the term of the continuity equation with respect to the unresolved scales in (24) is integrated by parts.

Inserting (44) in (24) and using the described modifications gives the resolved scale equation: Find u_h : $(0,T) \rightarrow X_h, p_h : (0,T) \rightarrow Y_h \text{ satisfying}$

$$(\hat{o}_{t}\boldsymbol{u}_{h},\boldsymbol{v}_{h}) + (2\boldsymbol{v}\mathbb{D}(\boldsymbol{u}_{h}),\mathbb{D}(\boldsymbol{v}_{h})) + b(\boldsymbol{u}_{h},\boldsymbol{u}_{h},\boldsymbol{v}_{h}) + (\nabla \cdot \boldsymbol{u}_{h},q_{h})$$

$$- (\nabla \cdot \boldsymbol{v}_{h},p_{h}) - (\mathbf{res}_{\mathbf{m},h},\nabla q_{h}) - (\mathbf{res}_{\mathbf{c},h},\nabla \cdot \boldsymbol{v}_{h})$$

$$+ b(\mathbf{res}_{\mathbf{m},h},\boldsymbol{u}_{h},\boldsymbol{v}_{h}) + b(\boldsymbol{u}_{h},\mathbf{res}_{\mathbf{m},h},\boldsymbol{v}_{h})$$

$$+ b(\mathbf{res}_{\mathbf{m},h},\mathbf{res}_{\mathbf{m},h},\boldsymbol{v}_{h}) = \langle \boldsymbol{f},\boldsymbol{v}_{h}\rangle$$

$$(45)$$

for all $(v_h, q_h) \in X_h \times Y_h$.

Concerning the actual choice of the convective term, it is advisable from the practical point of view that one does not need to compute a derivative of the residual of the momentum equation. For this reason, it is proposed in [10] to use the following form of the convective term, which is obtained from the divergence form with integration by

$$b(\mathbf{u}, \mathbf{v}, \mathbf{w}) = (\nabla \cdot (\mathbf{u}\mathbf{v}^T), \mathbf{w}) = -(\mathbf{u}\mathbf{v}^T, \nabla \mathbf{w}). \tag{46}$$

Direct calculations show that



$$(\nabla \mathbf{v})\mathbf{u} = (\mathbf{u} \cdot \nabla)\mathbf{v} \tag{47}$$

and

$$(uv^{T}, \nabla w) = \int_{\Omega} (uv^{T}) : \nabla w \ dx$$

$$= \int_{\Omega} v \cdot (\nabla w^{T} u) \ dx = (v, \nabla w^{T} u).$$
(48)

In the convective term of the resolved scales $b(\mathbf{u}_h, \mathbf{u}_h, \mathbf{v}_h)$ there is no residual and one can use in practice any other form of the convective term proposed in the literature.

In analogy to LES models, the terms $b(\mathbf{res}_{m,h}, \mathbf{u}_h, \mathbf{v}_h)$ and $b(\mathbf{u}_h, \mathbf{res}_{m,h}, \mathbf{v}_h)$ are called cross-stress terms. For the first cross-stress term, one obtains from (46), (48), and (47)

$$b(\mathbf{res}_{m,h}, \mathbf{u}_h, \mathbf{v}_h) = -(\mathbf{res}_{m,h}(\mathbf{u}_h)^T, \nabla \mathbf{v}_h)$$

$$= -((\nabla \mathbf{v}_h)^T \mathbf{res}_{m,h}, \mathbf{u}_h)$$

$$= -\int_{\Omega} (\mathbf{res}_{m,h})^T (\nabla \mathbf{v}_h) \mathbf{u}_h d\mathbf{x}$$

$$= -(\mathbf{res}_{m,h}, (\nabla \mathbf{v}_h) \mathbf{u}_h)$$

$$= -(\mathbf{res}_{m,h}, (\mathbf{u}_h \cdot \nabla) \mathbf{v}_h)$$
(49)

and for the second cross-stress term with (46) and (48)

$$b(\mathbf{u}_h, \mathbf{res}_{m,h}, \mathbf{v}_h) = -\left(\mathbf{u}_h (\mathbf{res}_{m,h})^T, \nabla \mathbf{v}_h\right)$$

= $-(\mathbf{res}_{m,h}, (\nabla \mathbf{v}_h)^T \mathbf{u}_h).$ (50)

The last convective term is called subgrid (or Reynoldsstress) term, again in analogy to LES, and from (46) it is given by

$$b(\mathbf{res}_{m,h}, \mathbf{res}_{m,h}, \nu_h) = -\left((\mathbf{res}_{m,h}((\mathbf{res}_{m,h})^T, \nabla \nu_h)). \quad (51)$$

As already mentioned, a diagonal tensor is used for τ with the components τ_m and τ_c , see (43). The proposal for choosing τ_m and τ_c in [10] is based on dimensional arguments and not on numerical analysis. A derivation of the stabilization parameter τ_m for compressible flow equations based on such arguments can be found in [131]. In this paper, a product of a Jacobian matrix, τ , and the transposed of the Jacobian is considered. The dimensional arguments lead to the conclusion that the blocks of this product are dimensionally equivalent to some other matrix. Based on this conclusion, an ansatz for the product is proposed, which contains the other matrix, and then the stabilization parameter is derived. Since the whole derivation is somewhat involved, its details will not be presented here but only the results.

Consider parametric finite elements with the bijective map $F_K: \hat{K} \to K$ and the inverse map $F_K^{-1}: K \to \hat{K}$ with $\mathbf{x} \mapsto \hat{\mathbf{x}}$. Differentiating F_K^{-1} leads to the definition of the symmetric tensor \mathbb{G} with

$$\mathbb{G}_{ij} = \sum_{k=1}^{3} \frac{\partial \hat{x}_k}{\partial x_i} \frac{\partial \hat{x}_k}{\partial x_j}, \quad i, j = 1, 2, 3.$$

Then, the stabilization parameter proposed in [10] is given by

$$\tau_{\mathrm{m}} = \left(\frac{4}{\Delta t^2} + (\boldsymbol{u}_h)^T \mathbb{G}(\boldsymbol{u}_h) + c_{\mathrm{inv}} v^2 \|\mathbb{G}\|_{\mathrm{F}}^2\right)^{-1/2},\tag{52}$$

where c_{inv} is the constant in the inverse estimate (14).

For the stabilization parameter τ_c , the vector \mathbf{g} with $g_i = \sum_{j=1}^{3} \partial \hat{x}_j / \partial x_i$ is defined and the proposal in [10] consists in setting

$$\tau_{c} = \left(\tau_{m} \mathbf{g}^{T} \mathbf{g}\right)^{-1}.\tag{53}$$

The stabilization parameters (52) and (53) will be discussed in detail for a special case in Example 1.

Example 1 Consider the reference cube $\hat{K} = [-1, 1]^3$ and let K be a cube with edges of length h which are parallel to the coordinate axes. Then the reference map has the form

$$F_K: \hat{K}
ightharpoonup K, \quad \hat{m{x}} \mapsto rac{1}{2} egin{pmatrix} h & 0 & 0 \ 0 & h & 0 \ 0 & 0 & h \end{pmatrix} \hat{m{x}} + m{b} = m{x}.$$

Considering the inverse map, one finds that

$$\frac{\partial \hat{x}_i}{\partial x_j} = \frac{2}{h} \tau_{ij}, \quad \mathbb{G}_{ij} = \frac{4}{h^2} \tau_{ij}, \quad \|\mathbb{G}\|_{\mathrm{F}}^2 = \frac{48}{h^4},$$
$$(\boldsymbol{u}_h)^T \mathbb{G}(\boldsymbol{u}_h) = \frac{4}{h^2} \|\boldsymbol{u}_h\|_2^2.$$

Then, the stabilization parameter τ_m becomes

$$\tau_{\rm m} = \left(\frac{4}{\Delta t^2} + \frac{4\|\boldsymbol{u}_h\|_2^2}{h^2} + \frac{48c_{\rm inv}v^2}{h^4}\right)^{-1/2}.$$
 (54)

For the parameter τ_c , one obtains $g_i = 2/h$ for i = 1, 2, 3, such that $\mathbf{g}^T \mathbf{g} = 12/h^2$ and

$$\tau_{\rm c} = \frac{h^2}{12\tau_{\rm m}}.\tag{55}$$

Now, the parameters (54) and (55) will be discussed for the different cases in which one of the terms in (54) dominates:

- The term $4/\Delta t^2$ dominates in (54), i.e., Δt is very small. Then one obtains $\tau_{\rm m} = \mathcal{O}(\Delta t)$ and $\tau_{\rm c} = \mathcal{O}(h^2/\Delta t)$.
- The term $4\|\mathbf{u}_h\|_2^2/h^2$ dominates in (54), i.e., there is a strong convection and $\Delta t \gtrsim h$. In this case, one gets $\tau_{\rm m} = \mathcal{O}(h)$ and $\tau_{\rm c} = \mathcal{O}(h)$.
- The term $48c_{\text{inv}}v^2/h^4$ is dominating in (54), i.e., the viscosity dominates or the mesh is very fine and



$$\Delta t \gtrsim h^2$$
. This situation leads to $\tau_{\rm m} = \mathcal{O}(h^2)$ and $\tau_{\rm c} = \mathcal{O}(1)$.

Thus, the parameter choice in the second and third case is the same as for equal-order discretizations of the Oseen equations, see [124, Part IV, Section 3.1] or [22]. In fact, in [10] the two-scale residual-based VMS method was applied with equal-order non-uniform rational B-splines (NURBS).

Considering the physical units of the stabilization parameters, one finds that

$$\tau_m \; : \; \left[\big(1/s^2 + m^2 \big/ (s^2 m^2) + m^4 \big/ (s^2 m^4) \big)^{-1/2} \right] = [\; s \;]$$

and

$$\tau_{c} \ : \ \left[\left(s/m^{2}\right)^{-1}\right] = \left[m^{2}/s\right].$$

Thus, τ_m is a time scale and τ_c is a viscosity scale, and they are respectively the time and viscous scales of the subgrid flow.

For $\Delta t \to 0$ it holds that $\tau_m \to 0$ and $\tau_c \to \infty$. An alternative definition of the stabilization parameters for small time steps, which avoids this behavior, was proposed in [79].

It can be expected that the parameter in the case of using velocity and pressure finite element spaces that satisfy the discrete inf-sup condition (9) has to be chosen in a different way than proposed in [10]. This expectation is based on the different choices for the Oseen equations, see [124, Part IV, Section 3.1]. In addition, numerical analysis for the transient Oseen equations with grad-div stabilization in [50] shows that $\tau_c = \mathcal{O}(1)$ is the asymptotic optimal choice in the convection-dominated regime, in contrast to $\tau_c = \mathcal{O}(h)$ as it was found in Example 1. Since to the best of our knowledge, the two-scale residual-based VMS method was not used so far with inf-sup stable pairs of finite element spaces, the asymptotic correct choice of the stabilization parameter seems to be an open problem in this case.

In [59] it is proposed to model the unresolved velocity scales or the subgrid scale velocity with

$$\partial_t \tilde{\boldsymbol{u}}' + \frac{1}{\tilde{\tau}_{\mathrm{m}}} \tilde{\boldsymbol{u}}' = \boldsymbol{f} - [\partial_t \boldsymbol{u}_h - v \Delta \boldsymbol{u}_h + (\boldsymbol{u}_h \cdot \nabla) \boldsymbol{u}_h + \nabla p_h],$$
(56)

instead of (44). A time-dependent evolution of the unresolved velocity scales of this form was proposed in [48], see also Sect. 5 for a VMS method based on time-dependent orthogonal subgrid scales.

4.2 Relations to Other Methods

From (45) and (49) it follows that



$$b(\mathbf{res}_{m,h}, \mathbf{u}_h, \mathbf{v}_h) - (\mathbf{res}_{m,h}, \nabla q_h)$$

= $-(\mathbf{res}_{m,h}, (\mathbf{u}_h \cdot \nabla)\mathbf{v}_h + \nabla q_h).$ (57)

This term has just the form of the stabilization term of the Streamline-Upwind Petrov-Galerkin (SUPG) method for the convection field u_h .

Inserting the concrete formula of the residual of the continuity equation gives the term

$$(\tau_c \nabla \cdot \boldsymbol{u}_h, \nabla \cdot \boldsymbol{v}_h), \tag{58}$$

which is just a so-called grad-div stabilization term.

Both terms (57) and (58) are classical stabilization terms for the incompressible Navier–Stokes equations.

There are similarities, but also differences, to the two-scale VMS method with orthogonal subgrid scales presented in Sect. 5. A discussion of these issues is postponed to Sect. 5.2.

4.3 Numerical Analysis

Numerical analysis for the two-scale residual-based VMS method (45) is not available. However, the grad-div stabilization and the SUPG method are analyzed for the Stokes, the Oseen, and the stationary Navier–Stokes equations.

The grad-div stabilization (58) arises from adding $-\tau_c \nabla(\nabla \cdot \boldsymbol{u}) = \boldsymbol{0}$ to the momentum equation in (1). Deriving the discrete weak form and applying integration by parts leads to the term $(\tau_c \nabla \cdot \boldsymbol{u}_h, \nabla \cdot \boldsymbol{v}_h)$. Since in finite element methods the velocity is generally not weakly divergence-free, i.e., $\nabla \cdot \boldsymbol{u}_h \neq 0$, the discretization (58) of this term has an effect on the finite element solution. Altogether, the grad-div stabilization can be considered as a penalization of the violation of the continuity equation for finite element velocities.

The grad-div stabilization was introduced in [54]. It is well understood for the Stokes equations

$$-v\Delta \mathbf{u} + \nabla p = \mathbf{f} \quad \text{in } \Omega,$$

$$\nabla \cdot \mathbf{u} = 0 \quad \text{in } \Omega$$
(59)

and for finite element methods which satisfy the discrete inf-sup condition (9). Numerical analysis, e.g., in [90, 117] shows that for finite element discretizations satisfying (9) the choice of the stabilization parameter $\tau_c = \mathcal{O}(1)$ with respect to the mesh width leads to optimal error estimates. However, a good choice of τ_c depends usually on (unknown) norms of the solution (\boldsymbol{u},p) of (59) and on whether or not the sequence of weakly divergence-free subspaces contained in the discretely divergence-free spaces $\boldsymbol{X}_{h,\text{div}}$ has an optimal approximation property.

The SUPG method was introduced in [28, 81] for stabilizing scalar convection-dominated convection-diffusion equations. Stabilizations of the Oseen equations and the

stationary Navier–Stokes equations which contain the SUPG term were analyzed in [53, 72, 111, 136], and extensions of the analysis can be found in [110, 114, 137]. Surveys of the results are provided in [22, 124].

The SUPG stabilization (57) was studied in particular for the Oseen equations

$$-v\Delta \mathbf{u} + (\mathbf{b} \cdot \nabla)\mathbf{u} + c\mathbf{u} + \nabla p = \mathbf{f} \quad \text{in } \Omega,$$

$$\nabla \cdot \mathbf{u} = 0 \quad \text{in } \Omega.$$
(60)

where b is a given weakly divergence-free convection field and $c(x) \ge 0$ in Ω . In the numerical analysis, the SUPG method was often considered with the grad-div stabilization (58) and the so-called pressure stabilization Petrov–Galerkin (PSPG) method. The PSPG method, introduced in [84], stabilizes pairs of finite element spaces that violate the discrete inf-sup condition (9).

Altogether, the SUPG/PSPG/grad-div finite element problem has the form: Given $f \in L^2(\Omega)$, find $(u_h, p_h) \in X_h \times Y_h$ such that

$$A((\boldsymbol{u}_h, p_h), (\boldsymbol{v}_h, q_h)) = L((\boldsymbol{v}_h, q_h)) \quad \forall \ (\boldsymbol{v}_h, q_h) \in \boldsymbol{X}_h \times \boldsymbol{Y}_h,$$
(61)

with

$$A((\boldsymbol{u}, p), (\boldsymbol{v}, q)) = v(\nabla \boldsymbol{u}, \nabla \boldsymbol{v}) + ((\boldsymbol{b} \cdot \nabla)\boldsymbol{u} + c\boldsymbol{u}, \boldsymbol{v})$$

$$- (\nabla \cdot \boldsymbol{v}, p) + (\nabla \cdot \boldsymbol{u}, q) + \sum_{K \in \mathcal{T}_h} \tau_{c,K} (\nabla \cdot \boldsymbol{u}, \nabla \cdot \boldsymbol{v})_K$$

$$+ \sum_{E \in \mathcal{E}_h} \gamma_E ([|p|]_E, [|q|]_E)_E + \sum_{K \in \mathcal{T}_h} (-v \Delta \boldsymbol{u} + (\boldsymbol{b} \cdot \nabla) \boldsymbol{u}$$

$$+ c\boldsymbol{u} + \nabla p, \tau_K^{\boldsymbol{v}} (\boldsymbol{b} \cdot \nabla) \boldsymbol{v} + \tau_K^{\boldsymbol{p}} \nabla q)_K$$

$$(62)$$

and

$$L((\mathbf{v},q)) = (\mathbf{f},\mathbf{v}) + \sum_{K \in \mathcal{T}_h} (\mathbf{f}, \tau_K^{\mathbf{v}}(\mathbf{b} \cdot \nabla)\mathbf{v} + \tau_K^p \nabla q)_K. \tag{63}$$

Here, $\tau_{c,K}$, γ_E , τ_K^{ν} , τ_K^{p} are local stabilization parameters and $[\ |\cdot|\]_E$ denotes the jump across the face E of a mesh cell K.

Main goals of the numerical analysis are to show the existence and uniqueness of a solution of (61) and to prove finite element error estimates. These estimates allow to derive information on asymptotic optimal choices of the stabilization parameters in (62), (63).

In the available analysis, the stabilization parameters for stabilizing velocity and pressure were set to be equal $\tau_{m,K} = \tau_K^v = \tau_K^p$. For all $K \in \mathcal{T}_h$, it is set

$$\tau_m = \max_{K \in \mathcal{T}_h} \tau_{m,K}, \quad \tau_c = \max_{K \in \mathcal{T}_h} \tau_{c,K}, \quad \gamma = \max_{E \in \mathcal{E}_h} \gamma_E.$$

The well-posedness of problem (61) can be proved by deriving an inf-sup condition for the bilinear form A from (62) with respect to an appropriate norm. The proof of this inf-sup condition poses some restrictions on the

stabilization parameters. Then a finite element error analysis can be performed. Equilibrating terms in the error bound gives for the convection-dominated case the following optimal choices of the stabilization parameters:

- for pairs of finite element spaces satisfying the discrete inf-sup condition (9) and the polynomial degree of the velocity space is higher by one than polynomial degree of pressure space: $\tau_{\rm m} = \mathcal{O}(h^2), \tau_{\rm c} = \mathcal{O}(1)$, and if $Y_h \not\subset H^1(\Omega)$ then $\gamma = \mathcal{O}(h)$,
- for pairs of finite element spaces that does not satisfy the discrete inf-sup condition and the polynomial degree of velocity and pressure space is the same: $\tau_{\rm m} = \mathcal{O}(h), \tau_{\rm c} = \mathcal{O}(h),$ and if $Y_h \not\subset H^1(\Omega)$ then $\gamma = \mathcal{O}(1).$

In simulations of turbulent flows, the use of anisotropic grids, in particular near the boundary, is often of great advantage. A numerical analysis of residual-based stabilized finite element methods (SUPG/PSPG/grad-div stabilization) of the Oseen equations on anisotropic meshes was performed in [2].

A numerical analysis of the SUPG stabilization for time-dependent problems is available so far only for scalar convection-diffusion equations in [103]. Optimal error estimates for the backward Euler scheme and for rather general assumptions on the data were derived for a stabilization parameter $\tau_{\rm m} \leq \Delta t/4$. Thus, the stabilization parameter depends on the length of the time step as in (52) and (54).

In [88], an explicit formula for the fine-scale Green's function (42) was derived. This function can be expressed in terms of the classical Green's function and the projection that defines the scale decomposition, see the beginning of Sect. 4.1 for possible approaches. A detailed analytical study of the fine-scale Green's function was performed for convection-diffusion equations in one dimension. It was shown that in the convection-dominated case the form of this function depends strongly on the projection. If the elliptic projection is used, then the fine-scale Green's function possesses the desirable properties to be localized and attenuated, in contrast to the situation for the L^2 projection.

4.4 Experience in Numerical Simulations

In [10] the two-scale residual-based VMS method was studied at an example for isotropic turbulence and at a benchmark problem of a turbulent channel flow with Reynolds number $Re_\tau=395$ based on the friction velocity and the channel half width. For the turbulent channel flow it was observed that the results for first and second order statistics obtained with quadratic NURBS are almost



identical to DNS results. A significant increase in accuracy was observed when using second order NURBS instead of first order NURBS (Q_1 finite elements). The authors consider the results with second order NURBS to be more accurate than those obtained with a spectral Fourier method from [87].

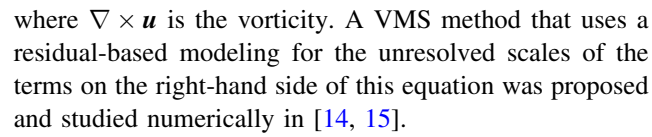
The two-scale residual-based VMS method from [10] and the algebraic VMS method AVM³ described in Sect. 9, both applied with Q_1/Q_1 finite elements, were compared in [63] for a turbulent channel flow problem and a turbulent flow in a lid driven cavity. With respect to several quantities of interest, the two-scale residual-based VMS method showed less accurate results. In these studies, the simulations with the two-scale residual-based VMS method were also somewhat less efficient. Computational studies in [65] for a turbulent flow around a cylinder showed only small differences between the residual-based VMS method and AVM³. From the point of view of efficiency, both VMS methods proved to be clearly superior to the popular dynamic Smagorinsky model.

In [59], equation (56) was discretized in a space consisting of bubble functions. The stabilization parameter $\tilde{\tau}_{\rm m}$ which was proposed in [59] possesses the asymptotic behavior $\tilde{\tau}_{\rm m} = \mathcal{O}(h)$ in the convection-dominated regime. Equal-order pairs of finite element spaces, e.g., Q_1/Q_1 , were used in the numerical studies. These studies were performed at the turbulent channel flow benchmark problems. It turned out that in the case of a length of the time step that was not too small, the differences of the results obtained with the steady-state model of the unresolved scales (44) and the time-dependent model (56) were small. However, for the time-dependent model (56), the results were more robust in the sense that the length of the time step did not possess much impact on the results. For the steady-state model, the length of the time step enters the definition of the stabilization parameters (52) and (53). In particular, τ_m becomes small, see the discussion of the stabilization parameters at the end of Sect. 4.1, and a notable impact of the length of the time step on second order statistics was observed.

A rotating turbulent flow, the so-called Taylor-Couette flow, was successfully simulated in [9] with the two-scale residual-based VMS method using C^1 NURBS, weak imposition of Dirichlet boundary conditions, and adaptive grid refinement.

A direct calculation shows that the nonlinear term can be split in the form

$$(\boldsymbol{u}\cdot\nabla)\boldsymbol{u}=(\mathbb{D}\boldsymbol{u})\boldsymbol{u}+\frac{1}{2}(\nabla\times\boldsymbol{u})\times\boldsymbol{u},$$



A residual-based VMS method with time-dependent subgrid scales for variable-density flows at low Mach number was proposed in [67].

5 Two-Scale VMS Method with Orthogonal Subscales

A residual-based VMS method that uses orthogonal subscales was developed in [44] for the Navier–Stokes problem. This model is referred as orthogonal subscales (OSS) method.

5.1 Derivation

As for the two-scale residual-based VMS method derived in Sect. 4.1, starting point of the OSS method is a decomposition of the spaces of form (23). The resolved scales are represented in a standard finite element space. The space of continuous solutions $\mathbf{Z} = \mathbf{X} \times \mathbf{Y}$ is decomposed into $\mathbf{Z} = \mathbf{Z}_h \oplus \mathbf{Z}'$, where $\mathbf{Z}_h = \mathbf{X}_h \times \mathbf{Y}_h$ represents the resolved scales, and $\mathbf{Z}' = \mathbf{X}' \times \mathbf{Y}'$ represents the unresolved scales. In this context, the space \mathbf{Z}' is called the space of subgrid scales or subscales. Correspondingly, the solution is decomposed as $\mathbf{U} = \mathbf{U}_h + \mathbf{U}'$ and the test functions in the form $\mathbf{V} = \mathbf{V}_h + \mathbf{V}'$. With the notations of Sect. 3, this corresponds to $\overline{\mathbf{X}} = \mathbf{X}_h$, $\overline{\mathbf{Y}} = \mathbf{Y}_h$.

The OSS method is derived as in [44] by considering first the transient Oseen equations, so that the convection velocity is a given solenoidal velocity field b. To present this method, let

$$\boldsymbol{M} = \operatorname{diag}(\boldsymbol{I}_d, 0),$$

where I_d is the $d \times d$ identity matrix, and consider an approximation of problem (24)–(25) in time by the trapezoidal rule, to analyze how does the time discretization affect the OSS method when using finite differences. Consider a uniform partition of the time interval [0, T] with time step Δt . The time step level at which the algorithmic solution is computed is denoted by a superscript. For $\theta \in [0,1]$ and $U'^{,n}$ known, the trapezoidal rule applied to Eq. (26) for the unresolved scales (with the convection velocity u = b) consists of finding $U'^{,n+\theta}$ as the solution of the problem



$$(\boldsymbol{M}\delta_{t}\boldsymbol{U}^{\prime,n},\boldsymbol{V}^{\prime}) + \langle \mathcal{L}_{\boldsymbol{b}}(\boldsymbol{U}^{\prime,n+\theta}), \boldsymbol{V}^{\prime} \rangle$$

$$= \langle \mathbf{Res}(\boldsymbol{U}_{h}^{n+\theta}), \boldsymbol{V}^{\prime} \rangle \forall \boldsymbol{V}^{\prime} \in \boldsymbol{Z}^{\prime},)$$
(64)

where $\delta_t U'^{,n} = \frac{1}{\Delta t} (U'^{,n+1} - U'^{,n})$, \mathcal{L}_b is the linear operator defined as

$$\mathcal{L}_{\boldsymbol{b}}(\boldsymbol{U}) = \begin{pmatrix} -v \Delta \boldsymbol{u} + (\boldsymbol{b} \cdot \nabla) \boldsymbol{u} + \nabla p \\ \nabla \cdot \boldsymbol{u} \end{pmatrix},$$

and $\operatorname{Res}(U_h^{n+\theta})$ is the residual associated to $U_h^{n+\theta}$

$$\mathbf{Res}(\boldsymbol{U}_h^{n+\theta}) = \boldsymbol{F} - \left[\boldsymbol{M} \delta_t \boldsymbol{U}_h^n + \mathcal{L}_{\boldsymbol{b}}(\boldsymbol{U}_h^{n+\theta}) \right], \quad \boldsymbol{F} = \begin{pmatrix} \boldsymbol{f} \\ 0 \end{pmatrix}.$$

The following notation is used throughout this section

$$f^{n+\theta} := \theta f^{n+1} + (1-\theta)f^n, \quad \delta_t f^n := \frac{1}{\Delta t} (f^{n+1} - f^n),$$

for any function f. For the sake of simplicity, it is considered throughout this section that F is time-independent and that the force vector belongs to the finite element space, or it is approximated by an element of this space. Equation (64) may be equivalently rewritten as

$$\left(M\frac{1}{\theta\Delta t}U'^{,n+\theta},V'\right) + \langle \mathcal{L}_{b}(U'^{,n+\theta}),V'\rangle
= \left(M\frac{1}{\theta\Delta t}U'^{,n},V'\right) + \langle \operatorname{Res}(U_{h}^{n+\theta}),V'\rangle,$$
(65)

from where a closed-form expression for U' has to be proposed.

The residual-based OSS strategy consists in setting the unresolved space as

$$Z' = Z_h^{\perp} \cap Z$$

where \mathbf{Z}_h^{\perp} is the $L^2(\Omega)$ -orthogonal complement of \mathbf{Z}_h , and in further approximating

$$\mathbf{Z}' pprox \mathbf{Z}'_h = \left[\sum_{K \in \mathcal{T}_h} \mathbf{H}^1_0(K) \right] \cap \mathbf{Z}_h^{\perp},$$

being thus \mathbf{Z}'_h a bubble finite element space. The goals is now to properly approximate $U' \approx U'_h \in \mathbf{Z}'_h$.

Denote $U_K' = U_h'|_K$ and assume that $\mathcal{L}_b(U_K'^{n+\theta})$ and $\operatorname{Res}(U_h^{n+\theta})$ have $L^2(K)$ regularity. The operator \mathcal{L}_b restricted to functions of $\mathbf{H}_0^1(K)$ is approximated by a diagonal operator, so that

$$M\frac{1}{\theta \Delta t}U_{K}^{\prime,n+\theta} + \mathcal{L}_{b}(U_{K}^{\prime,n+\theta}) \approx \left(M\frac{1}{\theta \Delta t} + \lambda_{K}\right)U_{K}^{\prime,n+\theta},$$
(66)

with λ_K being a $d \times d$ non-singular diagonal matrix. Then, Eq. (65) is discretized by

$$\left(U_K^{\prime,n+\theta} - \tau_{t,K} \left(M \frac{1}{\theta \Delta t} U_K^{\prime,n} + \mathbf{Res}(U_h^{n+\theta})|_K\right), V_K^{\prime}\right)_K \\
= 0 \quad \forall \ K \in \mathcal{T}_h.$$

for any $V_h' \in \mathbf{Z}_h'$, $V_K' = V_{h|_K}'$, $\tau_{t,K} = \left(M\frac{1}{\theta \Delta t} + \tau_K^{-1}\right)^{-1}$, and $\tau_K = \lambda_K^{-1}$. Thus, one obtains

$$\left(oldsymbol{U}_h^{\prime,n+ heta} - au_tigg(oldsymbol{M}rac{1}{ heta A t}U_h^{\prime,n} + \mathbf{Res}(U_h^{n+ heta})igg), V_h^\prime
ight)$$

$$=0 \quad \forall \ \boldsymbol{V}_{h}^{'} \in \boldsymbol{Z}_{h}^{\prime},$$

where τ_t denotes the time-dependent piecewise constant matrix function that takes the value $\tau_{t,K}$ on K. One can prove that space \mathbf{Z}_h' is dense in \mathbf{Z}_h^{\perp} in the L^2 norm, thus deducing

$$egin{aligned} \left(U_h'^{,n+ heta} - au_tigg(Mrac{1}{ heta \Delta t}U_h'^{,n} + \mathbf{Res}(U_h^{n+ heta})igg), V_h'
ight) \ &= 0 \quad orall \ V_h' \in \mathbf{Z}_h^{\perp}, \end{aligned}$$

and, as a consequence

$$\Pi_{\mathbf{Z}_h^{\perp}}\bigg(\mathbf{U}_h^{\prime,n+ heta}- au_tigg(Mrac{1}{ heta arDelta t}\mathbf{U}_h^{\prime,n}+\mathbf{Res}(\mathbf{U}_h^{n+ heta})igg)igg)=0,$$

where $\Pi_{\mathbf{Z}_h^{\perp}}$ denotes the $L^2(\Omega)$ -orthogonal projection on \mathbf{Z}_h^{\perp} . Since $U_h'^{,n+\theta} \in \mathbf{Z}_h' \subset \mathbf{Z}_h^{\perp}$, then $\Pi_{\mathbf{Z}_h^{\perp}}(U_h'^{,n+\theta}) = U_h'^{,n+\theta}$, and

$$oldsymbol{U}_h^{\prime,n+ heta} = \Pi_{oldsymbol{Z}_h^\perp}igg[au_tigg(oldsymbol{M}rac{1}{ heta \Delta t}oldsymbol{U}_h^{\prime,n} + \mathbf{Res}(oldsymbol{U}_h^{n+ heta})igg)igg].$$

To simplify the computations, a further approximations may be considered

$$U_h^{\prime,n+\theta} \approx \tau_t \Pi_{Z_h^{\perp}} \left(M \frac{1}{\theta \Delta t} U_h^{\prime,n} + \mathbf{Res}(U_h^{n+\theta}) \right). \tag{67}$$

Indeed, for all $V_h' \in \mathbf{Z}_h'$ one could write

$$\begin{split} &\left(\Pi_{\boldsymbol{Z}_{h}^{\perp}}\bigg(\boldsymbol{\tau}_{t}\bigg(\boldsymbol{M}\frac{1}{\theta \Delta t}\boldsymbol{U}_{h}^{\prime,n} + \mathbf{Res}(\boldsymbol{U}_{h}^{n+\theta})\bigg)\right), \boldsymbol{Z}_{h}^{\prime}\bigg) \\ &= \bigg(\boldsymbol{\tau}_{t}\bigg(\boldsymbol{M}\frac{1}{\theta \Delta t}\boldsymbol{U}_{h}^{\prime,n} + \mathbf{Res}(\boldsymbol{U}_{h}^{n+\theta})\bigg), \boldsymbol{Z}_{h}^{\prime}\bigg) \\ &= \sum_{K \in \mathcal{T}_{h}} \boldsymbol{\tau}_{t,K}\bigg(\boldsymbol{M}\frac{1}{\theta \Delta t}\boldsymbol{U}_{h}^{\prime,n} + \mathbf{Res}(\boldsymbol{U}_{h}^{n+\theta}), \boldsymbol{Z}_{h}^{\prime}\bigg)_{K} \\ &\approx \sum_{K \in \mathcal{T}_{h}} \boldsymbol{\tau}_{t,K}\bigg(\Pi_{\boldsymbol{Z}_{h}^{\perp}}\bigg(\boldsymbol{M}\frac{1}{\theta \Delta t}\boldsymbol{U}_{h}^{\prime,n} + \mathbf{Res}(\boldsymbol{U}_{h}^{n+\theta})\bigg), \boldsymbol{Z}_{h}^{\prime}\bigg)_{K} \\ &= \bigg(\boldsymbol{\tau}_{t}\Pi_{\boldsymbol{Z}_{h}^{\perp}}\bigg(\boldsymbol{M}\frac{1}{\theta \Delta t}\boldsymbol{U}_{h}^{\prime,n} + \mathbf{Res}(\boldsymbol{U}_{h}^{n+\theta})\bigg), \boldsymbol{Z}_{h}^{\prime}\bigg). \end{split}$$

Again, from (67), since $U_h'^{,n}\in Z_h'\subset Z_h^\perp$, then $\Pi_{Z_h^\perp}(U_h'^{,n})=U_h'^{,n}$, and



$$U_h^{\prime,n+\theta} \approx \tau_t \left[M \frac{1}{\theta \Delta t} U_h^{\prime,n} + \Pi_{\mathbf{Z}_h^{\perp}} (\mathbf{Res}(U_h^{n+\theta})) \right]. \tag{68}$$

Next, to introduce this approximation of $U_h^{\prime,n+\theta}$ in the equation for the resolved scale (24) discretized in time (with convection velocity u = b), denote by \mathcal{L}_b^* the adjoint operator of \mathcal{L}_b , given by

$$\mathcal{L}_{\boldsymbol{b}}^*(\boldsymbol{V}) = \begin{pmatrix} -v \Delta \boldsymbol{v} - (\boldsymbol{b} \cdot \nabla) \boldsymbol{v} - \nabla q \\ -\nabla \cdot \boldsymbol{v} \end{pmatrix}.$$

Observe that if $\mathcal{L}_b^*(V_h|_K)$ has $L^2(K)$ regularity, then using $U_h'|_{\partial_K} = 0$ for all $K \in \mathcal{T}_h$ one has

$$\begin{split} & (\boldsymbol{M}\delta_{t}\boldsymbol{U}'^{,n},\boldsymbol{V}_{h}) + \langle \mathcal{L}_{\boldsymbol{b}}(\boldsymbol{U}'^{,n+\theta}),\boldsymbol{V}_{h}\rangle \approx \langle \mathcal{L}_{\boldsymbol{b}}(\boldsymbol{U}'^{,n+\theta}),\boldsymbol{V}_{h}\rangle \\ & = \langle \mathcal{L}_{\boldsymbol{b}}^{*}(\boldsymbol{V}_{h}),\boldsymbol{U}_{h}'^{,n+\theta}\rangle \\ & = \sum_{K \in \mathcal{T}_{+}} \left(\mathcal{L}_{\boldsymbol{b}}^{*}(\boldsymbol{V}_{h}),\boldsymbol{U}_{h}'^{,n+\theta}\right)_{K}, \end{split}$$

where $(M\delta_t U'^{,n}, V_h) = 0$, since $M\delta_t U'^{,n}$ is orthogonal to \mathbf{Z}_h . Also, observe that $\Pi_{\mathbf{Z}_h^{\perp}}(M\delta_t U_h^n) = \mathbf{0}$, since $M\delta_t U_h^n$ is a finite element function, and $\Pi_{\mathbf{Z}_h^{\perp}}(\mathbf{F}) = \mathbf{0}$, because of the hypotheses on \mathbf{F} .

These modeling steps lead to the discretized equations for U_h : Given U_h^n , find $U_h^{n+1} \in \mathbf{Z}_h$ such that

$$\left(\boldsymbol{M}\delta_{t}\boldsymbol{U}_{h}^{n},\boldsymbol{V}_{h}\right) + \left\langle \mathcal{L}_{\boldsymbol{b}}(\boldsymbol{U}_{h}^{n+\theta}),\boldsymbol{V}_{h}\right\rangle \\
- \left(\mathcal{L}_{\boldsymbol{b}}^{*}(\boldsymbol{V}_{h}),\Pi_{\boldsymbol{Z}_{h}^{\perp}}\left(\mathcal{L}_{\boldsymbol{b}}(\boldsymbol{U}_{h}^{n+\theta})\right)\right)_{\boldsymbol{\tau}_{t}} \\
= \left\langle \boldsymbol{F},\boldsymbol{V}_{h}\right\rangle - \left(\mathcal{L}_{\boldsymbol{b}}^{*}(\boldsymbol{V}_{h}),\boldsymbol{M}\frac{1}{\theta\Delta t}\boldsymbol{U}_{h}^{\prime,n}\right)_{\boldsymbol{\tau}_{t}}, \tag{69}$$

for all $V_h \in \mathbf{Z}_h$, where $(\cdot, \cdot)_{\tau_t}$ stands for the inner product defined by

$$(U,V)_{ au_t} = (au_t U,V)_{\Omega} = \sum_{K \in {\mathcal T}_h} au_{t,K}(U,V)_K.$$

In practice, as performed in Sect. 4.1, the stabilizations of velocity and pressure are decoupled. Hence, one considers a structure for the stabilization matrices as

$$oldsymbol{ au}_{t,K} = egin{pmatrix} au_{ ext{m},K}^t oldsymbol{I}_d & oldsymbol{0} \ oldsymbol{0}^T & au_{ ext{c},K} \end{pmatrix},$$

where $au^t_{\mathrm{m},K}, au_{\mathrm{c},K} \in \mathbb{R}$ respectively are stabilization coefficients for velocity and pressure, and $au^t_{\mathrm{m},K} = \left(\frac{1}{\theta \Delta t} + au^{-1}_{\mathrm{m},K}\right)^{-1}$. Then, the $(\cdot,\cdot)_{ au_t}$ inner product has the structure

$$(\boldsymbol{U}, \boldsymbol{V})_{\tau_t} = \sum_{K \in \mathcal{T}_h} \tau_{m,K}^t(\boldsymbol{u}, \boldsymbol{v})_K + \sum_{K \in \mathcal{T}_h} \tau_{c,K}(p, q)_K.$$
 (70)

Inserting (70) in (69) leads to the discretized resolved scale equations

$$(\delta_{t}\boldsymbol{u}_{h}^{n},\boldsymbol{v}_{h}) + a(\boldsymbol{u}_{h}^{n+\theta},\boldsymbol{v}_{h}) + b(\boldsymbol{b},\boldsymbol{u}_{h}^{n+\theta},\boldsymbol{v}_{h}) + (\nabla \cdot \boldsymbol{u}_{h}^{n+\theta},q_{h})$$

$$- (\nabla \cdot \boldsymbol{v}_{h},p_{h}^{n+\theta}) + (\Pi_{X_{h}^{\perp}}(\boldsymbol{b} \cdot \nabla \boldsymbol{u}_{h}^{n+\theta} + \nabla p_{h}^{n+\theta}),\boldsymbol{b} \cdot \nabla \boldsymbol{v}_{h}$$

$$+\nabla q_{h})_{\tau_{m}^{\prime}} + (\Pi_{Y_{h}^{\perp}}(\nabla \cdot \boldsymbol{u}_{h}^{n+\theta}),\nabla \cdot \boldsymbol{v}_{h})_{\tau_{c}}$$

$$= \langle \boldsymbol{f},\boldsymbol{v}_{h}\rangle + \frac{1}{\theta\delta t}(\boldsymbol{u}_{h}^{\prime,n},\boldsymbol{b} \cdot \nabla \boldsymbol{v}_{h} + \nabla q_{h})_{\tau_{m}^{\prime}}$$

$$(71)$$

for all $(v_h, q_h) \in X_h \times Y_h$, with obvious notation. Second order derivatives of finite element functions within element interiors have been neglected in (71). They are exactly zero for linear elements, and for higher order interpolations, disregarding them leads to a method which is still consistent, in a sense pointed out in [44, Remark 4].

Problem (71) is the effective OSS method used as VMS discretization of the transient Oseen equations, where $\Pi_{X_h^{\perp}} = I - \Pi_{X_h}$, $\Pi_{Y_h^{\perp}} = I - \Pi_{Y_h}$, being Π_{X_h} (resp., Π_{Y_h}) the orthogonal projection on space X_h (resp., Y_h) with respect to the inner product $(\cdot, \cdot)_{\tau_m^t}$ (resp., $(\cdot, \cdot)_{\tau_c}$). A possible alternative is to assume that the subscales do not change in time, and thus

$$oldsymbol{U}_h^{\prime,n+ heta} = oldsymbol{U}_h^{\prime,n} = - au \Pi_{oldsymbol{Z}_h^\perp}ig[\mathcal{L}_{oldsymbol{b}}(oldsymbol{U}_h^{n+ heta})ig],$$

with

$$oldsymbol{ au} = egin{pmatrix} au_{
m m} oldsymbol{I}_d & oldsymbol{0} \ oldsymbol{0}^T & au_{
m c} \end{pmatrix}.$$

This approach would lead to the same stabilization terms as for the stationary problem. Since this basic assumption consists of neglecting the temporal variation of the subscales, these latter are called quasi-static subscales in this context. For quasi-static subscales, the second term in the right-hand side of (71) disappears and there is no need to store $\boldsymbol{u}_h^{\prime,n}$. However, when the quasi-static assumption is not used (cf. [48]), subscales need to be tracked by the formula derived from (68)

$$oldsymbol{u}_h^{\prime,n+ heta} = au_m^t rac{1}{ heta A t} oldsymbol{u}_h^{\prime,n} - au_m^t (oldsymbol{I} - \Pi_{X_h}) (oldsymbol{b} \cdot
abla oldsymbol{u}_h^{n+ heta} +
abla p_h^{n+ heta}).$$

As for dynamic LES closures, the OSS approach with dynamic subscales allows to model backscatter, as shown in [47, 118].

The extension to the Navier–Stokes problem follows by considering $b = u^{n+\theta}$ in (71). A fixed point (or Picard) algorithm could be considered for linearization (i.e., the advection velocity is given by $b = u^{n+\theta,i-1}$), which leads to



a transient Oseen problem for the velocity $\boldsymbol{u}_h^{n+\theta,i}$ within each iteration step to which applies the previous formulation. However, there is an important remark to be made. When the unknown velocity is split into its finite element component and the subscale, this decomposition also affects the advection velocity \boldsymbol{b} , that is to say, one will have $\boldsymbol{b} = \boldsymbol{u}_h^{n+\theta,i-1} + \boldsymbol{u}_h'^{,n+\theta,i-1}$. This splitting implies that the velocity subscale not only need to be tracked in time, but also along the iterative process.

In the literature, the stabilization coefficients $\tau_{m,K}$, $\tau_{c,K}$ are computed by

- (a) Dimensional or convergence (a priori error) analysis (cf. [41–43]), or by
- (b) Fourier analysis (cf. [44, 46]),

being the dimensional analysis approach the simplest way to recover the expressions for $\tau_{m,K}, \tau_{c,K}$, by taking $\tau_K = F(v, h_K, ||\boldsymbol{b}||_{\infty,K})$, where F is a matrix function whose structure aims at equalizing the dimensions of all terms of the method (applied in a first stage to simplified equations, such as convection-diffusion equations). In the case (a), one obtains for $\tau_{m,K}$ the expression

$$\tau_{m,K} = \left(c_1 \frac{v}{h_K^2} + c_2 \frac{\|\boldsymbol{b}\|_{\infty,K}}{h_K}\right)^{-1},\tag{72}$$

while in the case (b), one obtains for $\tau_{m,K}$ the expression

$$\tau_{m,K} = \left[\left(c_1 \frac{v}{h_K^2} \right)^2 + \left(c_2 \frac{\|\boldsymbol{b}\|_{\infty,K}}{h_K} \right)^2 \right]^{-1/2}, \tag{73}$$

where (72) and (73) yield a similar structure that takes into account the local balance between convection and diffusion, and are asymptotically equivalent in $v, h_K, ||\boldsymbol{b}||_{\infty,K}$. In both case, one has

$$\tau_{c,K} = \frac{h_K^2}{c_1 \tau_{mK}}.\tag{74}$$

In expressions (72)–(74), c_1 , c_2 are positive algorithmic constants properly tuned (usually by an a priori error analysis). In most papers on OSS, it is recommended to take the values $c_1 = 4$, $c_2 = \sqrt{c_1} = 2$ for linear elements (a choice justified from the analysis of the one-dimensional convection-diffusion equation and from many numerical experiments), and use the same values of the algorithmic constants for quadratic elements, but taking h_K half the element size (roughly the distance between locations of the degrees of freedom of the element).

Remark 1 The above derivation of expression (68) for U'_h is based upon the assumption that the operator \mathcal{L}_b restricted to $\mathbf{Z}_h|_K$ is approximated by a diagonal operator. This

assumption has been justified for the convection-diffusion equation in [39].

5.2 Relations to Other Methods

The OSS method is strongly related to the two-scale residual-based VMS method developed in [10] and described in Sect. 4.1. Indeed, both are two-scale VMS methods which are residual-based (see [38, tions 11.1, 11.7.2]), that is the basic procedure is to keep all terms in the residual-driven structure of the resolved flow equations and to perform an approximated analytical element-wise solution of the small-scale flow. Thus, both methods are consistent methods, in the sense that the continuous solution exactly satisfies the discrete equations, whenever it is smooth enough. The two methods contain models for the Reynolds-stress and both cross-stress terms, in contrast to classical stabilization procedures such as SUPG for instance, that accounts for only one of the crossstress terms (see Sect. 4.2), thus making both methods powerful and efficient tools for the challenging computation of turbulent flows, specially in transient and nonequilibrium regimes. Moreover, these procedures do not make use of the statistical theory of equilibrium turbulence, and no ad-hoc eddy viscosity modeling is required for both methods. At this respect, it has been analyzed that one of the relevant features of the OSS method is that it introduces the right amount of numerical diffusion on the large scales which is asymptotically equivalent, as the Reynolds number increases, to the eddy viscosity dissipated by the unresolved scales (cf. [47, 70, 118]), given a sufficiently fine computational mesh with characteristic mesh cell size h in the inertial subrange of the studied (isotropic) turbulent flow.

One may note that the main difference between the two methods consists in the approximation of the unresolved scales. In the OSS method, only the orthogonal projection of the residual on the mean scales space is included. Indeed, if one considers the quasi-static version of the OSS method, the unresolved scales are approximated as

$$U' \approx \tau \Pi_h(\operatorname{Res}(U_h)),$$
 (75)

where $\Pi_h = \Pi_{\mathbf{Z}_h^{\perp}}$, while for the two-scale residual-based VMS method this approximation holds but with the essential difference $\Pi_h = I$, and thus

$$U' \approx \tau(\operatorname{Res}(U_h)).$$
 (76)

5.3 Numerical Analysis

A numerical analysis for the OSS method applied to the Navier–Stokes problem, with convection velocity split into



its finite element component and the subscale, is not available. The subgrid terms have a complex structure that includes convective interactions between large and small scales, thus setting serious technical problems just to prove stability. However, several results from the numerical analysis of the OSS method have been obtained for the convection-diffusion-reaction equations in [42], for the Oseen equations in [45, 48], and also for its extension to the steady linearized primitive equations of the ocean in [37], always in the context of uniformly regular grids.

In [42], the stability and error analysis of the OSS method for the advection-diffusion-reaction equations is performed, proving optimal error estimates. This analysis have been further extended to the (stationary) Oseen equations. In [45], it is shown that the OSS formulation adapted to the Oseen equations is stable and optimally convergent to smooth solutions under proper regularity assumptions on the advection velocity, and an adequate choice of the algorithmic parameters on which the method depends. Also a simple modification of the OSS method that introduces less coupling in the discrete velocity-pressure equations and possesses slightly better stability properties has been analyzed: the idea is to control separately the components of $\boldsymbol{b} \cdot \nabla \boldsymbol{u}_h$ and $\nabla p_h \tau_m$ -orthogonal to \boldsymbol{X}_h , that is to use a sort of "term-by-term" stabilization, which would lead to the stabilizing term

$$\begin{split} \left(\Pi_{X_h^{\perp}}(\boldsymbol{b} \cdot \nabla \boldsymbol{u}_h), \boldsymbol{b} \cdot \nabla \boldsymbol{v}_h \right)_{\tau_{\mathrm{m}}} + & \left(\Pi_{X_h^{\perp}}(\nabla p_h), \nabla q_h \right)_{\tau_{\mathrm{m}}'} \\ & + \left(\Pi_{Y_h^{\perp}}(\nabla \cdot \boldsymbol{u}_h), \nabla \cdot \boldsymbol{v}_h \right)_{\tau_{\mathrm{c}}} \end{split}$$

to be added to the standard Galerkin formulation, where the parameters τ_m and τ'_m could even be taken different. Dropping the orthogonal projections, this method reduces to a general version of the method analyzed in [32], which has a consistency error that makes it only applicable with P_1 finite elements. In any case, the numerical analysis is based upon specific discrete inf-sup conditions for the stabilized approximations, which allow the use of equal velocity-pressure interpolations and are essential for the stability of the methods. Also, optimal control on the streamline derivative of the velocity field is guaranteed. In [48], the stability analysis is extended to the transient Oseen equations with tracking in time of the subscales.

In [37], the extension of the analysis to the steady linearized primitive equations is performed, by also adding a convergence analysis. Optimal error estimates are obtained for smooth flows, again under proper regularity assumptions on the advection velocity. The performed analysis is an extension of the unified analysis of stabilized and mixed methods carried out for Stokes equations in [33]. The main contribution from the analytical point of view is the proof of a specific discrete inf-sup condition for the surface

pressure, that allows to estimate its L^2 norm in terms of the subgrid scales of the surface pressure gradient, that are specifically bounded by the OSS discretization.

5.4 Experience in Numerical Simulations

Numerical studies with OSS method applied to incompressible flows may be found in numerous publications. On the one hand, the numerical simulations were performed to test the optimal convergence rate of the method for smooth flows. On the other hand, the goal was to test the performance of the method in simulating turbulent flows. Different variants of the method were tested, depending on the following factors: Quasi-static or transient subscales, timestep dependency or not of the stabilization parameter, linear or nonlinear splitting of the convective velocity with respect to the subscales. Most of the comparisons were performed with respect to the algebraic subgrid scale method (ASGS), which consists in taking the subscales in the space of the residuals, and thus is equivalent to the twoscale residual based VMS method described in Sect. 4.1 when quasi-static subscales are used, the time-step dependency is included in the stabilization parameter, and the nonlinear scale splitting is applied in the finite element equation only, and not in the subscale equation. The numerical results highlighted the excellent accuracy of the OSS method in the simulation of turbulent incompressible flows.

In [44], the numerical examples presented, the classical cavity flow problem in two dimensions at Reynolds number Re = 5000 and the two-dimensional flow around a cylinder at Re = 100, aimed to demonstrate that the OSS method introduces less numerical diffusion than the ASGS method, while being equally stable. In particular, peaks were better captured. Likewise, in spite of the smaller amount of numerical diffusion, the evolution to the steady state was similar using the OSS and the ASGS method. Thus, the OSS can be considered as an alternative to reach steady states in a flow calculation. In general, considering transient subscales led to better results, both in terms of accuracy (with higher amplitudes and frequencies, that is, less numerical dissipation), and of stability, eliminating some pressure oscillations in time encountered when the subscales are considered quasi-static. However, if Δt is much larger than τ_m , it seemed to be not necessary to track the subscales in time, since considering them as quasi-static gave very similar results. It is also stated that, concerning the computational cost for transient calculations, the OSS formulation was very competitive with respect to the ASGS method, sometimes even cheaper, since less stabilizing terms appear. Moreover, these terms do not depend on the whole residual of the Navier-Stokes equations,



which in some situations may be expensive or very difficult to evaluate. Examples for such situations are the presence of thermal or electromagnetic couplings, Coriolis forces, and, above all, nonlinear viscosities, coming either from nonlinear constitutive models or from turbulence modeling.

The case of a turbulent flow over a cuboid-shaped surface was considered in [118]. A Reynolds number Re = 4500 based on the inflow velocity and obstacle height was considered. In this work, the OSS approach with transient subscales was implemented, and it was shown capable to predict backscatter, as just for dynamic LES models, mainly close to boundary and shear layers, where it is known it could appear. Also, the possibility to add a simple Smagorinsky model to the OSS formulation was considered. In this case, the numerical results showed that the numerical dissipation is of the same order as the subgrid dissipation introduced by adding the Smagorinsky model, except in the zone of strong anisotropy (boundary and shear layers), where the dissipation coming from adding the Smagorinsky model was higher than the numerical one. The numerical evidences obtained here have been also experienced and summarized in [47], where a more comprehensive comparison between the performance of the OSS discretization for fully developed turbulent flows with and without the Smagorinsky model was analyzed. In particular, two long term three-dimensional simulations, namely a flow over a plate and a telescope, were reported. The first example considers a flow over a circular plate supported on a column and inclined. It showed how the -7/3 slope of the Kolmogorov pressure spectrum was well approximated by the OSS method. The second example, the flow around a telescope, was intended to demonstrate that the OSS method is also applicable to real flow problems. This problem consists in the aerodynamic analysis around a building enclosing a large telescope, where modeling turbulence is crucial to determine the optical quality of the site where the telescope is placed. Again, the scientifically relevant issue is whether or not the OSS model is able to capture the inertial range of the Kolmogorov spectrum: it was observed that the pressure spectrum computed by using the OSS method displays the correct -7/3 slope without using the Smagorinsky model. The computation of some other relevant punctual statistics revealed, as expected, that results are more dissipative with the addition of the Smagorinsky model than without it.

Finally, an assessment of the OSS formulation modeling turbulent flows was performed in [49]. The OSS formulation was tested for the decay of homogeneous isotropic turbulence (DHIT), the Taylor–Green vortex (TGV) problem, and the turbulent channel flow (TCF). Thus, both bounded and unbounded flows are considered.

The DHIT problem consists in analyzing the statistics of the turbulent flow in a 3D box of size $\Omega=(0,2\pi)^3$ with periodic boundary conditions in all directions, which is started with a field having a predetermined energy spectrum. Structured meshed with N^3 linear, quadratic, and cubic hexahedral elements (Q_1,Q_2,Q_3) , respectively) were used, taking the mesh width h=1/32,1/64,1/128, so that the h-p refinement analysis is also performed, as in [10]. The viscosity value was set such that the associated Taylormicroscale Reynolds number is $\mathrm{Re}_{\lambda}=952$, which results in $v\approx 3.5\times 10^{-4}$.

The TGV problem aimed to show, in a relatively simple flow, the basic turbulence decay mechanisms like the turbulent energy cascade, the production of small eddies, and the enhancement of dissipation by the stretching of vortex lines. The computational domain is the unit cube with periodical boundary conditions. The initial flow generates 8 vortices with the same vortex scale. The problem is solved using Re = 1600. The same structured meshes and elements as in the DHIT problem were used. The TGV test is characterized by its laminar evolution at the initial time steps, when the flow is strongly anisotropic due to the structured large-scale vortices directly related to the initial condition. If the Reynolds number is large enough, the vortex-stretching process, which activates the energy cascade effect, transfers energy from large to small scales and the flow becomes unstable and turbulent. According to [23], the flow becomes nearly isotropic for Re > 1000.

The TCF problem consists of a fluid that flows between two parallel walls driven by an imposed pressure gradient which is defined by the Reynolds number based on the wall shear velocity, Re_{τ} . The attention was restricted to the cases $\text{Re}_{\tau} \in \{180, 395\}$. The problem was solved using the coarsest mesh from previous test, 32^3 linear hexahedral (Q_1) mesh cells, with refinement in the wall-normal direction following a hyperbolic function.

Overall, OSS and ASGS yielded similar results, all displaying the features of turbulent flows when reproducing global outputs such as energy spectra. These methods were stable and converged to reference solutions, both when the mesh was refined and when the polynomial order was increased. Further, the effect of small time steps when the stabilization parameters depend on them has been analyzed. Apart from the quality of the results, the OSS method with dynamic subscales was convenient in terms of numerical performance. It required more nonlinear iterations than ASGS, but less iterations of the linear solver, altogether leading to lower computational cost. This fact has been explained by plotting the number of solver iterations required to converge as the time step size is reduced, for a fixed mesh in space. The number of iterations (and as a result the condition number of the system matrix) blew up



exponentially for ASGS whereas it remained bounded for OSS. In both formulations, ASGS and OSS, the use of dynamic subscales has been found to be crucial for non-linear convergence. In fact, in some cases quasi-static subscales failed to converge.

All these numerical experiments suggest that the dynamic nonlinear OSS model turns out to be really highperforming in terms of efficiency and robustness, showing enormous potential in simulating turbulent flows, also with respect to purely classical LES model, such as the dynamic Smagorinsky model [52] or the adaptive local deconvolution model [76] specifically designed as an implicit LES model, when using a similar number of degrees of freedom. In particular, an excellent agreement with respect to DNS data was recovered on coarser meshes, in terms of total kinetic energy evolution, computation of energy spectra (-5/3 law), dissipation rate evolution, and specific statistics of first and second order (such as mean streamwise velocity, root mean square velocity fluctuations, Reynolds shear stress). The results also showed that the dynamic nonlinear OSS formulation results to be unconditionally stable when the skew-symmetric form of the convective term is used for the resolved scale equation.

To conclude this section, the high capability of the OSS method in modeling turbulence without any additional eddy viscosity term was pointed out, which is due to its intrinsic dissipative structure, which furnishes an additional argument in favor of the position to consider turbulence modeling a numerical issue.

6 Local Projection Stabilization (LPS) Methods as Two-Scale VMS Methods

Local Projection Stabilization (LPS) methods are stabilization methods that provide specific stabilization of any single operator term that could be a source of instability for the numerical discretization. They were introduced in [12] and they could be viewed as simplifications of the methods described in Sects. 4 and 5. LPS methods are not fully consistent, but are of optimal order with respect to the finite element interpolation. Moreover they are simpler to implement than residual-based methods.

6.1 Basic Ideas and Derivation

As a single rule, the structure of LPS method is achieved by retaining in the OSS method (69) the specific interactions that stabilize convection or pressure gradient, and by changing the global L^2 projection by local L^2 projections. This leads to a family of methods, associated to the choice of the actual local L^2 projection. The main derivation of

LPS methods will be introduced for the Oseen equations (60). The stabilization effect is achieved by adding least-squares terms that give a weighted control on the fluctuations of the quantity of interest. This control is based upon a projection operation $\pi_h: L^2(\Omega) \mapsto D_h$ into a discontinuous finite element space D_h (the "projection" space). This space is built on a grid \mathcal{M}_h formed by macro-elements built from the grid \mathcal{T}_h . The component-wise extension of π_h to vector functions is denoted by π_h . The LPS approximation of the Oseen equations reads: Find $(\boldsymbol{u}_h, p_h) \in \boldsymbol{X}_h \times Y_h$ such that for any $(\boldsymbol{v}_h, q_h) \in \boldsymbol{X}_h \times Y_h$,

$$A((\boldsymbol{u}_h, p_h), (\boldsymbol{v}_h, q_h)) + S_h((\boldsymbol{u}_h, p_h), (\boldsymbol{v}_h, q_h)) = \langle \boldsymbol{f}, \boldsymbol{v}_h \rangle,$$
(77)

where

$$A((\boldsymbol{u}_h, p_h), (\boldsymbol{v}_h, q_h)) = v(\nabla \boldsymbol{u}_h, \nabla \boldsymbol{v}_h) + (\boldsymbol{b} \cdot \nabla \boldsymbol{u}_h + c \, \boldsymbol{u}_h, \, \boldsymbol{v}_h) - (\nabla \cdot \boldsymbol{v}_h, p_h) + (\nabla \cdot \boldsymbol{u}_h, q_h),$$

and

$$S_{h}((\boldsymbol{u}_{h}, p_{h}), (\boldsymbol{v}_{h}, q_{h})) = \sum_{M \in \mathcal{M}_{h}} \tau_{M} (\boldsymbol{\kappa}_{h}(\boldsymbol{b} \cdot \nabla \boldsymbol{u}_{h}), \boldsymbol{\kappa}_{h}(\boldsymbol{b} \cdot \nabla \boldsymbol{v}_{h}))_{K} + \sum_{M \in \mathcal{M}_{h}} \mu_{M} (\boldsymbol{\kappa}_{h}(\nabla p_{h}), \boldsymbol{\kappa}_{h}(\nabla q_{h}))_{K}.$$

$$(78)$$

Here, $\kappa_h = I - \pi_h$ is the "fluctuation" operator, while τ_M and μ_M are stabilization coefficients. Additional terms stabilizing (for instance) the discretization of the divergence (grad-div term) can be added.

The stability of LPS methods is based upon local inf-sup conditions (see Sect. 6.2 below): The local restriction $X_h(M)$ of the velocity space X_h (the "approximation" space) to any macro-element $M \in \mathcal{M}_h$ must be rich enough in degrees of freedom with respect to $D_h(M)$, much as in mixed methods the global velocity space X_h must be rich enough with respect to the pressure space Y_h to achieve the discrete inf-sup condition (9). With this purpose, two main approaches of LPS methods have been proposed (see [73]): In the one-level approach, the approximation space is enriched such that the local inf-sup condition holds and both X_h and D_h are built on the same mesh. In the twolevel approach, the projection space is built on a coarser mesh level to satisfy the local inf-sup condition. It is possible to consider overlapping sets of macro elements (see [13]).

6.2 Numerical Analysis

In [115], a general stability and convergence theory of LPS schemes for the Oseen equations is given, see also [124, Part IV,Sections 4 and 5] for a comprehensive



presentation. A priori error estimates were obtained, with the same optimal order of convergence as for the SUPG/PSPG method. The key idea in the error analysis of the local projection scheme is the construction of an interpolant into X_h which exhibits an additional orthogonality property with respect to the discontinuous space D_h . To describe this analysis to some extent, assume that the discrete velocity and pressure spaces are built as $X_h = \left[H_0^1(\Omega)\right]^d \cap Z_h^d$, $Y_h = L_0^2(\Omega) \cap Z_h$, where Z_h is a standard finite element space of polynomial order r without containing essential boundary conditions. The following assumptions are assumed to hold:

Assumption A1 There exists an interpolation operator $i_h: H^1(\Omega) \mapsto Z_h$ such that $i_h: H^1_0(\Omega) \mapsto Z_h \cap H^1_0(\Omega)$, and for all $w \in H^l(M)$, $M \in \mathcal{M}_h$

$$||w - i_h w||_{0,M} + h_M |w - i_h w|_{1,M} \le C h_M^l |w|_{l,\omega(M)},$$

$$1 \le l \le r + 1,$$
(79)

on a suitable patch $\omega(M) \supset M$.

Assumption A2 The fluctuation operator $\kappa_h = I - \pi_h$ satisfies

$$\|\kappa_h q\|_{0,M} \le C h_M^l |q|_{l,M} \quad \forall \ q \in H^l(M), \ \forall \ M \in \mathcal{M}_h,$$

 $0 \le l \le r.$

Assumption A3 There is a positive constant β such that the local inf-sup condition

$$\inf_{q_h \in D_h(M)} \sup_{v_h \in Z_h(M)} \frac{\left(v_h, q_h\right)_M}{\left\|v_h\right\|_{0,M} \left\|q_h\right\|_{0,M}} \ge \beta \quad \forall \ M \in \mathcal{M}_h, h > 0$$

holds, where
$$D_h(M) := \{d_h|_M : d_h \in D_h\}$$
 and $Z_h(M) := \{w_h|_M : w_h \in Z_h\}.$

Assumptions A1 and A3 ensure stability of the LPS discretization (77), in the sense that if $\max\{v, c, \tau_M, h_M^2/\mu_M\} \leq C$ for all $M \in \mathcal{M}_h$, then, there is a constant $\gamma > 0$ independent of v and h such that

$$\inf_{(\boldsymbol{v}_h,q_h)\in\boldsymbol{X}_h\times\boldsymbol{Y}_h}\sup_{(\boldsymbol{w}_h,r_h)\in\boldsymbol{X}_h\times\boldsymbol{Y}_h}\frac{(A+S_h)((\boldsymbol{v}_h,q_h)(\boldsymbol{w}_h,r_h))}{||(\boldsymbol{v}_h,q_h)||_h||(\boldsymbol{w}_h,r_h)||_h}\geq\gamma,$$

where the $||\cdot||_h$ denotes the grid-dependent norm

$$||(\mathbf{v},q)||_{h} := [\mathbf{v} \, |\mathbf{v}|_{1} + c \, ||\mathbf{v}||_{0} + (\mathbf{v}+c) \, ||q||_{0} + S_{h}((\mathbf{v},q),(\mathbf{v},q))]^{1/2}.$$

Optimal error estimates are obtained under assumptions A1, A2 and A3: Assuming that the solution (\boldsymbol{u},p) of the Oseen equations (60) belongs to $[H_0^1(\Omega)\cap H^{r+1}(\Omega)]^d\times L_0^2(\Omega)\cap H^{r+1}(\Omega)$, the choice of stabilization parameters $\tau_M\simeq h_M/\|\boldsymbol{b}\|_{r,\infty,M}$ and $\mu_M\simeq h_M$ is asymptotically optimal and leads to

$$\begin{aligned} &||(\boldsymbol{u},p) - (\boldsymbol{u}_h,p_h)||_h \\ &\leq C \left(\sum_{M \in \mathcal{M}_h} (v + h_M) \, h_M^{2r} \left(\|\boldsymbol{u}\|_{r+1,\omega(M)}^2 + \|p\|_{r+1,\omega(M)}^2 \right) \right)^{1/2}. \end{aligned}$$

The key for the proof of this result is the existence of an interpolation operator $j_h: H^1(\Omega) \mapsto Z_h$ satisfying the following orthogonality and approximation properties:

$$(w - j_h w, q_h) = 0 \quad \forall \ q_h \in D_h, \ w \in H^1(\Omega),$$
$$\|w - j_h w\|_{0,M} + h_M |w - j_h w|_{1,M} \le C h_M^l \|w\|_{l,\omega(M)}$$
$$\forall \ w \in H^l(\Omega).$$

with $1 \le l \le r + 1$, for all $M \in \mathcal{M}_h$, where $\omega(M)$ is the union of all elements of \mathcal{M}_h that intersect M. The existence of such an interpolation operator turns out to be a consequence of Assumptions 1 and 3.

Assumptions A1 and A2 are standard in finite element approximations, and are satisfied by well-known families of them. However, the local inf-sup condition required by A3 is less standard. Several families of finite element spaces satisfying this assumption may be found in references [12, 13, 73, 115], among others.

Recently, extensions of the analysis of LPS methods to the instationary Navier–Stokes equations have been developed. In [4], the case of inf-sup stable pairs of finite element spaces was considered, where the second term in S_h from (78) can be neglected. In addition, a grad-div stabilization term (58) was introduced in the discrete problem. For the continuous-in-time case, error estimates were proved with constants that do not depend on inverse powers of v. To obtain this property, the grad-div term played an essential role. The analysis was extended in [3, 5] to fully discrete problems with BDF2 as temporal discretization and a decoupling of velocity and pressure computation via a pressure projection scheme.

6.3 LPS by Interpolation

A further simplification of LPS schemes is achieved when the local L^2 projection operator π_h is replaced by an interpolation operator from $[L^2(\Omega)]^d$ onto a projection space \mathbf{D}_h formed by continuous finite elements (see [34]). To describe this approach, assume that the discrete velocity and pressure spaces X_h and Y_h are formed by piecewise polynomial functions of degree l at most

$$X_h = (V_h^l(\Omega) \cap H_0^1(\Omega))^d, \quad Y_h = V_h^l(\Omega) \cap L_0^2(\Omega), \tag{80}$$

where $V_h^l = P_l$ on simplices and $V_h^l = Q_l$ on quadrilaterals or hexahedra. It is assumed that π_h is some stable approximation operator from $[L^2(\Omega)]^d$ into $\mathbf{D}_h = \left[V_h^{l-1}(\Omega)\right]^d$. This interpolant may be defined as



$$\forall x \in \overline{\Omega}, \, \pi_h(\mathbf{v})(x) = \sum_{a \in \mathcal{N}} \Pi_h(\mathbf{v})(a) \varphi_a(x), \tag{81}$$

where \mathcal{N} is the set of Lagrange interpolation nodes of $V_h^l(\Omega)$, φ_a are the Lagrange basis functions associated to \mathcal{N} and Π_h is some interpolation operator by local averaging of Scott–Zhang or Clément kind. $\Pi_h(\mathbf{v})(a)$ may be reduced to a single nodal value if \mathbf{v} is piecewise smooth. The fluctuation operator $\mathbf{\kappa}_h = \mathbf{I} - \mathbf{\pi}_h$ satisfies also the following extension of Assumption 2: There exists a constant C_p , independent of h, such that

$$\forall \mathbf{v}_h \in [W^{l,p}(\Omega)]^d, \forall K \in \mathcal{T}_h, |\mathbf{\kappa}_h(\mathbf{v}_h)|_{r,p,K} \leq C_p h_K^{l-r} |\mathbf{v}_h|_{l,p,\omega(K)},$$
(82)

for $r = \{0,1\}$, $1 \le p \le +\infty$, $r \le l$. These two assumptions are verified by quasi-local approximation operators such as the Girault–Lions [61], Bernardi–Maday–Rapetti [16], or Scott–Zhang [129] type operators and local L^2 interpolation operators such as those considered in standard LPS methods [115]. The LPS method by interpolation is still stated by (77), but assuming that the grids \mathcal{T}_h and \mathcal{M}_h coincide.

The stability of this LPS method by interpolation follows from a specific inf-sup condition, that will be stated, for simplicity, for uniformly regular grids. That is, there exist two positive constants C_1 and C_2 such that

$$C_1 h < h_K < C_2 h$$
, $\forall K \in \mathcal{T}_h$, $\forall h > 0$.

Lemma 2 Assume that the family of grids is uniformly regular. Then, the following inf-sup condition holds

$$\forall q_{h} \in Y_{h}, \|q_{h}\|_{0} \leq C \left(\sup_{\mathbf{v}_{h} \in \mathbf{X}_{h}} \frac{(\nabla \cdot \mathbf{v}_{h}, q_{h})}{|\mathbf{v}_{h}|_{1}} + h \|\mathbf{\kappa}_{h}(\nabla q_{h})\|_{0} \right). \tag{83}$$

Proof The proof is based upon an inf-sup condition, which is the global equivalent of the local inf-sup conditions of LPS methods (Assumption 3), that is stated without proof

$$\forall g_h \in V_h^{l-1}(\Omega), \|g_h\|_0 \le C \sup_{\nu_h \in V_h^l(\Omega) \cap H_0^1(\Omega)} \frac{(\nu_h, g_h)}{\|\nu_h\|_0}. \tag{84}$$

As $\pi_h(\nabla q_h) \in \left[V_h^{l-1}\right]^d$, the inf-sup condition (84) yields

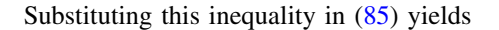
$$\|\pi_h(\nabla q_h)\|_0 \le C \sup_{\nu_h \in X_h} \frac{(\pi_h(\nabla q_h), \nu_h)}{\|\nu_h\|_0}.$$
 (85)

As $\kappa_h = \mathbf{I} - \pi_h$, it follows that

$$|(\boldsymbol{\pi}_h(\nabla q_h), \boldsymbol{\nu}_h)| \le |(\nabla q_h, \boldsymbol{\nu}_h)| + ||\boldsymbol{\kappa}_h(\nabla q_h)||_0 ||\boldsymbol{\nu}_h||_0.$$

With the inverse estimate (14), one finds

$$h \sup_{\mathbf{v}_h \in X_h} \frac{(\pi_h(\nabla q_h), \mathbf{v}_h)}{\|\mathbf{v}_h\|_0} \leq C \left(\sup_{\mathbf{v}_h \in X_h} \frac{(\nabla q_h, \mathbf{v}_h)}{|\mathbf{v}_h|_1} + h \|\mathbf{\kappa}_h(\nabla q_h)\|_0 \right).$$



$$h \|\boldsymbol{\pi}_h(\nabla q_h)\|_0 \le C \left(\sup_{\boldsymbol{\nu}_h \in \boldsymbol{X}_h} \frac{(\nabla \cdot \boldsymbol{\nu}_h, q_h)}{|\boldsymbol{\nu}_h|_1} + h \|\boldsymbol{\kappa}_h(\nabla q_h)\|_0 \right).$$
(86)

By [139], there exist two positive constants C_1 and C_2 independent of h such that

$$\forall q_h \in Y_h, \quad C_1 \|q_h\|_0 \le \sup_{\mathbf{v}_h \in X_h} \frac{(\nabla \cdot \mathbf{v}_h, q_h)}{|\mathbf{v}_h|_1} + C_2 h \|\nabla q_h\|_0.$$
(87)

Since $\|\nabla q_h\|_0 \le \|\kappa_h(\nabla q_h)\|_0 + \|\pi_h(\nabla q_h)\|_0$, combining (86) and (87) completes the proof. \square

The inf-sup condition (83) is the basis for the stability of the method as stated in the following theorem.

Theorem 2 Assume that the grids are uniformly regular, $f \in [L^2(\Omega)]^d$, $b \in [L^r(\Omega)]^d$ for some r > d and the stabilized coefficients τ_K and μ_K are of order h_K^2 . Then the discrete problem (77) has a unique solution. Moreover, there exists a constant C > 0, independent of h and v, such that

$$v|\mathbf{u}_h|_1 + \sqrt{v} S_h((\mathbf{u}_h, p_h), (\mathbf{u}_h, p_h))^{1/2} \le ||\mathbf{f}||_{-1},$$
 (88)

$$||p_h||_0 \le C \left(1 + \frac{1}{\sqrt{\nu}} + \frac{||\boldsymbol{b}||_{0,r}}{\sqrt{\nu}} + \frac{||\boldsymbol{b}||_{0,r}}{\nu} + c\right) ||\boldsymbol{f}||_0.$$
 (89)

Proof Problem (77) is equivalent to a square linear system of dim X_h + dim Y_h equations. Hence uniqueness of the solution is equivalent to its existence. So one can proceed assuming that there exists a solution and prove that it is unique. And to prove this, it is enough to prove estimates (88) and (89). It is assumed for brevity that c = constant > 0.

1) Setting $v_h = u_h$ and $q_h = p_h$ in (77) gives

$$v |\mathbf{u}_h|_1^2 + c ||\mathbf{u}_h||_0^2 + S_h((\mathbf{u}_h, p_h), (\mathbf{u}_h, p_h)) = \langle \mathbf{f}, \mathbf{u}_h \rangle.$$

Then, it follows that

$$|\mathbf{u}_{h}|_{1} \leq \frac{1}{v} \|\mathbf{f}\|_{-1}, \|\mathbf{u}_{h}\|_{0} \leq \frac{1}{c} \|\mathbf{f}\|_{0}, S_{h}((\mathbf{u}_{h}, p_{h}), (\mathbf{u}_{h}, p_{h})) \leq \frac{1}{4v} \|\mathbf{f}\|_{-1}^{2}.$$

$$(90)$$

2) To obtain the pressure estimate, the inf-sup condition (83) is used

$$C\|p_h\|_0 \leq \sup_{\mathbf{v}_h \in X_h} \frac{(\nabla \cdot \mathbf{v}_h, p_h)}{|\mathbf{v}_h|_1} + h \|\mathbf{\kappa}_h(\nabla p_h)\|_0 := I + II.$$

As $\mu_K \simeq h^2$, the second term is bounded by

$$|II| \le S_h((\boldsymbol{u}_h, p_h), (\boldsymbol{u}_h, p_h))^{1/2} \le \frac{C}{\sqrt{\nu}} ||\boldsymbol{f}||_{-1}.$$



To bound the first term, take $q_h = 0$ in (77), leading to

$$(\nabla \cdot \mathbf{v}_{h}, p_{h}) = (\mathbf{b} \cdot \nabla \mathbf{u}_{h}, \mathbf{v}_{h}) + v(\nabla \mathbf{u}_{h}, \nabla \mathbf{v}_{h}) + c(\mathbf{u}_{h}, \mathbf{v}_{h}) + \sum_{K \in \mathcal{T}_{h}} \tau_{K}(\mathbf{\kappa}_{h}(\mathbf{b} \cdot \nabla \mathbf{u}_{h}), \mathbf{\kappa}_{h}(\mathbf{b} \cdot \nabla \mathbf{v}_{h}))_{K} - \langle \mathbf{f}, \mathbf{v}_{h} \rangle.$$

$$(91)$$

Due to the third estimate in (90), the stabilizing term has the bound

$$\left| \sum_{K \in \mathcal{T}_{h}} \tau_{K}(\boldsymbol{\kappa}_{h}(\boldsymbol{b} \cdot \nabla \boldsymbol{u}_{h}), \boldsymbol{\kappa}_{h}(\boldsymbol{b} \cdot \nabla \boldsymbol{v}_{h}))_{K} \right|$$

$$\leq \frac{C}{\sqrt{\nu}} \|\boldsymbol{f}\|_{-1} \|\boldsymbol{\kappa}_{h}(\boldsymbol{b} \cdot \nabla \boldsymbol{v}_{h})\|_{\tau},$$

$$(92)$$

where for
$$r\in L^2(\Omega),\ \|r\|_{\tau}=\left(\sum_{K\in\mathcal{T}_h}\tau_K\|r\|_{0,K}^2\right)^{1/2}.$$
 The

support of the P_1 basis functions associated to the grid \mathcal{T}_h

is denoted by
$$\mathcal{O}_i$$
, $i = 1, ..., R$. Then, $\overline{\Omega} = \bigcup_{i=1}^{R} \mathcal{O}_i$, and any

mesh cell $K \in \mathcal{T}_h$ belongs to at most m macroelements \mathcal{O}_i , for some m independent of h. This property follows from the regularity of the family of grids. Then, one gets

$$\|\boldsymbol{\kappa}_h(\boldsymbol{b}\cdot\nabla\boldsymbol{\nu}_h)\|_{\tau}^2 \leq C h^2 \sum_{i=1}^R \|\boldsymbol{\kappa}_h(\boldsymbol{b}\cdot\nabla\boldsymbol{\nu}_h)\|_{0,\mathcal{O}_i}^2.$$
 (93)

As π_h is locally stable and $\boldsymbol{b} \in [L^r(\Omega)]^d$, r > d, it follows that

$$\|\mathbf{\kappa}_{h}(\mathbf{b} \cdot \nabla \mathbf{v}_{h})\|_{\tau}^{2} \leq C h^{2} \sum_{i=1}^{R} \sum_{K \subset \mathcal{O}_{i}} \|\mathbf{b} \cdot \nabla \mathbf{v}_{h}\|_{0,\omega(K)}^{2}$$

$$\leq C h^{2} \sum_{i=1}^{R} \sum_{K \subset \mathcal{O}_{i}} \|\mathbf{b}\|_{0,r,\omega(K)}^{2} \|\nabla \mathbf{v}_{h}\|_{0,r^{*},\omega(K)}^{2},$$

with $1/r + 1/r^* = 1/2$. Due to the uniform regularity of the grids, the inverse estimate

$$\forall K \in \mathcal{T}_h, \forall p \in P_l(K), \|p\|_{0,r^*,K} \le \hat{C} h^{d/r^* - d/2} \|p\|_{0,K}$$

holds. Then,
$$\|\nabla \nu_h\|_{0,r^*,\omega(K)}^2 \le \hat{C} \, h^{2d/r^*-d} \sum_{T \subset \omega(K)} \|\nabla \nu_h\|_{0,T}^2$$

and therefore one obtains the following estimate

$$\|\boldsymbol{\kappa}_{h}(\boldsymbol{b}\cdot\nabla\boldsymbol{v}_{h})\|_{\tau}^{2} \leq C h^{2(1-d/r)} \sum_{i=1}^{R} \sum_{K\subset\mathcal{O}_{i}} \|\boldsymbol{b}\|_{0,r,\omega(K)}^{2} \|\nabla\boldsymbol{v}_{h}\|_{0,\omega(K)}^{2}$$
$$\leq C h^{2(1-d/r)} \|\boldsymbol{b}\|_{0,r}^{2} \|\nabla\boldsymbol{v}_{h}\|_{0}^{2},$$

where it was used that a mesh cell belongs to at most m macroelements. Combining the last inequality with (92) gives

$$\left| \sum_{K \in \mathcal{T}_h} \tau_K(\boldsymbol{\kappa}_h(\boldsymbol{b} \cdot \nabla \boldsymbol{u}_h), \boldsymbol{\kappa}_h(\boldsymbol{b} \cdot \nabla \boldsymbol{v}_h))_K \right|$$

$$\leq \frac{C}{\sqrt{\nu}} h^{1-d/r} ||\boldsymbol{f}||_{-1} ||\boldsymbol{b}||_{0,r} ||\nabla \boldsymbol{v}_h||_{0}.$$

To bound the remaining terms in (91), one uses (90)

$$|(\boldsymbol{b} \cdot \nabla \boldsymbol{u}_{h}, \boldsymbol{v}_{h}) + v (\nabla \boldsymbol{u}_{h}, \nabla \boldsymbol{v}_{h}) + c (\boldsymbol{u}_{h}, \boldsymbol{v}_{h}) - \langle \boldsymbol{f}, \boldsymbol{v}_{h} \rangle|$$

$$\leq C \Big((v + \|\boldsymbol{b}\|_{0,r}) |\boldsymbol{u}_{h}|_{1} + c \|\boldsymbol{f}\|_{0} + \|\boldsymbol{f}\|_{-1} \Big) |\boldsymbol{v}_{h}|_{1}$$

$$\leq C \Big(1 + \frac{\|\boldsymbol{b}\|_{0,r}}{v} + c \Big) \|\boldsymbol{f}\|_{0} |\boldsymbol{v}_{h}|_{1}.$$

Finally, by substituting the two last inequalities into (91) one obtains

$$|I| \le C \left(1 + \frac{\|\boldsymbol{b}\|_{0,r}}{\sqrt{v}} + \frac{\|\boldsymbol{b}\|_{0,r}}{v} + c \right) \|\boldsymbol{f}\|_{0}. \tag{94}$$

Combining the estimates for I and II with the inf-sup condition (84) one deduces (89). \square

The error estimates are based upon this stability result, and the approximation properties of operator π_h . The proof will be omitted for brevity.

Theorem 3 Assume that the hypotheses of Theorem 2 hold, that the operator π_h satisfies (82), that $\mathbf{b} \in [H^s(\Omega)]^d$ with s > l - 1 and that the solution of the Oseen problem (60) verifies $(\mathbf{u}, p) \in [H^{l+1}(\Omega)]^d \times H^l(\Omega)$. Then the following error estimates hold:

$$|\mathbf{u} - \mathbf{u}_h|_1 \le C(\|\mathbf{b}\|_c, \|\mathbf{f}\|_0, \mathbf{v}) h^l,$$
 (95)

$$||p - p_h||_0 < C(||\boldsymbol{b}||_c, ||\boldsymbol{f}||_0, v) h^l,$$
 (96)

where $C(\|\boldsymbol{b}\|_s, \|\boldsymbol{f}\|_0, v)$ is a constant depending on $\|\boldsymbol{b}\|_s$, $\|\boldsymbol{f}\|_0$ and v that grows as $1/\sqrt{v}$.

These stability and error estimates also hold for general regular grids (not uniformly regular), although the proof is much more involved (see [34]). Moreover, in [1], a finite element error analysis of the LPS method by interpolation for the time-dependent Navier–Stokes equations is presented.

6.4 Application to the Simulation of Turbulent Flows

A finite element three-scales projection-based VMS-LPS steady turbulence model that includes general non-linear wall laws is presented in [36, 125]. Good accuracy is obtained with benchmark turbulent flow problems on coarse grids. This is a model with the structure (34) that includes a multi-scale Smagorinsky modeling of the eddy



viscosity, which contains the restriction to the sub-filter scales through a projection/interpolation operator (introduced in Sect. 3.2), and a LPS by interpolation stabilization of convection and pressure gradient, in order to use the same interpolation for velocity and pressure. In addition, it includes wall-laws modeling of the turbulent boundary layer. This provides a discretization with a reduced computational cost, but that keeps the same high-order accuracy with respect to standard projection-stabilized methods. This model is presented here without wall-laws for brevity. The numerical experiences with this model are presented in Sect. 10.5.

Consider the steady version of the Navier-Stokes equations (2): Find $(\mathbf{u},p) \in X \times Y$ such that for all $(\mathbf{v},q) \in X \times Y$

$$a(\mathbf{u}, \mathbf{v}) + b(\mathbf{u}, \mathbf{u}, \mathbf{v}) - (\nabla \cdot \mathbf{v}, p) = \langle \mathbf{f}, \mathbf{v} \rangle, (\nabla \cdot \mathbf{u}, q) = 0.$$
(97)

These equations are discretized by approximating the spaces X and Y by the spaces X_h and Y_h defined by (80), and the variational formulation by: Find $(\mathbf{u}_h, p_h) \in X_h \times Y_h$ such that:

$$a(\mathbf{u}_{h}, \mathbf{v}_{h}) + b_{s}(\mathbf{u}_{h}, \mathbf{u}_{h}, \mathbf{v}_{h}) - (p_{h}, \nabla \cdot \mathbf{v}_{h}) + c(\mathbf{u}_{h}; \mathbf{u}_{h}, \mathbf{v}_{h}) + s_{\text{conv}}(\mathbf{u}_{h}; \mathbf{u}_{h}, \mathbf{v}_{h}) = \langle \mathbf{f}, \mathbf{v}_{h} \rangle,$$

$$(\nabla \cdot \mathbf{u}_{h}, q_{h}) + s_{\text{pres}}(p_{h}, q_{h}) = 0,$$
(98)

for any $(v_h, q_h) \in X_h \times Y_h$.

The trilinear form b_s is the skew-symmetric one of the convection form b given in (7). The use of b_s instead of b is needed to keep a correct energy balance at the discrete level, that follows as $b_s(u_h, v_h, v_h) = 0$.

The form c is associated to the VMS-Smagorinsky modeling of the eddy viscosity (35)

$$c(\mathbf{u}_h; \mathbf{u}_h, \mathbf{v}_h) = 2(\mathbf{v}_{\mathsf{T}}(\widehat{\mathbf{u}}_h) \mathbb{D}(\widehat{\mathbf{u}}_h), \mathbb{D}(\widehat{\mathbf{v}}_h)), \tag{99}$$

where the eddy viscosity v_T is defined by (36)

$$v_{\mathrm{T}}(\mathbf{v})(\mathbf{x}) = (C_{S}h_{K})^{2} \|\mathbb{D}(\mathbf{v}|_{K})(\mathbf{x})\|_{\mathrm{F}} \quad \text{for } \mathbf{x} \in \mathrm{K},$$

and

$$\widehat{\boldsymbol{u}}_h = \boldsymbol{\rho}_h^* \boldsymbol{u}_h, \quad \widehat{\boldsymbol{v}}_h = \boldsymbol{\rho}_h^* \boldsymbol{v}_h, \quad \boldsymbol{\rho}_h^* = \boldsymbol{I} - \boldsymbol{\rho}_h,$$

Here, ρ_h is a uniformly stable (in $H^1(\Omega)$ -norm) interpolation operator (the "restriction" operator) on \widehat{X}_h , where

$$\widehat{X}_h = \left[V_h^{l-1}(\Omega) \right]^d, \tag{100}$$

or

$$\widehat{X}_h = \left[V_H^l(\Omega) \right]^d, \tag{101}$$

and $V_H^l(\Omega)$ in (101) is a sub-space of $V_h^l(\Omega)$ with larger grid size H > h (typically, H = 2h or H = 3h). The restriction operator ρ_h must be uniformly bounded with respect to h,

satisfy optimal error estimates (79), and preserve the slip boundary conditions. In the framework of Sect. 3.2, the large scales space is given by

$$\overline{X}_h = (I - \rho_h)X_h,$$

However neither the space \overline{X}_h nor \widehat{X}_h appears in the discretization, only the restriction operator ρ_h is needed.

In this way, this VMS method appears as a LES method where the cutoff length δ is of the same order as the grid size h. This size of the cutoff length is reasonable as setting $\delta \gg h$ then the numerical solution would solve scales much smaller than the modeled ones, while setting $\delta \ll h$ would generate a large error in the computation of the modeled scales.

The forms s_{conv} and s_{pres} in (98) correspond to a LPS method, given by

$$s_{\text{conv}}(\boldsymbol{u}_h; \boldsymbol{u}_h, \boldsymbol{v}_h) = \sum_{K \in \mathcal{T}_h} \tau_{m,K}(\boldsymbol{\sigma}_h^*(\boldsymbol{u}_h \cdot \nabla \boldsymbol{u}_h), \boldsymbol{\sigma}_h^*(\boldsymbol{u}_h \cdot \nabla \boldsymbol{v}_h))_K,$$

$$s_{\text{pres}}(p_h, q_h) = \sum_{K \in \mathcal{T}_h} \tau_{c,K}(\boldsymbol{\sigma}_h^*(\nabla p_h), \boldsymbol{\sigma}_h^*(\nabla q_h))_K.$$

Here, $\sigma_h^* = I - \sigma_h$, where σ_h is some locally stable (in the L^2 norm) projection or interpolation operator on the projection space $\mathbf{D}_h = \left[V_h^{l-1}(\Omega)\right]^d$, satisfying optimal error estimates, similarly to operator π_h given by (81). Also, $\tau_{m,K}$ and $\tau_{c,K}$ are stabilization coefficients for convection and pressure gradient, respectively, given by

$$\tau_{c,K} = \tau_{m,K} = \left\{ \left[c_1 \frac{v + \overline{v}_{T}|_K}{(h_K/l)^2} \right] + \left[c_2 \frac{U_K}{(h_K/l)} \right] \right\}^{-1}, \quad (102)$$

by adapting the expressions (72), where $\overline{v}_T|_K$ is the local mean value for the eddy viscosity on the mesh cell K, and U_K is the mean speed on K.

Model (98) includes the main features and assumptions of a three-scale VMS method. The method is based on a variational formulation and the decomposition of the scales is defined by projection in the large-scales space \overline{X}_h . The turbulence model is applied only to the small resolved scales.

Here, the steady version will be considered while the unsteady one will be studied in Sect. 10. This model has a relatively simple structure as a turbulence model. It may be programmed with ease from an existing finite element solver for Navier–Stokes equations. The main difficulty is the computation of the interpolation operators that appear in the stabilizing and eddy diffusion terms, but it may simply be computed from point wise values of the functions to interpolate, as was mentioned in Sect. 6.3.

The existence of solutions of model (98) is based upon a linearization of the model equations: Given $w_h \in X_h$, find $(z_h, r_h) \in X_h \times Y_h$ such that



$$a(\mathbf{z}_{h}, \mathbf{v}_{h}) + b_{s}(\mathbf{w}_{h}, \mathbf{z}_{h}, \mathbf{v}_{h}) - (r_{h}, \nabla \cdot \mathbf{v}_{h}) + c(\mathbf{w}_{h}; \mathbf{z}_{h}, \mathbf{v}_{h}) + s_{\text{conv}}(\mathbf{w}_{h}; \mathbf{z}_{h}, \mathbf{v}_{h}) = \langle \mathbf{f}, \mathbf{v}_{h} \rangle,$$

$$(\nabla \cdot \mathbf{z}_{h}, q_{h}) + s_{\text{pres}}(r_{h}, q_{h}) = 0,$$

$$(103)$$

for any $(v_h, q_h) \in X_h \times Y_h$. The mapping $w_h \in X_h \mapsto z_h \in X_h$ admits a fixed point by Brouwer's Fixed Point Theorem which is the solution of model (98). This follows from the stability estimates (that are stated here just for the solution of (98)):

$$v \| \mathbb{D}(\boldsymbol{u}_{h}) \|_{0} + c(\boldsymbol{u}_{h}; \boldsymbol{u}_{h}, \boldsymbol{u}_{h}) + s_{\text{conv}}(\boldsymbol{u}_{h}; \boldsymbol{u}_{h}, \boldsymbol{u}_{h}) + s_{\text{pres}}(p_{h}, p_{h}) \leq C \| \boldsymbol{f} \|_{-1}, \| p_{h} \|_{0} \leq C \left(1 + \frac{1}{\sqrt{v}} + \frac{|\boldsymbol{u}_{h}|_{1}}{\sqrt{v}} + \frac{|\boldsymbol{u}_{h}|_{1}}{v} \right) \| \boldsymbol{f} \|_{0},$$
(104)

where the second estimate is obtained from the first one and the inf-sup condition (84), similarly to (94). A convergence result of solutions of (98) to a solution of the steady-state Navier–Stokes equations (97) can be proved.

Theorem 4 The sequence $\{(\mathbf{u}_h, p_h)\}_{h>0}$ of solutions of the VMS-LPS model (98) contains a sub-sequence which is weakly convergent in $[H^1(\Omega)]^d \times L^2(\Omega)$ to a solution of the steady Navier–Stokes equations (97).

Proof (Sketch) The eddy viscosity and convection-stabilization terms vanish in the limit due to the estimates

$$\frac{|c(\boldsymbol{u}_h; \boldsymbol{u}_h, \boldsymbol{v}_h)|}{|s_{\text{conv}}(\boldsymbol{u}_h; \boldsymbol{u}_h, \boldsymbol{v}_h)|}$$
(105)

The pressure stabilizing term also vanishes in the limit. To prove this, one uses a representation formula. By [33], there exists a family of vectorial bubble finite element spaces \mathbb{Z}_h (formed by functions that vanish on the edges of all elements), a family of bilinear uniformly continuous and uniformly coercive forms on $[H_0^1(\Omega)]^d$, $\mathcal{S}_h(\cdot,\cdot)$ such that

$$s_{\text{pres}}(r_h, q_h) = \mathcal{S}_h(\mathcal{R}_h(\sigma_h^*(\nabla r_h)), \mathcal{R}_h(\sigma_h^*(\nabla q_h)))$$

$$\forall r_h, q_h \in Y_h.$$

Here, $\mathcal{R}_h : [H^{-1}(\Omega)]^d \to \mathbb{Z}_h$ is the static condensation operator associated to \mathcal{S}_h , defined as: Given $\varphi \in [H^{-1}(\Omega)]^d$, $\mathcal{R}_h(\varphi)$ is the only element of \mathbb{Z}_h that satisfies: $\mathcal{S}_h(\mathcal{R}_h(\varphi), z_h) = \langle \varphi, z_h \rangle$, $\forall z_h \in \mathbb{Z}_h$. Then

$$s_{\text{pres}}(p_h, p_h) = \mathcal{S}_h(\mathcal{R}_h(\sigma_h^*(\nabla p_h)), \mathcal{R}_h(\sigma_h^*(\nabla p_h))),$$

and by estimate (104), one deduces that the sequence $\{\mathcal{R}_h(\sigma_h^*(\nabla p_h))\}_{h>0}$ is uniformly bounded in $[H_0^1(\Omega)]^d$. Then, this sequence is weakly convergent to zero in $[H_0^1(\Omega)]^d$, see [32, Lemma 4.1]. Assume that $q \in \mathcal{D}(\Omega) \cap L_0^2(\Omega)$. Then, $\sigma_h^*(\nabla q_h)$ strongly converges to zero in $L^2(\Omega)$. As

$$s_{\text{pres}}(p_h, q_h) = \mathcal{S}_h(\mathcal{R}_h(\sigma_h^*(\nabla p_h)), \mathcal{R}_h(\sigma_h^*(\nabla q_h)))$$
$$= \langle \sigma_h^*(\nabla q_h), \mathcal{R}_h(\sigma_h^*(\nabla p_h)) \rangle,$$

one concludes that

$$\lim_{h\to 0} s_{\text{pres}}(p_h, q_h) = 0.$$

The remaining terms in (98) pass to the limit in a standard way. One then concludes that the limit (\boldsymbol{u},p) satisfies formulation (97) for all $\boldsymbol{v} \in \boldsymbol{X}$ and $q \in \mathcal{D}(\Omega) \cap L_0^2(\Omega)$. By density it also holds for $q \in Y = L_0^2(\Omega)$. \square

For smooth velocity and pressure (u,p) and small data, method (98) satisfies error estimates of optimal order. It also satisfies an asymptotic energy balance: Indeed, define the deformation energy $E_{\rm D}$, the subgrid eddy dissipation energy $E_{\rm SC}$ and the energy $E_{\rm SC}$ and $E_{\rm SP}$, respectively, corresponding to the convection and the pressure stabilizing terms by:

$$E_{D}(\boldsymbol{u}) = a(\boldsymbol{u}, \boldsymbol{u}) = 2v \|\mathbb{D}(\boldsymbol{u})\|_{2}^{2},$$

$$E_{S}(\boldsymbol{u}_{h}) = c(\boldsymbol{u}_{h}; \boldsymbol{u}_{h}, \boldsymbol{u}_{h}) = 2 \sum_{K \in \mathcal{T}_{h}} (C_{S}h_{K})^{2} \int_{K} |\mathbb{D}(\widehat{\boldsymbol{u}}_{h})|^{3} d\boldsymbol{x},$$

$$E_{SC}(\boldsymbol{u}_{h}) = s_{conv}(\boldsymbol{u}_{h}; \boldsymbol{u}_{h}, \boldsymbol{u}_{h}) = \sum_{K \in \mathcal{T}_{h}} \tau_{v,K} \|\sigma_{h}^{*}(\boldsymbol{u}_{h} \cdot \nabla \boldsymbol{u}_{h})\|_{2,K}^{2},$$

$$E_{SP}(p_{h}) = s_{pres}(p_{h}, p_{h}) = \sum_{K \in \mathcal{T}_{h}} \tau_{c,K} \|\sigma_{h}^{*}(\nabla p_{h})\|_{2,K}^{2}.$$

$$(106)$$

Then, if the sequence $\{(\boldsymbol{u}_h,p_h)\}_{h>0}$ is strongly convergent in $[H^1(\Omega)]^d \times L^2(\Omega)$ to a solution (\boldsymbol{u},p) of the Navier-Stokes equations (2) with regularity $[H^2(\Omega)]^d \times H^1(\Omega)$, it holds

$$\lim_{h\to 0} E_{\mathrm{D}}(\boldsymbol{u}_h) = E_{\mathrm{D}}(\boldsymbol{u}), \quad \lim_{h\to 0} E_{\mathrm{S}}(\boldsymbol{u}_h) = \lim_{h\to 0} E_{\mathrm{SC}}(\boldsymbol{u}_h)$$

$$= \lim_{h\to 0} E_{\mathrm{SP}}(p_h) = 0,$$

and then

$$\lim_{h\to 0} [E_{\mathrm{D}}(\boldsymbol{u}_h) + E_{\mathrm{S}}(\boldsymbol{u}_h) + E_{\mathrm{SC}}(\boldsymbol{u}_h) + E_{\mathrm{SP}}(p_h)] = E_{\mathrm{D}}(\boldsymbol{u}),$$

Thus, the total energy balance is asymptotically maintained in such a way that the deformation energy passes to the limit. In addition, the dissipated eddy energy and the subgrid energy due to stabilizing terms asymptotically vanish.

If the the sequence $\{(\boldsymbol{u}_h,p_h)\}_{h>0}$ is only weakly convergent in $[H^1(\Omega)]^d \times L^2(\Omega)$ to (\boldsymbol{u},p) , one cannot ensure that $\lim_{h\to 0} E_{\rm SP}(p_h) = 0$. Thus, it is only possible to prove an asymptotic energy inequality of the form

$$E_{\mathrm{D}}(\boldsymbol{u}) \leq \liminf_{h \to 0} [E_{\mathrm{D}}(\boldsymbol{u}_h) + E_{\mathrm{S}}(\boldsymbol{u}_h) + E_{\mathrm{SC}}(\boldsymbol{u}_h) + E_{\mathrm{SP}}(p_h)].$$



7 Three-Scale Bubble VMS Method

This section presents the bubble VMS methodology with a three-scale decomposition of the flow field using bubble functions for the small resolved velocity scales. Bubble VMS methods can be considered as a direct realization of a three-scale VMS method for finite elements by discretizing both equations (32) and (33) with a finite element method. Earlier direct realizations used Fourier spectral methods, at least in the direction of homogeneous isotropic turbulence, and a separation into large and small resolved scales was performed via the norm of the wave number vector, e.g., see [86, 87].

7.1 Derivation

There are several realizations of bubble VMS methods which differ in some details, e.g., see [31, 62, 68, 69, 98, 112, 113]. Here, exemplary the derivation of one of these realizations is presented.

Consider the decomposition of the resolved scales (\boldsymbol{u}_h, p_h) into large scales $(\overline{\boldsymbol{u}}, \overline{p})$ and small resolved scales $(\widehat{\boldsymbol{u}}, \widehat{p})$. Equation (32) for the large scale test function, after having neglected the coupling terms of the large and the unresolved scales, takes the form

$$(\hat{o}_t \boldsymbol{u}_h, \overline{\boldsymbol{v}}) + (2\boldsymbol{v} \mathbb{D}(\boldsymbol{u}_h), \mathbb{D}(\overline{\boldsymbol{v}})) + b(\boldsymbol{u}_h, \boldsymbol{u}_h, \overline{\boldsymbol{v}}) - (\nabla \cdot \overline{\boldsymbol{v}}, p_h) + (\nabla \cdot \boldsymbol{u}_h, \overline{\boldsymbol{q}}) = (\boldsymbol{f}, \overline{\boldsymbol{v}}).$$

Applying the splitting of the resolved scales yields

$$(\partial_{t}\overline{\boldsymbol{u}},\overline{\boldsymbol{v}}) + (2v\mathbb{D}(\overline{\boldsymbol{u}}),\mathbb{D}(\overline{\boldsymbol{v}})) + b(\overline{\boldsymbol{u}},\overline{\boldsymbol{u}},\overline{\boldsymbol{v}}) - (\nabla \cdot \overline{\boldsymbol{v}},\overline{p}) + (\nabla \cdot \overline{\boldsymbol{u}},\overline{q}) = (\boldsymbol{f},\overline{\boldsymbol{v}}) - \{(\partial_{t}\widehat{\boldsymbol{u}},\overline{\boldsymbol{v}}) + (2v\mathbb{D}(\widehat{\boldsymbol{u}}),\mathbb{D}(\overline{\boldsymbol{v}})) + b(\boldsymbol{u}_{h},\widehat{\boldsymbol{u}},\overline{\boldsymbol{v}}) + b(\widehat{\boldsymbol{u}},\overline{\boldsymbol{u}},\overline{\boldsymbol{v}}) - (\nabla \cdot \overline{\boldsymbol{v}},\widehat{p}) + (\nabla \cdot \widehat{\boldsymbol{u}},\overline{q})\}.$$

$$(107)$$

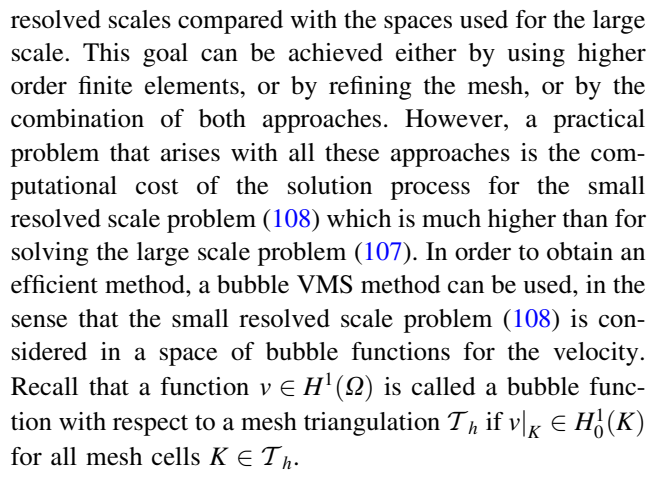
Similarly, one derives an equation for the small resolved scale test function

$$(\hat{o}_{t}\widehat{\boldsymbol{u}},\widehat{\boldsymbol{v}}) + (2(\boldsymbol{v} + \boldsymbol{v}_{T})\mathbb{D}(\widehat{\boldsymbol{u}}), \mathbb{D}(\widehat{\boldsymbol{v}})) + b(\boldsymbol{u}_{h}, \widehat{\boldsymbol{u}}, \widehat{\boldsymbol{v}}) - (\nabla \cdot \widehat{\boldsymbol{v}}, \widehat{\boldsymbol{p}}) + (\nabla \cdot \widehat{\boldsymbol{u}}, \widehat{\boldsymbol{q}}) = (\boldsymbol{f}, \widehat{\boldsymbol{v}}) - \{(\hat{o}_{t}\overline{\boldsymbol{u}}, \widehat{\boldsymbol{v}}) + (2\boldsymbol{v}\mathbb{D}(\overline{\boldsymbol{u}}), \mathbb{D}(\widehat{\boldsymbol{v}})) + b(\boldsymbol{u}_{h}, \overline{\boldsymbol{u}}, \widehat{\boldsymbol{v}}) - (\nabla \cdot \widehat{\boldsymbol{v}}, \overline{\boldsymbol{p}}) + (\nabla \cdot \overline{\boldsymbol{u}}, \widehat{\boldsymbol{q}})\}.$$

$$(108)$$

Here, the eddy viscosity term is already included, which models the effect of the unresolved scales onto the small resolved scales with v_T being the subgrid turbulent viscosity.

In bubble finite element VMS methods, standard finite element spaces are used for the large scales, $\overline{X} \times \overline{Y} = X_h \times Y_h$. As pointed out in Sect. 3.2, the main goal of the bubble finite element VMS method is to use a higher resolution spaces for the approximation of the



With respect to the model for the small resolved scale pressure, it was proposed in [62, 68, 69] to model the small resolved scale pressure in the form

$$\widehat{p} = -\sum_{K \in \mathcal{T}_h} \tau_{c}(\nabla \cdot \overline{\boldsymbol{u}}), \tag{109}$$

which is the same model as proposed in [10] for the twoscale residual-based VMS, see Sect. 4.1. In (109), $\{\tau_{c}\}_{K\in\mathcal{T}_{h}}$ is a family of stabilization parameters which are usually defined to be piecewise constant. Using this proposal, the small resolved pressure does not appear any longer in the large scale equation but its influence on the large scales is modeled. The contribution of the small resolved pressure (109) into the large scale equation leads to a so-called grad-div stabilization term. Since the small resolved pressure \hat{p} disappeared, a divergence constraint for the small resolved velocity \hat{u} is no longer required. And, since there is no longer a divergence constraint for \hat{u} , it does not make sense to have a term with this contribution in the divergence constraint for the large scale equation (107). Hence, all terms in the model (107) and (108) coming from the divergence constraint which includes small resolved scales will be neglected by setting

$$(\nabla \cdot \widehat{\boldsymbol{u}}, \overline{q}) = (\nabla \cdot \overline{\boldsymbol{u}}, \widehat{q}) = (\nabla \cdot \widehat{\boldsymbol{u}}, \widehat{q}) = 0.$$

Inserting these modifications in the small resolved scale problem (108), one obtains a simplified vector-valued equation for \hat{u} . Motivated by the desire to construct an efficient method, the small resolved velocity is searched in a bubble space. Note that the space of these bubble functions \hat{X}_{bub} is infinite-dimensional. However, from the practical point of view, this space has to be a finite-dimensional space.

Usually, some further simplifying assumptions are made for the terms with the small resolved velocity scales. The equation for the small resolved velocity scales is only solved once for each time step, i.e., at the beginning, which yields the solution $\hat{u}^{(1)}$. Consequently, this equation is



linearized and all terms with \overline{u} are treated explicitly. Therefore, the temporal derivatives in (107) and (108) have to be modified. Denoting quantities at time level n with a subscript n, one can use for the large scale equation (107)

$$\hat{\sigma}_t \hat{\boldsymbol{u}} \approx \frac{\hat{\boldsymbol{u}}^{n+1} - \hat{\boldsymbol{u}}^n}{\Delta t_{n+1}} \approx \frac{\hat{\boldsymbol{u}}^{(1)} - \hat{\boldsymbol{u}}^n}{\Delta t_{n+1}},\tag{110}$$

where $\Delta t_{n+1} = t_{n+1} - t_n$ is the current time step. In the small resolved scale equation, one assumes that the temporal change in the large scales can be neglected, i.e., $\partial_t \overline{u} = 0$. Moreover, for reasons of efficiency, the gradient form of the viscous term is used in the small resolved scale equation and some right-hand side terms in the large scale equation. With the gradient form, the small resolved scale equation decouples into three scalar equations since the system matrix becomes a block diagonal matrix.

Inserting the models and the simplifying assumptions for the small resolved scales into (107) and (108) leads to the following system of equations: Find $\overline{u}:[0,T]\to \overline{X}, \overline{p}:(0,T]\to \overline{Y}$ satisfying

$$(\hat{o}_{t}\overline{\boldsymbol{u}},\overline{\boldsymbol{v}}) + (2\boldsymbol{v}\mathbb{D}(\overline{\boldsymbol{u}}),\mathbb{D}(\overline{\boldsymbol{v}})) + b(\overline{\boldsymbol{u}},\overline{\boldsymbol{u}},\overline{\boldsymbol{v}}) - (\nabla \cdot \overline{\boldsymbol{v}},\overline{\boldsymbol{p}}) + (\nabla \cdot \overline{\boldsymbol{u}},\overline{\boldsymbol{q}}) + \sum_{K \in \mathcal{T}_{h}} \tau_{c}(\nabla \cdot \overline{\boldsymbol{u}},\nabla \cdot \overline{\boldsymbol{v}})_{K} = (\boldsymbol{f},\overline{\boldsymbol{v}}) - \left\{ \left(\frac{\widehat{\boldsymbol{u}}^{(1)} - \widehat{\boldsymbol{u}}^{n}}{\Delta t_{n+1}},\overline{\boldsymbol{v}} \right) + \left(\boldsymbol{v}\nabla\widehat{\boldsymbol{u}}^{(1)},\nabla\overline{\boldsymbol{v}} \right) + b\left(\overline{\boldsymbol{u}}^{n} + \widehat{\boldsymbol{u}}^{(1)},\widehat{\boldsymbol{u}}^{(1)},\overline{\boldsymbol{v}} \right) + b\left(\widehat{\boldsymbol{u}}^{(1)},\overline{\boldsymbol{u}}^{n},\overline{\boldsymbol{v}} \right) \right\}$$

$$(111)$$

for all $(\overline{v}, \overline{q}) \in \overline{X} \times \overline{Y}$. The equation for computing the small resolved scales $\widehat{u}^{(1)} : [0, T] \to \widehat{X}_{\text{bub}}$ reads as

$$\left(\frac{\widehat{\boldsymbol{u}}^{(1)} - \widehat{\boldsymbol{u}}^{n}}{\Delta t_{n+1}}, \widehat{\boldsymbol{v}}\right) + \left((\boldsymbol{v} + \boldsymbol{v}_{T})\nabla\widehat{\boldsymbol{u}}^{(1)}, \nabla\widehat{\boldsymbol{v}}\right) + b\left(\boldsymbol{u}_{h}^{n}, \widehat{\boldsymbol{u}}^{(1)}, \widehat{\boldsymbol{v}}\right) \\
= (\boldsymbol{f}, \widehat{\boldsymbol{v}}) - \left\{\left(\boldsymbol{v}\nabla\overline{\boldsymbol{u}}^{n}, \nabla\widehat{\boldsymbol{v}}\right) + b\left(\boldsymbol{u}_{h}^{n}, \overline{\boldsymbol{u}}^{n}, \widehat{\boldsymbol{v}}\right) - (\nabla \cdot \widehat{\boldsymbol{v}}, \overline{p}^{n}) \\
+ \sum_{K \in \mathcal{T}_{h}} \tau_{c}(\nabla \cdot \overline{\boldsymbol{u}}^{n}, \nabla \cdot \widehat{\boldsymbol{v}})_{K}\right\}$$
(112)

for all $\widehat{\mathbf{v}} \in \widehat{\mathbf{X}}_{\text{bub}}$.

Note that both models for the small resolved scale (109) and (112) can be interpreted in the way that the small resolved scales are driven from the residual of the large scales. The small resolved pressure is driven from the residual of the continuity equation and the small resolved velocity from the residual of the momentum equation.

In all bubble VMS methods, a principal question arises concerning an unphysical property introduced by using bubble functions for modeling the small resolved scales. These scales are represented by the bubble functions and are allowed to move within a mesh cell but, due to the homogeneous Dirichlet boundary conditions on the faces of the mesh cells, they cannot move directly from one mesh cell to their neighbors. Hence, the small resolved scales are bound to the mesh cells and there will be no direct interaction between these scales across the mesh cell boundaries. However, by the coupling of the small resolved scales to the large scales in (111), the information contained in the small resolved scales is distributed indirectly to the other mesh cells.

7.2 Relations to Other Methods

The use of bubble functions for stabilizing dominant convection was already proposed independently of VMS methods. These bubble functions solve equations with the residual obtained with a standard finite element method. For this reason, this approach is called residual-free bubble (RFB) method. This idea was first proposed for scalar convection-diffusion equations in [27] and applications to laminar incompressible flows can be found, e.g., in [57]. Thus, the bubble VMS method can be considered as a generalization of the RFB method in the sense that a turbulence model is introduced in the equation for the small resolved velocity scales.

7.3 Numerical Analysis

A numerical analysis for the bubble VMS method as presented in Sect. 7.1 does not seem to be available. However, error estimates for the closely related RFB method were derived for convection-diffusion equations and the Oseen equations.

Concerning scalar convection-diffusion equations, a priori error estimates for finite elements on simplicial meshes were proved in [7, 25, 26]. The case of bilinear elements was studied in [122].

In [55], an approximate RFB method for the Oseen equations is analyzed for the non-conforming Crouzeix–Raviart pair of finite element spaces. It was shown that the exact RFB method is identical to some SUPG-type stabilization in the case of constant coefficients. This SUPG-type stabilization was used as approximation for the RFB method. An optimal estimate for the error in a norm including the stabilization could be proved with a constant independent of inverse powers of ν .

7.4 Experience in Numerical Simulations

The use of a bubble VMS method requires to approximate the solution in the infinite-dimensional bubble space. In



[62, 68, 69, 98] each mesh cell was triangulated with a local grid and an approximation of the small resolved velocity with Q_1 finite elements was computed. In contrast, bubbles with a fixed polynomial degree were used in [31, 112, 113]. The methods from [31, 112, 113] do not use an eddy viscosity model in the bubble equations but a stabilization is obtained by applying an upwind-type method to the convective term. Another option that was studied in [31, 98, 113] was to use quasi-static small resolved scales, i.e., to neglect the temporal derivative for the bubble functions. This approach saves to store the values for the small resolved scales from the previous discrete time.

A comparison of a bubble VMS method with the unusual stabilized finite element method (USFEM) from [56] and the Smagorinsky LES model (with dynamic C_S or fixed $C_S = 0.1$) was presented in [69]. To stabilize the used equal-order pairs of finite element spaces, the Pressure Stabilization Petrov-Galerkin (PSPG) method was applied. As already mentioned, the local systems in the bubble VMS method were solved on local grids in each hexahedral mesh with Q_1 elements. For the use of the dynamic Smagorinsky model in the bubble VMS, a second local grid was applied that was somewhat finer than the first local grid. The numerical studies included turbulent circulating flow in a lid-driven cavity at various Reynolds numbers and a plane mixing layer example in two dimensions. For lid-driven cavity flow, the bubble VMS method led, in comparison with the USFEM and the other methods, to a remarkable good results.

Numerical studies in [98] compared the bubble VMS method with the projection-based VMS method presented in Sect. 8. Benchmark problems of turbulent channel flows were considered with the inf-sup stable finite element pair $Q_2/P_1^{\rm disc}$ on hexahedral grids. For the bubble VMS method inf-sup stable pairs of finite elements on anisotropic grids were used. The static Smagorinsky models (38) with $C_S =$ 1 and (37) with $C_S \in \{0.5, 1\}$ were used for the bubble VMS method. For quantities of interest, numerical studies for the flow at $Re_{\tau} = 195$ showed slightly better results for the quasi-static bubble VMS method compared with the projection-based VMS method. On the other hand, the projection-based VMS method gave superior results at $Re_{\tau} = 395$. It is mentioned that the implementation of the bubble VMS was rather complicated. In addition, it turned out that the dominating term of the model is the grad-div term which evolves from modeling the small resolved pressure. Incorporating only this term, without modeling the small resolved velocity, led to stable simulations. However, applying in addition to the grad-div stabilization also the bubble model for the small resolved velocity improved the accuracy of the results. It is also mentioned that the large values of C_S were needed for the solution of the problem (112) on the coarse grids ($5 \times 5 \times 5$ sub cells) for the local problems. Altogether, the use of the bubble VMS method is not recommended in [98].

In summary, bubble VMS methods which approximate the solution for the small resolved velocity on local grids were implemented and studied from two groups. None of these groups seems to use this type of VMS method any longer.

The bubble VMS method from [112, 113] was studied in [113] at an isotropic turbulence problem, a turbulent channel flow, and a turbulent flow around a cylinder. It was shown that similar results can be obtained as, e.g., with the two-scale residual-based VMS method presented in Sect. 4 and the AVM³ method described in Sect. 9. It was observed that with quasi-static small resolved scales the method loses stability for small time steps. The method from [112, 113] was improved in [31]. The improved method can be applied also on tetrahedral grids and in the case of quasi-static small resolved scales there is no instability for small time steps. For a turbulent channel flow problem, simulated with the P_1/P_1 finite element method, similar results were obtained as with the residualbased VMS method from Sect. 4 with Q_1/Q_1 finite elements. Results computed with P_2/P_2 finite elements were considerably more accurate than results with P_1/P_1 for the same number of degrees of freedom.

8 Three-Scale Velocity Deformation Tensor Projection-Based VMS Method

This section presents a method where the scale separation into large and small resolved scales is defined with the velocity deformation tensor. Having defined in this way small resolved velocity scales, an additional viscous term is introduced where the turbulence model is acting directly only on the small resolved scales. To shorten notation, this method is called in this section just "three-scale projection-based VMS method".

8.1 Definition of the Method

First, the projection-based VMS method will be defined. It will be shown in Sect. 8.2 that a special case fits perfectly into the general concept of a three-scale VMS method described in Sect. 3.2.

Let $X_h \times Y_h$ be finite element spaces for the velocity and pressure which satisfy the discrete inf-sup stability condition (9), let L_H be a finite-dimensional space of symmetric $d \times d$ tensor-valued functions defined on Ω and let v_T be a non-negative function that might depend on the finite element velocity and pressure and on the mesh width. Then,



the semidiscrete projection-based VMS method (continuous-in-time) is defined as follows: Find $\boldsymbol{u}_h:[0,T]\to\boldsymbol{X}_h,$ $p_h:(0,T]\to Y_h,$ and $\mathbb{G}_H:[0,T]\to L_H$ satisfying

$$(\hat{o}_{t}\boldsymbol{u}_{h},\boldsymbol{v}_{h}) + (2\boldsymbol{v}\mathbb{D}(\boldsymbol{u}_{h}),\mathbb{D}(\boldsymbol{v}_{h})) + b(\boldsymbol{u}_{h},\boldsymbol{u}_{h},\boldsymbol{v}_{h}) - (\nabla \cdot \boldsymbol{v}_{h},p_{h}) + (2\boldsymbol{v}_{T}(\boldsymbol{u}_{h},h)(\mathbb{D}(\boldsymbol{u}_{h}) - \mathbb{G}_{H}),\mathbb{D}(\boldsymbol{v}_{h})) = \langle \boldsymbol{f},\boldsymbol{v}_{h}\rangle(\nabla \cdot \boldsymbol{u}_{h},q_{h}) = 0 (\mathbb{D}(\boldsymbol{u}_{h}) - \mathbb{G}_{H},\mathbb{L}_{H}) = 0,$$

$$(113)$$

for all $(v_h, q_h) \in X_h \times Y_h$ and $\mathbb{L}_H \in L_H$.

The main features and assumptions of a three-scale VMS method can be observed quite well already in (113). The method is based on a variational formulation and the decomposition of the scales is defined by projection in the last equation of (113). The large scales are represented by \mathbb{G}_H and the small resolved scales by $\mathbb{D}(u_h) - \mathbb{G}_H$. Thus $\mathbb{D}(u_h)$ represents all resolved scales. In the last term on the left-hand side of the first equation in (113) it can be seen that the turbulence model is applied directly only to the small resolved scales.

The method (113) was proposed in [93] based on ideas from [105]. To apply this method, one has to choose two parameters: the additional viscosity $v_T(\boldsymbol{u}_h, h)$ and the space L_H .

Concerning $v_T(u_h, h)$, numerical studies with method (113) presented in [93, 98, 99, 104, 123] used a Smagorinsky models of the form

$$v_{\mathrm{T}} = C_{\mathrm{S}} \delta^{2} \| \mathbb{D}(\boldsymbol{u}_{h}) \|_{\mathrm{F}},\tag{114}$$

$$v_{\mathrm{T}} = C_{\mathrm{S}} \delta^{2} \| \mathbb{D}(\boldsymbol{u}_{h}) - \mathbb{G}_{H} \|_{\mathrm{F}}, \tag{115}$$

$$v_{\rm T} = C_S \frac{\delta^2}{|K|^{1/2}} \|\mathbb{D}(\boldsymbol{u}_h) - \mathbb{G}_H\|_{L^2(K)}. \tag{116}$$

The other parameter in (113) is the space of symmetric tensors L_H . The last equation in (113) states that the tensor \mathbb{G}_H is just the $L^2(\Omega)$ projection of $\mathbb{D}(\boldsymbol{u}_h)$ into L_H : $P_{L_H}: L \to L_H, \ \mathbb{D}(\boldsymbol{v}) \to P_{L_H} \mathbb{D}(\boldsymbol{v}) = \mathbb{G}_H$

$$(P_{L_H} \mathbb{D}(\mathbf{v}) - \mathbb{D}(\mathbf{v}), \mathbb{L}_H) = 0 \quad \forall \ \mathbb{L}_H \in L_H. \tag{117}$$

With this notation and using the short form (21), one can reformulate (113) as follows: Find $u_h: [0,T] \to X_h$, $p_h: (0,T] \to Y_h$ satisfying

$$A(\mathbf{u}_h; (\mathbf{u}_h, p_h), (\mathbf{v}_h, q_h)) + (2\mathbf{v}_{\mathrm{T}}(\mathbf{u}_h, h)(I - P_{L_H})\mathbb{D}(\mathbf{u}_h), \mathbb{D}(\mathbf{v}_h)) = \mathbf{f}(\mathbf{v}_h)$$
(118)

for all $(v_h, q_h) \in X_h \times Y_h$.

The space L_H plays the role of a large scale space such that $(I - P_{L_H}) \mathbb{D}(\boldsymbol{u}_h)$ represents small resolved scales of $\mathbb{D}(\boldsymbol{u}_h)$. Of course, only scales should be subtracted from $\mathbb{D}(\boldsymbol{u}_h)$ that are contained in this tensor. Hence, it is required that $L_H \subset \{\mathbb{D}(\boldsymbol{v}_h) : \boldsymbol{v}_h \in \boldsymbol{X}_h\}$.

Since L_H represents large scales, it has to be in some sense a coarse finite element space. Similarly to LPS methods, there are essentially two possibilities:

- If X_h is a higher order finite element space, L_H can be defined as low order finite element space on the same grid as X_h . This approach is studied in [93] and it will be discussed below.
- The second possibility, in particular if X_h is a low order discretization, consists in defining L_H on a coarser grid, see [96] for a study of this approach in the case of convection-dominated convection-diffusion equations.

Since $\mathbb{D}(u_h)$ is a discontinuous piecewise polynomial tensor, choosing its $L^2(\Omega)$ projection in the same way seems to be natural. Thus, L_H should consist of discontinuous piecewise polynomial tensors as well. It was elaborated in [93] that for the sake of an efficient implementation of the one-grid method, the use of discontinuous tensors for L_H is mandatory.

A projection-based VMS method which computes the projection in a post-processing step was proposed and studied in [106]. That means, in the first step of this approach, one can use the Galerkin finite element discretization of the Navier–Stokes equations. Using the solution obtained in this step, one computes in a second step the final solution by applying a projection. In [106] the projection is constructed in such a way that it has the form of the eddy viscosity term in (113). This approach can be considered as an operator splitting. Its advantage is that it is not intrusive, i.e., one can use for the first step an existing code and needs to implement the projection only as an addon.

8.2 Imbedding of the Method into the Basic Concept of a Three-Scale VMS Method

In the case v_T being a positive constant, method (113) can be transformed to the abstract form (32)–(33) of a three-scale VMS method. To this end, the three-scale partitioning given in Sect. 3.2 has to be described by appropriately chosen function spaces and projections.

Clearly, the continuous pair of spaces (X, Y) contains all scales. The finite element spaces (X_h, Y_h) contain the large and the small resolved scales.

Let $X_H \subset [H^1(\Omega)]^d$ be a discrete space such that $L_H = \mathbb{D}(X_H)$. The space X_H should be coarser than X_h . But in the definition of X_H , no essential boundary conditions, like no-slip conditions, are incorporated. Thus, in general $X_H \not\subset X_h$. The pair of spaces for the large scales is given by (X_H, Y_H) where Y_H is chosen such that a discrete inf-sup condition of type (9) is fulfilled for (X_H, Y_H) . Then, the large scales $P_H u$ of the velocity are defined by an elliptic



projection into X_H and the large scales $P_H p$ of the pressure by the $L^2(\Omega)$ projection into Y_H ; $P_H: (X,Y) \to (X_H,Y_H)$

$$(\mathbb{D}(\boldsymbol{u} - P_H \boldsymbol{u}), \mathbb{D}(\overline{\boldsymbol{v}}_H)) = 0 \quad \forall \quad \overline{\boldsymbol{v}}_H \in \boldsymbol{X}_H,$$

$$(\boldsymbol{u} - P_H \boldsymbol{u}, 1) = 0,$$

$$(p - P_H p, q_H) = 0 \quad \forall \quad q_H \in Y_H.$$
(119)

Lemma 3 Commutation of the definition of the large scales and differentiation. Let $v \in X$, $L_H = \mathbb{D}(X_H)$ and denote by $P_{L_H}\mathbb{D}(v)$ the $L^2(\Omega)$ projection of $\mathbb{D}(v)$ into L_H defined in the last equation of (113). Then

$$P_{L_H} \mathbb{D}(\mathbf{v}) = \mathbb{D}(P_H \mathbf{v}) \quad \forall \ \mathbf{v} \in \mathbf{X}. \tag{120}$$

Proof From $L_H = \mathbb{D}(V_H)$ and $P_{L_H}\mathbb{D}(v) \in L_H$ it follows that there is a $w_H \in X_H$ such that $P_{L_H}\mathbb{D}(v) = \mathbb{D}(w_H)$. Using the last equation of (113) gives

$$(\mathbb{D}(\mathbf{v} - \mathbf{w}_H), \mathbb{L}_H) = 0 \quad \forall \ \mathbb{L}_H \in L_H. \tag{121}$$

On the other hand, since $L_H = \mathbb{D}(X_H)$, (119) is equivalent to

$$(\mathbb{D}(\mathbf{v} - P_H \mathbf{v}), \mathbb{L}_H) = 0 \quad \forall \ \mathbb{L}_H \in L_H. \tag{122}$$

The statement of the lemma follows now directly from (121) and (122) since the elliptic projection is unique. \Box

Let v_T be a positive constant. A straightforward calculation, using that P_{L_H} is a $L^2(\Omega)$ projection and $(I - P_{L_H})$ is in the orthogonal complement, shows that

$$(v_{\mathrm{T}}(I - P_{L_H}) \mathbb{D}(\boldsymbol{u}_h), \mathbb{D}(\boldsymbol{v}_h)) = (v_{\mathrm{T}}(I - P_{L_H}) \mathbb{D}(\boldsymbol{u}_h), (I - P_{L_H}) \mathbb{D}(\boldsymbol{v}_h)).$$

Thus, (118) can be reformulated as follows: Find u_h : $[0,T] \to X_h$, p_h : $(0,T] \to Y_h$ satisfying

$$A(\mathbf{u}_{h}; (\mathbf{u}_{h}, p_{h}), (\mathbf{v}_{h}, q_{h})) + (2v_{T}(I - P_{L_{H}})\mathbb{D}(\mathbf{u}_{h}), (I - P_{L_{H}})\mathbb{D}(\mathbf{v}_{h})) = \mathbf{f}(\mathbf{v}_{h})$$
(123)

for all $(v_h, q_h) \in X_h \times Y_h$. Decomposing $X_h = X_H + \widehat{X}_h$ and $Y_h = Y_H + \widehat{Y}_h$ with $\widehat{X}_h = (I - P_H)X_h$, $\widehat{Y}_h = (I - P_H)Y_h$, one obtains with (120)

$$(I-P_{L_H})\mathbb{D}(\boldsymbol{v}_h)=\mathbb{D}(\boldsymbol{v}_h-P_H\boldsymbol{v}_h)=\mathbb{D}((I-P_H)\boldsymbol{v}_h)=\mathbb{D}(\widehat{\boldsymbol{v}}_h).$$

The decompositions $\boldsymbol{u}_h = \overline{\boldsymbol{u}}_H + \widehat{\boldsymbol{u}}_h$, $p_h = \overline{p}_H + \widehat{p}_H$, $\boldsymbol{v}_h = \overline{\boldsymbol{v}}_H + \widehat{\boldsymbol{v}}_h$, and $q_h = \overline{q}_H + \widehat{q}_H$ are inserted into (123). Using the linearity of $A(\cdot;\cdot,\cdot)$ with respect to the second and third component and writing the arising equation formally as a coupled system gives

$$\begin{array}{l}
A(\overline{u}_H + \widehat{u}_h; (\overline{u}_H, \overline{p}_H), (\overline{v}_H, \overline{q}_H)) \\
+ A(\overline{u}_H + \widehat{u}_h; (\widehat{u}_h, \widehat{p}_h), (\overline{v}_H, \overline{q}_H)) = f(\overline{v}_H)
\end{array} (124)$$

for all test functions $(\overline{v}_H, \overline{q}_H) \in X_H \times Y_H$ and

$$A(\overline{u}_{H} + \widehat{u}_{h}; (\overline{u}_{H}, \overline{p}_{H}), (\widehat{v}_{h}, \widehat{q}_{h}))$$

$$+ A(\overline{u}_{H} + \widehat{u}_{h}; (\widehat{u}_{h}, \widehat{p}_{h}), (\widehat{v}_{h}, \widehat{q}_{h}))$$

$$+ (2v_{T} \mathbb{D}(\widehat{u}_{h}), \mathbb{D}(\widehat{v}_{h})) = f(\widehat{v}_{h})$$

$$(125)$$

for all test functions from $\widehat{X}_h \times \widehat{Y}_h$. The coupled system (124)–(125) possesses exactly the form (32)–(33). The unresolved scales are modeled only in the equation for the small resolved scales (125) with the model

$$c(\mathbf{u}_h; (\overline{\mathbf{u}}_H, \overline{p}_H), (\widehat{\mathbf{u}}_h, \widehat{p}_h), (\widehat{\mathbf{v}}_h, \widehat{q}_h)) = (2v_T \mathbb{D}(\widehat{\mathbf{u}}_h), \mathbb{D}(\widehat{\mathbf{v}}_h))$$

and this model influences the large scales solely indirectly by the coupling of (124) and (125).

8.3 Relations to Other Methods

Let $L_H \subset \{\mathbb{D}(v_h) : v_h \in X_h\}$. The limit cases of L_H lead to two well known discrete models. In the case that $L_H = \{\mathbb{D}(v_h) : v_h \in X_h\}$, the second term on the left-hand side of (118) vanishes and the Galerkin finite element discretization of the Navier–Stokes equations is recovered. If $L_H = \{\mathbb{O}\}$, one obtains an artificial viscosity stabilization of the Navier–Stokes equations with a possible non-linear artificial viscosity. If, e.g., v_T is the Smagorinsky eddy viscosity model, the Smagorinsky LES model is recovered. In this sense one can say that the three-scale projection-based VMS method is in between the Galerkin discretization and an LES model of eddy viscosity type.

Comparing representation (113) with (144) shows that, apart from the PSPG-type stabilization, the coarse space projection-based VMS method and AVM³ have principally the same form.

8.4 Numerical Analysis

A numerical analysis for projection-based VMS methods was presented in several papers. In all cases, the principal way of performing the analysis was the same as for the Galerkin discretization of the Navier–Stokes equations. The main goal was to show that the inclusion of the VMS model leads to error bounds where certain constants depend on a reduced Reynolds number (and not on the Reynolds number as for the Galerkin discretization). These results show in some sense that the projection-based VMS method possesses a smaller complexity than the Galerkin finite element method.

The first analysis was presented in [94] for method (113) and the case of a constant turbulent viscosity v_T . Two error estimates with constants depending on a reduced Reynolds number were derived. In [95], the case of v_T being a Smagorinsky-type eddy viscosity including the small



resolved scales was studied. In this paper, the additional viscous term is defined differently than in (113), namely as deformation tensor of small resolved scales \hat{u}_h and not as the small resolved scales of the deformation tensor $\mathbb{D}(u_h) - \mathbb{G}_H$, i.e., differentiation and projection are interchanged in these definitions. The analysis for v_T being a Smagorinsky-type viscosity required the use of different function spaces than for a constant viscosity. Finally, the results of [94] were generalized in [123] to the case of v_T being a piecewise constant viscosity. The analysis from [123] was extended in [109] to the case of thermally coupled incompressible flows.

For the sake of keeping the presentation as simple as possible and of concentrating on the main issue, namely the reduced Reynolds number in the error bound, an error estimate for the case of v_T being a constant will be presented here.

For the finite element error analysis it will be assumed that Ω is a bounded domain with polyhedral Lipschitz boundary, no-slip boundary conditions are prescribed, (X_h, Y_h) are assumed to satisfy the discrete inf-sup condition (9), and the continuous-in-time case is considered. Concerning the parameters of the VMS method it is assumed that v_T is a positive constant and that $L_H \subseteq \mathbb{D}(X_h)$.

If v_T is a positive constant, the projection-based VMS method can be rewritten in the form (123), i.e., it reads as: Find $u_h : [0,T] \to X_h$, $p_h : (0,T] \to Y_h$ satisfying

$$(\partial_{t}\boldsymbol{u}_{h},\boldsymbol{v}_{h}) + (2\boldsymbol{v}\mathbb{D}(\boldsymbol{u}_{h}),\mathbb{D}(\boldsymbol{v}_{h}))$$

$$+ b_{s}(\boldsymbol{u}_{h},\boldsymbol{u}_{h},\boldsymbol{v}_{h}) - (\nabla \cdot \boldsymbol{v}_{h},p_{h}) + (2\boldsymbol{v}_{T}(I - P_{L_{H}}))$$

$$\mathbb{D}(\boldsymbol{u}_{h}), (I - P_{L_{H}})\mathbb{D}(\boldsymbol{v}_{h})) = (\boldsymbol{f},\boldsymbol{v}_{h}) \quad \forall \ \boldsymbol{v}_{h} \in \boldsymbol{X}_{h}$$

$$(\nabla \cdot \boldsymbol{u}_{h},q_{h}) = 0 \quad \forall \ q_{h} \in Y_{h},$$

$$(126)$$

where the projection P_{L_H} was defined in (117).

The error analysis will be performed in the space $X_{h,\mathrm{div}}$. For simplicity let $f = f_h$. Then the velocity from (126) can be computed equivalently by solving the following problem: Find $u_h: [0,T] \to X_{h,\mathrm{div}}$ such that

$$(\partial_{t}\boldsymbol{u}_{h},\boldsymbol{v}_{h}) + (2\boldsymbol{v}\mathbb{D}(\boldsymbol{u}_{h}),\mathbb{D}(\boldsymbol{v}_{h})) + b_{s}(\boldsymbol{u}_{h},\boldsymbol{u}_{h},\boldsymbol{v}_{h}) + (2\boldsymbol{v}_{T}(I - P_{L_{H}})\mathbb{D}(\boldsymbol{u}_{h}), (I - P_{L_{H}})\mathbb{D}(\boldsymbol{v}_{h})) = (\boldsymbol{f},\boldsymbol{v}_{h})$$

$$(127)$$

for all $v_h \in X_{h,\text{div}}$.

In the finite element error analysis, the error of the solution of (126) to the solution of the Navier–Stokes equations (2) will be studied. The goal consists in deriving an error bound which depends in the most terms on a reduced Reynolds number or equivalently on an increased

effective viscosity, in contrast to the error bound (20) for the Galerkin finite element method. In the limit case $L_H = \{\mathbb{O}\}$, method (126) becomes the Smagorinsky LES model. Finite element error estimates to the solution of the continuous Smagorinsky LES model with constants independent of ν were derived in [91, 101].

Next, an additional viscosity will be defined. Since P_{L_H} is an $L^2(\Omega)$ projection, it follows for $\mathbf{v} \in \mathbf{X}$ and $\|\mathbb{D}(\mathbf{v})\|_0 > 0$ that

$$v_{T} \| (I - P_{L_{H}}) \mathbb{D}(\mathbf{v}) \|_{0}^{2} = v_{T} \left(\| \mathbb{D}(\mathbf{v}) \|_{0}^{2} - \| P_{L_{H}} \mathbb{D}(\mathbf{v}) \|_{0}^{2} \right)$$

$$= v_{T} \left(1 - \frac{\| P_{L_{H}} \mathbb{D}(\mathbf{v}) \|_{0}^{2}}{\| \mathbb{D}(\mathbf{v}) \|_{0}^{2}} \right) \| \mathbb{D}(\mathbf{v}) \|_{0}^{2}$$

$$=: v_{\text{add}}(\mathbf{v}) \| \mathbb{D}(\mathbf{v}) \|_{0}^{2}.$$
(128)

In addition, from $0 \le ||P_{L_H} \mathbb{D}(\mathbf{v})||_0 \le ||\mathbb{D}(\mathbf{v})||_0$ one obtains

$$0 \le v_{\text{add}}(\mathbf{v}) \le v_{\text{T}}.\tag{129}$$

Note that if \mathbf{v} depends on t then $v_{\mathrm{add}}(\mathbf{v})$, too. From (129) it follows that $v_{\mathrm{add}}(\mathbf{v}(t,\cdot)) \in L^{\infty}(0,T)$ if v_{T} is bounded almost everywhere in the time interval. If $\|\mathbb{D}(\mathbf{v})\|_0 = 0$ then $\mathbf{v} = \mathbf{0}$ since $\mathbf{v} \in \mathbf{X}$. In this case, one sets $v_{\mathrm{add}}(\mathbf{v}) = 0$.

The finite element error analysis requires some assumptions on the regularity of the solution and the data of the Navier–Stokes equations. It will be assumed that

$$f \in (L^2(0, T; X^*)), \quad \mathbf{u}_0 \in X,$$
 (130)

and that (2) possesses a solution (u, p) with

$$\nabla \mathbf{u} \in (L^4(0, T; L^2))^{d \times d}, \ \partial_t \mathbf{u} \in (L^2(0, T; \mathbf{X}^*))^d,$$

$$p \in L^2(0, T; L^2).$$
(131)

Note, these assumptions imply that Serrin's condition is fulfilled from what follows that the solution of (2) is unique, see Sect. 2.1.

Before presenting the error analysis, an outline of the proof, following the approach in [74, 75], will be given.

- 1. The stability of u and u_h is proved, i.e., it is shown that certain norms of u and u_h are bounded a priori by the data of the problem: f, u_0 , v, see Lemma 4.
- 2. An error equation is derived by subtracting (127) from (2) for test functions from $X_{h,\text{div}}$. The error is split into an approximation term η and a (finite element) remainder ϕ_h

$$e = u - u_h = (u - \widetilde{u}_h) - (u_h - \widetilde{u}_h) =: \eta - \phi_h,$$
(132)

where $\widetilde{u}_h \in X_{h,\text{div}}$ is a projection of u which satisfies certain interpolation properties. An example for such a



projection is the Stokes projection, see (15)–(17). Then, ϕ_b is taken as test function in the error equation.

3. The right-hand side of the error equation is estimated such that one obtains an inequality of the form

$$\frac{d}{dt} \|\boldsymbol{\phi}_h\|_0^2 + g_1(t, \boldsymbol{\phi}_h) \le g_2(t, \boldsymbol{\eta}, \boldsymbol{u}) + g_3(t, \boldsymbol{u}) \|\boldsymbol{\phi}_h\|_0^2,$$
(133)

where all functions are non-negative for almost all $t \in [0, T]$.

- 4. It has to be checked that Gronwall's lemma can be applied to (133), i.e., one has to show that all functions in (133) belong to $L^1(0,T)$. The application of Gronwall's lemma yields an estimate for ϕ_h .
- 5. The error estimate for e is proved by applying the triangle inequality to (132).

Lemma 4 The solution \mathbf{u}_h of the finite element problem (127) satisfies

$$\|\boldsymbol{u}_{h}(t)\|_{0}^{2} + \int_{0}^{t} (2v + 2v_{\text{add}}(\boldsymbol{u}_{h}(\tau))) \|\mathbb{D}(\boldsymbol{u}_{h})(\tau)\|_{0}^{2} d\tau$$

$$\leq \|\boldsymbol{u}_{0,h}\|_{0}^{2} + \int_{0}^{t} \frac{C}{2v + 2v_{\text{add}}(\boldsymbol{u}_{h}(\tau))} \|\boldsymbol{f}\|_{X^{*}}^{2} d\tau.$$
(134)

Consequently, it is $\mathbf{u}_h \in (L^{\infty}(0,T;L^2))^d$ and $\mathbb{D}(\mathbf{u}_h) \in (L^2(0,T;L^2))^{d \times d}$. The velocity solution of the continuous problem (2) fulfills $\mathbf{u} \in (L^{\infty}(0,T;L^2))^d$ and $\mathbb{D}(\mathbf{u}) \in (L^2(0,T;L^2))^{d \times d}$.

Proof Setting $v_h = u_h$ in (127), using

$$(\partial_t \boldsymbol{u}_h, \boldsymbol{u}_h) = \frac{1}{2} \frac{d}{dt} \|\boldsymbol{u}_h\|_0^2,$$

and the skew symmetry of $b_s(\cdot, \cdot, \cdot)$, the definition of v_{add} , (128), the standard estimate of the dual pairing, Korn's inequality (13), and integrating over (0, t) with $t \le T$ gives

$$\frac{1}{2} \|\boldsymbol{u}_{h}(t)\|_{0}^{2} + \int_{0}^{t} (2v + 2v_{\text{add}}(\boldsymbol{u}_{h}(\tau))) \|\mathbb{D}(\boldsymbol{u}_{h})(\tau)\|_{0}^{2} d\tau
\leq \frac{1}{2} \|\boldsymbol{u}_{0,h}\|_{0}^{2} + \int_{0}^{t} \|\boldsymbol{f}(\tau)\|_{\boldsymbol{X}^{*}} \|\nabla \boldsymbol{u}_{h}(\tau)\|_{0} d\tau
\leq \frac{1}{2} \|\boldsymbol{u}_{0,h}\|_{0}^{2} + \int_{0}^{t} \frac{C}{2v + 2v_{\text{add}}(\boldsymbol{u}_{h}(\tau))} \|\boldsymbol{f}(\tau)\|_{\boldsymbol{X}^{*}}^{2} d\tau
+ \int_{0}^{t} \frac{2v + 2v_{\text{add}}(\boldsymbol{u}_{h}(\tau))}{2} \|\mathbb{D}(\boldsymbol{u}_{h})(\tau)\|_{0}^{2} d\tau.$$

Subtraction of the last term gives (134). $\mathbb{D}(\boldsymbol{u}_h) \in (L^2(0,T;L^2))^{d\times d}$. Taking then the supremum of $t \in (0,T)$ gives the statement $\boldsymbol{u}_h \in (L^{\infty}(0,T;L^2))$.

The proof for the solution of the continuous problem uses the same techniques, compare also (5) for the

regularity of an appropriately defined variational velocity solution. \Box

The stability estimate (134) shows that the bound for u_h does not depend on v^{-1} as for the Galerkin discretization, see (18), but on the inverse of a presumably larger viscosity term.

Theorem 5 Let $(\mathbf{u}, p) \in X \times Y$ be the solution of (2) and let $\mathbf{u}_h \in X_{h,\text{div}}$ be the solution of (127) where $v_T \ge 0$ is a constant. Let the regularity assumptions (131) be fulfilled and let $\widetilde{\mathbf{u}}_h$ be a projection of \mathbf{u} into $X_{h,\text{div}}$ such that $\mathbf{\eta} = \mathbf{u} - \widetilde{\mathbf{u}}_h \in X_{h,\text{div}}$ satisfies optimal interpolation estimates of form (16) and (17). Let the reduced Reynolds number $\operatorname{Re}_{\text{red}}(\mathbf{v}_h)$ defined by

$$\operatorname{Re}_{\operatorname{red}}(\mathbf{v}_h) = \left(2v + \inf_{t \in (0,T]} 2v_{\operatorname{add}}(\mathbf{v}_h(t))\right)^{-1} \le 2v^{-1}.$$
 (135)

Then, the error $\mathbf{u} - \mathbf{u}_h$ satisfies for $T \ge 0$

$$\begin{split} &\|(\boldsymbol{u}-\boldsymbol{u}_{h})(T)\|_{0}^{2} + (\operatorname{Re}_{\operatorname{red}}(\boldsymbol{u}_{h}-\widetilde{\boldsymbol{u}}_{h}))^{-1}\|\mathbb{D}(\boldsymbol{u}-\boldsymbol{u}_{h})\|_{L^{2}(0,T;L^{2})}^{2} \\ &\leq C \inf_{\lambda_{h} \in L^{2}(0,T;Y_{h})} \left\{ \|(\boldsymbol{u}-\widetilde{\boldsymbol{u}}_{h})(T)\|_{0}^{2} \\ &+ (\operatorname{Re}_{\operatorname{red}}(\boldsymbol{u}_{h}-\widetilde{\boldsymbol{u}}_{h}))^{-1}\|\mathbb{D}(\boldsymbol{u}-\widetilde{\boldsymbol{u}}_{h})\|_{L^{2}(0,T;L^{2})}^{2} \\ &+ \exp\left(C(\operatorname{Re}_{\operatorname{red}}(\boldsymbol{u}_{h}-\widetilde{\boldsymbol{u}}_{h}))^{3}\|\mathbb{D}(\boldsymbol{u})\|_{L^{4}(0,T;L^{2})}^{4}\right) \\ &\left[\|\boldsymbol{u}_{0,h}-\widetilde{\boldsymbol{u}}_{h}(0)\|_{0}^{2} + (\boldsymbol{v}+\boldsymbol{v}_{T})\|\mathbb{D}(\boldsymbol{u}-\widetilde{\boldsymbol{u}}_{h})\|_{L^{2}(0,T;L^{2})}^{2} \\ &+ (\operatorname{Re}_{\operatorname{red}}(\boldsymbol{u}_{h}-\widetilde{\boldsymbol{u}}_{h}))\left[\|\partial_{t}(\boldsymbol{u}-\widetilde{\boldsymbol{u}}_{h})\|_{L^{2}(0,T;X^{*})}^{2} \\ &+ \|\boldsymbol{p}-\lambda_{h}\|_{L^{2}(0,T;L^{2})}^{2} + \|\mathbb{D}(\boldsymbol{u}-\widetilde{\boldsymbol{u}}_{h})\|_{L^{4}(0,t;L^{2})}^{2} \|\mathbb{D}(\boldsymbol{u})\|_{L^{4}(0,t;L^{2})}^{2} \\ &+ \left((\operatorname{Re}_{\operatorname{red}}(\boldsymbol{u}_{h}))^{1/2}\|\boldsymbol{u}_{0,h}\|_{0}^{2} + (\operatorname{Re}_{\operatorname{red}}(\boldsymbol{u}_{h}))^{3/2}\|\boldsymbol{f}\|_{L^{2}(0,T;X^{*})}^{2} \right) \\ &\times \|\mathbb{D}(\boldsymbol{u}-\widetilde{\boldsymbol{u}}_{h})\|_{L^{4}(0,t;L^{2})}^{2} \right] + \boldsymbol{v}_{T}\|(\boldsymbol{I}-\boldsymbol{P}_{L_{H}})\mathbb{D}(\boldsymbol{u})\|_{L^{2}(0,T;L^{2})}^{2} \right] \right\} \end{split}$$

for arbitrary $\widetilde{\boldsymbol{u}}_h \in \boldsymbol{X}_{h.\text{div}}$.

Proof The splitting of the error (132) is performed with the help of a projection $\widetilde{u}_h \in X_{h,\mathrm{div}}$ of u. Let $t \in [0,T]$ be arbitrary. It is required that the projection fulfills the approximation properties (16) and (17) such that, e.g., the Stokes projection can be chosen. Korn's inequality (13), (16) with k = 1, and the regularity assumptions (131) imply that

$$\nabla \boldsymbol{\eta} \in (L^4(0, T; L^2))^{d \times d}. \tag{137}$$

Now, Step 2 of the proof is carried out by a straightforward calculation, yielding



$$\frac{1}{2} \frac{d}{dt} \|\boldsymbol{\phi}_{h}\|_{0}^{2} + (2v + 2v_{\text{add}}(\boldsymbol{\phi}_{h})) \|\mathbb{D}(\boldsymbol{\phi}_{h})\|_{0}^{2}
= (\partial_{t}\boldsymbol{\eta}, \boldsymbol{\phi}_{h}) + (2v\mathbb{D}(\boldsymbol{\eta}), \mathbb{D}(\boldsymbol{\phi}_{h})) + (2v_{\text{T}}(I - P_{L_{H}}))
\times \mathbb{D}(\boldsymbol{\eta}), (I - P_{L_{H}}) \mathbb{D}(\boldsymbol{\phi}_{h}))
+ b_{s}(\boldsymbol{u}, \boldsymbol{u}, \boldsymbol{\phi}_{h}) - b_{s}(\boldsymbol{u}_{h}, \boldsymbol{u}_{h}, \boldsymbol{\phi}_{h})
- (2v_{\text{T}}(I - P_{L_{H}}) \mathbb{D}(\boldsymbol{u}), (I - P_{L_{H}}) \mathbb{D}(\boldsymbol{\phi}_{h}))
- (p - \lambda_{h}, \nabla \cdot \boldsymbol{\phi}_{h})$$
(138)

with arbitrary $\lambda_h \in Y_h$.

In Step 3 of the proof, one has to get an inequality of form (133) by estimating the terms on the right-hand side of (138). All bilinear terms are estimated essentially in the same way: using the Cauchy-Schwarz inequality (or the estimate for the dual pairing), Korn's inequality (13) and Young's inequality (11). In addition, (128) is used. One obtains

 $(\partial_t \boldsymbol{\eta}, \boldsymbol{\phi}_h) \leq \|\partial_t \boldsymbol{\eta}\|_{\boldsymbol{X}^*} \|\nabla \boldsymbol{\phi}_h\|_0 \leq C \|\partial_t \boldsymbol{\eta}\|_{\boldsymbol{X}^*} \|\mathbb{D}(\boldsymbol{\phi}_h)\|_0$

$$\leq \frac{2\nu + 2\nu_{\text{add}}(\phi_{h})}{8} \|\mathbb{D}(\phi_{h})\|_{0}^{2} + \frac{C}{2\nu + 2\nu_{\text{add}}(\phi_{h})} \|\partial_{t}\eta\|_{X^{*}}^{2},
(2\nu\mathbb{D}(\eta), \mathbb{D}(\phi_{h})) \leq 2\nu\|\mathbb{D}(\eta)\|_{0}\|\mathbb{D}(\phi_{h})\|_{0}
\leq \frac{\nu}{8} \|\mathbb{D}(\phi_{h})\|_{0}^{2} + 8\nu\|\mathbb{D}(\eta)\|_{0}^{2},
(\nabla \cdot \phi_{h}, p - \lambda_{h}) \leq \|p - \lambda_{h}\|_{0} \|\nabla \cdot \phi_{h}\|_{0} \leq C\|p - \lambda_{h}\|_{0} \|\mathbb{D}(\phi_{h})\|_{0}
\leq \frac{2\nu + 2\nu_{\text{add}}(\phi_{h})}{8} \|\mathbb{D}(\phi_{h})\|_{0}^{2} + \frac{C}{2\nu + 2\nu_{\text{add}}(\phi_{h})} \|p - \lambda_{h}\|_{0}^{2},
(\nu_{T}(I - P_{L_{H}})\mathbb{D}(\eta), (I - P_{L_{H}})\mathbb{D}(\phi_{h}))
\leq \frac{\nu_{T}}{16} \|(I - P_{L_{H}})\mathbb{D}(\phi_{h})\|_{0}^{2} + 4\nu_{T} \|(I - P_{L_{H}})\mathbb{D}(\eta)\|_{0}^{2},
(\nu_{T}(I - P_{L_{H}})\mathbb{D}(\omega), (I - P_{L_{H}})\mathbb{D}(\phi_{h}))
\leq \nu_{T} \|(I - P_{L_{H}})\mathbb{D}(\omega)\|_{0} \|(I - P_{L_{H}})\mathbb{D}(\phi_{h})\|_{0}
\leq \frac{\nu_{\text{add}}(\phi_{h})}{16} \|\mathbb{D}(\phi_{h})\|_{0}^{2} + 4\nu_{T} \|(I - P_{L_{H}})\mathbb{D}(\phi_{h})\|_{0}
\leq \frac{\nu_{\text{add}}(\phi_{h})}{16} \|\mathbb{D}(\phi_{h})\|_{0}^{2} + 4\nu_{T} \|(I - P_{L_{H}})\mathbb{D}(\omega)\|_{0}^{2}.$$

The trilinear term is first decomposed into three terms. A direct calculation gives

$$b_{s}(\boldsymbol{u},\boldsymbol{u},\boldsymbol{\phi}_{h}) - b_{s}(\boldsymbol{u}_{h},\boldsymbol{u}_{h},\boldsymbol{\phi}_{h})$$

= $b_{s}(\boldsymbol{\eta},\boldsymbol{u},\boldsymbol{\phi}_{h}) - b_{s}(\boldsymbol{\phi}_{h},\boldsymbol{u},\boldsymbol{\phi}_{h}) + b_{s}(\boldsymbol{u}_{h},\boldsymbol{\eta},\boldsymbol{\phi}_{h}).$

The terms on the right-hand side are estimated separately using the estimate (8) of the trilinear term. One obtains by

applying (8) and Young's inequality (11) for the first term

$$\begin{split} b_{s}(\pmb{\eta}, \pmb{u}, \pmb{\phi}_{h}) \\ &\leq C \|\pmb{\eta}\|_{0}^{1/2} \|\mathbb{D}(\pmb{\eta})\|_{0}^{1/2} \|\mathbb{D}(\pmb{u})\|_{0} \|\mathbb{D}(\pmb{\phi}_{h})\|_{0} \\ &\leq \frac{2v + 2v_{\text{add}}(\pmb{\phi}_{h})}{8} \|\mathbb{D}(\pmb{\phi}_{h})\|_{0}^{2} + \frac{C}{2v + 2v_{\text{add}}(\pmb{\phi}_{h})} \\ \|\pmb{\eta}\|_{0} \|\mathbb{D}(\pmb{\eta})\|_{0} \|\mathbb{D}(\pmb{u})\|_{0}^{2}, \end{split}$$

for the second term

$$b_{s}(\phi_{h}, \boldsymbol{u}, \phi_{h})$$

$$\leq C \|\phi_{h}\|_{0}^{1/2} \|\mathbb{D}(\boldsymbol{u})\|_{0} \|\mathbb{D}(\phi_{h})\|_{0}^{3/2}$$

$$\leq \frac{2v + 2v_{\text{add}}(\phi_{h})}{8} \|\mathbb{D}(\phi_{h})\|_{0}^{2} + \frac{C}{(2v + 2v_{\text{add}}(\phi_{h}))^{3}}$$

$$\|\phi_{h}\|_{0}^{2} \|\mathbb{D}(\boldsymbol{u})\|_{0}^{4},$$

and for the third term

$$b_{s}(\boldsymbol{u}_{h}, \boldsymbol{\eta}, \boldsymbol{\phi}_{h})$$

$$\leq C \|\boldsymbol{u}_{h}\|_{0}^{1/2} \|\mathbb{D}(\boldsymbol{u}_{h})\|_{0}^{1/2} \|\mathbb{D}(\boldsymbol{\eta})\|_{0} \|\mathbb{D}(\boldsymbol{\phi}_{h})\|_{0}$$

$$\leq \frac{2v + 2v_{\text{add}}(\boldsymbol{\phi}_{h})}{8} \|\mathbb{D}(\boldsymbol{\phi}_{h})\|_{0}^{2} + \frac{C}{2v + 2v_{\text{add}}(\boldsymbol{\phi}_{h})}$$

$$\|\boldsymbol{u}_{h}\|_{0} \|\mathbb{D}(\boldsymbol{u}_{h})\|_{0} \|\mathbb{D}(\boldsymbol{\eta})\|_{0}^{2}.$$

Collecting terms gives

$$\frac{1}{2} \frac{d}{dt} \| \boldsymbol{\phi}_{h} \|_{0}^{2} + \frac{2v + 2v_{\text{add}}(\boldsymbol{\phi}_{h})}{4} \| \mathbb{D}(\boldsymbol{\phi}_{h}) \|_{0}^{2} \\
\leq \left[\frac{C}{2v + 2v_{\text{add}}(\boldsymbol{\phi}_{h})} \| \partial_{t} \boldsymbol{\eta} \|_{X^{*}}^{2} + (8v + 8v_{\text{add}}(\boldsymbol{\eta})) \| \mathbb{D}(\boldsymbol{\eta}) \|_{0}^{2} \\
+ \frac{C}{2v + 2v_{\text{add}}(\boldsymbol{\phi}_{h})} \| p - \lambda_{h} \|_{0}^{2} + 8v_{\text{T}} \| (I - P_{L_{H}}) \mathbb{D}(\boldsymbol{u}) \|_{0}^{2} \\
+ \frac{C}{2v + 2v_{\text{add}}(\boldsymbol{\phi}_{h})} \left(\| \boldsymbol{\eta} \|_{0} \| \mathbb{D}(\boldsymbol{\eta}) \|_{0} \| \mathbb{D}(\boldsymbol{u}) \|_{0}^{2} \\
+ \| \boldsymbol{u}_{h} \|_{0} \| \mathbb{D}(\boldsymbol{u}_{h}) \|_{0} \| \mathbb{D}(\boldsymbol{\eta}) \|_{0}^{2} \right) \right] \\
+ \left[\frac{C}{(2v + 2v_{\text{add}}(\boldsymbol{\phi}_{h}))^{3}} \| \mathbb{D}(\boldsymbol{u}) \|_{0}^{4} \right] \| \boldsymbol{\phi}_{h} \|_{0}^{2}.$$

Applying the definition of the reduced Reynolds number (135) and using that $v_{\rm add}(\eta) \le v_{\rm T}$, see (129), finishes Step 3 of the proof:



$$\frac{d}{dt} \|\phi_{h}\|_{0}^{2} + \frac{(\operatorname{Re}_{\operatorname{red}}(\phi_{h}))^{-1}}{2} \|\mathbb{D}(\phi_{h})\|_{0}^{2}
\leq C \left[(\operatorname{Re}_{\operatorname{red}}(\phi_{h})) \|\partial_{t} \eta\|_{X^{*}}^{2} + (v + v_{T}) \|\mathbb{D}(\eta)\|_{0}^{2}
+ (\operatorname{Re}_{\operatorname{red}}(\phi_{h})) \|p - \lambda_{h}\|_{0}^{2} + v_{T} \|(I - P_{L_{H}})\mathbb{D}(\boldsymbol{u})\|_{0}^{2}
+ (\operatorname{Re}_{\operatorname{red}}(\phi_{h})) (\|\boldsymbol{\eta}\|_{0} \|\mathbb{D}(\boldsymbol{\eta})\|_{0} \|\mathbb{D}(\boldsymbol{u})\|_{0}^{2}
+ \|\boldsymbol{u}_{h}\|_{0} \|\mathbb{D}(\boldsymbol{u}_{h})\|_{0} \|\mathbb{D}(\boldsymbol{\eta})\|_{0}^{2} \right]
+ C(\operatorname{Re}_{\operatorname{red}}(\phi_{h}))^{3} \|\mathbb{D}(\boldsymbol{u})\|_{0}^{4} \|\phi_{h}\|_{0}^{2}. \tag{139}$$

To perform Step 4 of the proof, the $L^1(0,T)$ -regularity of the terms appearing in (139) has to be studied. Let $t \in (0,T]$ be arbitrary. One obtains with Poincaré's inequality (12), Korn's inequality (13), the Cauchy-Schwarz inequality, (131), and (137)

$$\int_{0}^{t} \| \boldsymbol{\eta}(\tau) \|_{0} \| \mathbb{D}(\boldsymbol{\eta})(\tau) \|_{0} \| \mathbb{D}(\boldsymbol{u})(\tau) \|_{0}^{2} d\tau
\leq C \int_{0}^{t} \| \mathbb{D}(\boldsymbol{\eta})(\tau) \|_{0}^{2} \| \mathbb{D}(\boldsymbol{u})(\tau) \|_{0}^{2} d\tau
\leq C \| \mathbb{D}(\boldsymbol{\eta}) \|_{L^{4}(0, t, L^{2})}^{2} \| \mathbb{D}(\boldsymbol{u}) \|_{L^{4}(0, t, L^{2})}^{2} < \infty.$$

Similarly it follows with Hölder's inequality, Lemma 4, and (137) that

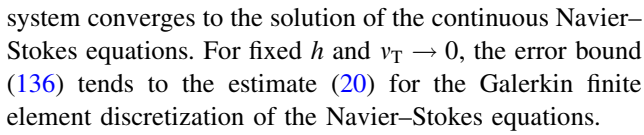
$$\int_{0}^{t} \|\mathbf{u}_{h}(\tau)\|_{0} \|\mathbb{D}(\mathbf{u}_{h})(\tau)\|_{0} \|\mathbb{D}(\mathbf{\eta})(\tau)\|_{0}^{2} d\tau
\leq \|\mathbf{u}_{h}\|_{L^{\infty}(0,t;L^{2})} \int_{0}^{t} \|\mathbb{D}(\mathbf{u}_{h})(\tau)\|_{0} \|\mathbb{D}(\mathbf{\eta})(\tau)\|_{0}^{2} d\tau
\leq \|\mathbf{u}_{h}\|_{L^{\infty}(0,t;L^{2})} \|\mathbb{D}(\mathbf{u}_{h})\|_{L^{2}(0,t;L^{2})} \|\mathbb{D}(\mathbf{\eta})\|_{L^{4}(0,t;L^{2})}^{2}
\leq C(\operatorname{Re}_{\operatorname{red}}(\mathbf{u}_{h}))^{1/2} (\|\mathbf{u}_{0,h}\|_{0}^{2} + \operatorname{Re}_{\operatorname{red}}(\mathbf{u}_{h})\|\mathbf{f}\|_{L^{2}(0,t;X^{*})}^{2})
\|\mathbb{D}(\mathbf{\eta})\|_{L^{4}(0,t;L^{2})}^{2} < \infty.$$

The $L^1(0,T)$ -regularity of the other terms is a direct consequence of (131), (16), (17) and (137).

Applying Gronwall's inequality and performing the last step of the proof are straightforward. \Box

Even if the constants in the error bound (136) do not depend on negative powers of v, there is an implicit dependency on such powers via the norms of u.

For the convergence of the error bound (136), the last term is the crucial one since in contrast to all other terms it does not possess a factor with the interpolation error $u - \tilde{u}_h$. As the mesh width $h \to 0$, the last term tends to zero if $v_T \to 0$ or if L_H tends to $\mathbb{D}(X)$. In both cases, the Galerkin finite element discretization (6) of the Navier–Stokes equations is recovered asymptotically. Otherwise, in particular if v_T and L_H are fixed and $h \to 0$, one cannot expect that the solution of the projection-based VMS



Let $(u,p) \in H^{k+1}(\Omega) \times H^k(\Omega)$ for all times, $k \ge 1$, and consider the pair of spaces P_k/P_{k-1} or Q_k/Q_{k-1} , $k \ge 2$. Neglecting in the following discussion the squares at the terms in (136), then the optimal order of convergence of the left-hand side of (136) is h^k . All interpolation errors on the right-hand side of (136) converge at least with h^k . The last term in the error bound contains the L^2 projection of the deformation tensor into L_H . Hence, it is of order H^k , where H is the mesh parameter connected with L_H . Hence, for not spoiling the convergence of the error bound, the additional viscosity has to be chosen such that $v_T = c(h/H)^{2k}$. In practice, e.g., if L_H is defined on the same grid as x_h , an explicit value for H is not available. But one can think of H being H = Ch with C > 1. In this case, v_T should be just a constant independent of the mesh width.

There is no improvement in the constant in the exponential, i.e., $\operatorname{Re}_{\operatorname{red}} = 2v^{-1}$, if there is a time t at which $v_{\operatorname{add}}(\phi_h(t)) = 0$. Using the definition (128) of v_{add} , one finds that this situation is equivalent to $\|P_{L_H}\mathbb{D}(\phi_h(t))\|_0^2 = \|\mathbb{D}(\phi_h(t))\|_0^2$ or equivalently, since P_{L_H} is the L^2 projection, to $(I - P_{L_H})\mathbb{D}(\mathbf{u}_h) = (I - P_{L_H})\mathbb{D}(\widetilde{\mathbf{u}}_h)$. (140)

That means, the small resolved scales of u_h and \tilde{u}_h are the same. However, this situation is unlikely for turbulent flows since these scales of u_h are considerably influenced by the model that is used for the unresolvable small scales whereas the interpolation \tilde{u}_h does not possess any information about this model, e.g., if \tilde{u}_h is defined by the Stokes projection. In this case, (140) is only likely if there are only large scales in the flow, which is not the case in turbulent flows.

From the mathematical point of view, the difficulty consists in the fact that the equations for laminar flows and turbulent flows are the same, namely the Navier–Stokes equations (1). Since the analysis is carried out for (1), it is not possible to distinguish between the two kinds of flows and the results must also hold for the case of laminar flows. For such flows, $v_{\rm add}(\phi_h(t))$ may vanish and the error estimate (20) of the Galerkin finite element method is recovered, in which the constants depend on v^{-1} .

8.5 Experience in Numerical Simulations

As already mentioned at the end of Sect. 8.1, the three-scale projection-based VMS method can be implemented as a one-grid method and as a two-grid method. For the simulation of turbulent flows, so far only the one-grid version was used.



The implementation of this version is described in detail in [93]. It turned out that choosing L_H to be a space of discontinuous tensors and using a basis that is L^2 orthogonal are essential for an efficient implementation. Both requirements can be easily fulfilled by choosing a basis of piecewise Legendre polynomials. Using a discontinuous space for L_H makes also sense from the point of view that the functions of L_H are L^2 projections of deformation tensors of finite element functions, which are usually discontinuous functions, too.

If L_H is the same space during the whole simulation, one has to assemble four additional matrices at the initial time. Three additional matrices have to be assembled every time the computed velocity u_h changes since these matrices contain the factor v_T and v_T is chosen usually to be a Smagorinsky-type model of form (114)–(116). After having assembled these matrices, one has to compute few sparse matrix-matrix products. The resulting sparse matrices have to be added to the matrices obtained in the Galerkin finite element discretization of the Navier-Stokes equations. Satisfying the two requirements on L_H stated above, it was shown in [93] that the resulting additional matrices possess the same sparsity pattern as the matrices from the Galerkin method. Thus, there is no need to change the sparsity structure of the matrices in an existing code for simulating the incompressible Navier-Stokes equations.

The three-scale projection-based VMS method was studied comprehensively at turbulent channel flow problems in [97, 98, 104]. Several options for choosing the projection space (which was always static in time) and the eddy viscosity model were compared. The simulations were always performed on quite coarse hexahedral grids with the $Q_2/P_1^{\rm disc}$ pair of finite element spaces. Often, the combination of choosing L_H to be the space of piecewise constant symmetric tensors, the large-small Smagorinsky model (114), δ as twice of the length of the shortest edge of the mesh cell, and $C_S = 0.01$ gave results which were among the best ones (and better than for the Smagorinsky LES model). In [104] it was shown that the projectionbased VMS method is less sensitive to the choice of the parameters in the Smagorinsky model than the Smagorinsky LES model. This property is due to the fact that the eddy viscosity model influences much less scales directly in the VMS approach compared with the LES method.

In [98] it was concluded that the choice of L_H has a much larger impact on the results compared with the choice of v_T . Based on this observation, a method for choosing the space L_H adaptively was proposed in [99]. The basic idea of this method consists in applying a lot of eddy viscosity in strongly turbulent regions and to switch off the eddy viscosity in laminar regions. The local turbulence intensity was estimated with the size of the local small resolved

scales $\|\mathbb{D}(\boldsymbol{u}_h) - \mathbb{G}_H\|_{L^2(K)}$. Based on these local values, four spaces were assigned to $L_H(K)$:

- $L_H(K) = \{\mathbb{O}\}$: the eddy viscosity is applied locally to all resolved scales,
- $\bullet \quad L_H(K) = P_0(K),$
- $\bullet \quad L_H(K) = P_1(K),$
- $L_H(K) = \mathbb{D}(X_h(K))$: the eddy viscosity is switched off locally.

The proof of concept for this method as well as a number of parameter studies for choosing the adaptive projection space can be found in [99]. It turned out that the projection space was chosen in the studied examples (turbulent channel flow, turbulent flow around a cylinder) as it was expected. With appropriately chosen parameters in the selection process for the local projection spaces, the results for the channel flow problem were better than with static spaces for L_H . For the turbulent flow around the cylinder, the results were similar. Every change of the space L_H requires a new assembling of all seven additional matrices.

The use of the three-scale projection-based VMS method with adaptive choice of the projection space on tetrahedral grids with the Bernardi–Raugel element [17] is described and studied in [100].

In [123], the three-scale projection-based VMS method was studied in combination with a grad-div stabilization term. Numerical studies for an isotropic turbulence example showed that the grad-div term dominates the VMS term.

Usually, the computing times of the projection-based VMS method with static projection space are a few percent longer than for the Smagorinsky LES model (but the results are more accurate). Applying the adaptive choice of the projection space leads usually again to somewhat longer computing times.

The three-scale projection-based VMS method with adaptively chosen projection space was used in the simulation of turbulent flows in population balance systems, modeling droplets in clouds, in [19, 20, 128]. In all cases, a good agreement of the simulated flow fields with experimental wind tunnel data were obtained.

For the projection-based VMS method that computes the projection as a post-processing step, it was observed in [106] that one obtains similar results for computing isotropic turbulence as for the method of form (113).

9 Three-Scale Algebraic VMS-Multigrid Methods

Algebraic VMS-multigrid methods aim at introducing an additional viscous term in the discrete momentum equation where the turbulent viscosity is directly applied to some



small resolved scales. This goal is the same as for the three-scale projection-based VMS method presented in Sect. 8. However, the scale separation into large and small resolved scales is performed in a completely different way in both methods.

The algebraic variational multiscale-multigrid method (AVM³) was proposed and applied to convection-dominated convection-diffusion problems in [64]. It was further developed and extended for application to turbulent flows in [63, 65]. Finally, the use of a more sophisticated turbulence model was proposed in [121].

9.1 Scale Separation by Plain Aggregation AMG

In AVM³, the construction of the small resolved scales uses an idea from AMG (Algebraic Multi-Grid) methods. The motivation for this approach comes from the desire to define the scale separation of the resolved scales without introducing another finite element space or another grid.

AMG methods are a proposal for transferring the ideas of geometric multigrid methods to problems where coarser geometric grids are not available, see [135]. To this end, a multilevel structure is constructed that is solely based on the matrix, which represents the problem on the given grid. In AMG methods, coarser levels, discrete operators on these levels, and transfer operators (restriction and prolongation) are constructed. For the scale separation in AVM³, only the construction of one coarse level and the corresponding transfer operators are needed. In AMG methods, transfer operators play a crucial role for the efficiency of solving the linear system of equations. There are several possibilities for constructing coarser levels in AMG methods, e.g., smoothed aggregation [127] or plain aggregation [138]. It is suggested for AVM³ in [64] to use the plain aggregation AMG to extract the small resolved scales. The scale separation based on the plain aggregation AMG will be described next.

The degrees of freedom on the given grid correspond to the rows of the given matrix A. In [63, 64], some root degree of freedom i is chosen and an aggregate is formed from the union of all degrees of freedom j for which the matrix entry a_{ij} does not vanish. Then, these degrees of freedom are removed from the list, a next root degree of freedom is chosen and this procedure is continued until all degrees of freedom belong to an aggregate. The aggregates represent the degrees of freedom on the next coarser level. Denoting the fine and the coarse level in terms of the mesh width h of the geometric grid corresponding to the fine level, then the aggregates on the coarse level were denoted in [63, 64] by 3h.

Operators for the restriction of the residual R_h^{3h} and the prolongation of functions P_{3h}^h have to be defined. To this end, consider the matrix \tilde{A} which differs from A only in the

way the Dirichlet boundary conditions are replaced with outflow boundary conditions. Let \tilde{A}_0 be a matrix whose columns span the kernel of \tilde{A} , i.e., it holds

$$\tilde{A}\tilde{A}_0 = 0. \tag{141}$$

The matrix on the coarse grid can be defined with the socalled Galerkin projection

$$\tilde{A}^{3h} = R_h^{3h} \tilde{A} P_{3h}^h.$$

Denoting the matrix which spans the kernel of \tilde{A}^{3h} by \tilde{A}_0^{3h} gives

$$0 = \tilde{A}^{3h} \tilde{A}_0^{3h} = R_h^{3h} \tilde{A} P_{3h}^h \tilde{A} P_{3h}^{3h} \tilde{A}_0^{3h}. \tag{142}$$

From (141) it follows that this equation is satisfied if

$$P_{3h}^{h}\tilde{A}_{0}^{3h}=\tilde{A}_{0}.$$

Based on this relation, the operators P_{3h}^h and \tilde{A}_0^{3h} can be determined simultaneously, for details see [64]. Finally, one sets

$$R_h^{3h} = (P_{3h}^h)^T$$
.

Note that these operators are linear operators between finite-dimensional spaces and thus they can be represented with matrices. For more details on the construction of the operators and further considerations on AMG methods, it is referred to [64].

The operator for defining the large scales is given by

$$S_h^{3h}: \boldsymbol{X}_h \to \boldsymbol{X}_h, \quad \boldsymbol{u}_{3h} = P_{3h}^h R_h^{3h} \boldsymbol{u}_h,$$

that is, in the first step u_h is restricted to the aggregates and in the second step, the representation of the aggregates in the finite element space is obtained. The small resolved scales are defined by

$$\mathbf{u}_h = \mathbf{u}_{3h} + \widehat{\mathbf{u}}_h \quad \Longleftrightarrow \quad \widehat{\mathbf{u}}_h = \mathbf{u}_h - \mathbf{u}_{3h}. \tag{143}$$

In AVM³ presented in [63], the definition of the aggregates is based on the matrix that contains the complete discretization of the velocity-velocity coupling of the Navier–Stokes equations, including terms coming from stabilizations.

9.2 Derivation

The derivation of Algebraic VMS-multigrid methods starts by considering first the two-scale decomposition of the velocity and pressure

$$\boldsymbol{u} = \boldsymbol{u}_h + \boldsymbol{u}', \quad p = p_h + p'$$

where $(u_h, p_h) \in X_h \times Y_h$. The same decomposition is applied to the corresponding test functions. After having neglected the equation with the unresolved scale test



functions, the equation with the test function from the finite element spaces remains

$$(\partial_{t}\boldsymbol{u}_{h},\boldsymbol{v}_{h}) + (2v\mathbb{D}(\boldsymbol{u}_{h}),\mathbb{D}(\boldsymbol{v}_{h})) + b(\boldsymbol{u}_{h},\boldsymbol{u}_{h},\boldsymbol{v}_{h}) + (\nabla \cdot \boldsymbol{u}_{h},q_{h})$$

$$- (\nabla \cdot \boldsymbol{v}_{h},p_{h})$$

$$= (\boldsymbol{f},\boldsymbol{v}_{h}) - \left[(\partial_{t}\boldsymbol{u}',\boldsymbol{v}_{h}) + (2v\mathbb{D}(\boldsymbol{u}'),\mathbb{D}(\boldsymbol{v}_{h})) + b(\boldsymbol{u}_{h},\boldsymbol{u}',\boldsymbol{v}_{h}) + b(\boldsymbol{u}',\boldsymbol{u}_{h},\boldsymbol{v}_{h}) + b(\boldsymbol{u}'\boldsymbol{u}',\boldsymbol{v}_{h}) - (\nabla \cdot \boldsymbol{v}_{h},p') \right] - (\nabla \cdot \boldsymbol{u}',q_{h}).$$

$$(144)$$

Consider now the terms in the brackets, and the splitting of the test function $v_h = v_{3h} + \hat{v}_h$. Then, the assumptions for three-scale VMS methods from Sect. 3.2 are taken into account:

- The direct impact of the unresolved scales and the large scales is negligible, i.e., all the terms in the brackets with test function v_{3h} are neglected.
- The direct impact of the unresolved scales onto the small resolved scales is modeled with a turbulence model, i.e., all terms in the brackets with test function ν

 ^ˆ

$$\nabla \cdot \left(C_{S} h^{2} \| \mathbb{D}(\widehat{\boldsymbol{u}}_{h}) \|_{F} \mathbb{D}(\widehat{\boldsymbol{u}}_{h}) \right) = \nabla \cdot \left(v_{T}(\widehat{\boldsymbol{u}}_{h}) \mathbb{D}(\boldsymbol{u})_{h} \right)$$

$$(145)$$

was used, see [63].

A realization of the AVM³ can be found so far only for the pair of finite element spaces Q_1/Q_1 for velocity and pressure on hexahedral grids. Thus, the introduction of an additional consistent stabilization was suggested in [63] which includes the PSPG stabilization term as a model of the last term on the right-hand side of (144)

$$(\nabla \cdot \boldsymbol{u}', q_h) \approx \sum_{K \in \mathcal{T}_h} (\partial_t \boldsymbol{u}_h - v \Delta \boldsymbol{u}_h + (\boldsymbol{u}_h \cdot \nabla) \boldsymbol{u}_h + \nabla p_h - \boldsymbol{f}, \tau_{m,K} \nabla q_h)_K$$

where $\{\tau_{m,K}\}_{K \in \mathcal{T}_h}$ denote the stabilization parameters. This additional term in the AVM³ formulation circumvents the violation of the discrete inf-sup condition in the case of equal-order pairs of velocity-pressure finite element spaces.

Inserting the models described above in (144), the AVM³ reads as follows: Find $u_h : [0, T] \to X_h$ and $p_h : (0, T] \to Y_h$ satisfying

$$(\hat{o}_{t}\boldsymbol{u}_{h},\boldsymbol{v}_{h}) + (2\boldsymbol{v}\mathbb{D}(\boldsymbol{u}_{h}),\mathbb{D}(\boldsymbol{v}_{h})) + b(\boldsymbol{u}_{h},\boldsymbol{u}_{h},\boldsymbol{v}_{h}) + (\nabla \cdot \boldsymbol{u}_{h},q_{h}) - (\nabla \cdot \boldsymbol{v}_{h},p_{h}) + (2\boldsymbol{v}_{T}(\hat{\boldsymbol{u}}_{h})\mathbb{D}(\hat{\boldsymbol{u}}_{h}),\mathbb{D}(\boldsymbol{v}_{h})) + \sum_{K \in \mathcal{T}_{h}} (\hat{o}_{t}\boldsymbol{u}_{h} - \boldsymbol{v}\Delta\boldsymbol{u}_{h} + (\boldsymbol{u}_{h} \cdot \nabla)\boldsymbol{u}_{h} + \nabla p_{h},\tau_{m,K}\nabla q_{h})_{K} = (\boldsymbol{f},\boldsymbol{v}_{h}) + \sum_{K \in \mathcal{T}_{h}} (\boldsymbol{f},\tau_{m,K}\nabla q_{h})_{K}.$$

$$(146)$$

The small resolved scales \hat{u}_h are computed with the help of the AMG approach sketched in Sect. 9.1.

In [121] it was proposed to use a more sophisticated turbulence model than the Smagorinsky model (145), a so-called multifractal model of u'. Multifractal modeling of unresolved scales is based on physical considerations, see [29, 30] for a detailed derivation. As final result, the unresolved velocity scales can be represented in the form

$$\mathbf{u}' = C_{\text{sgs}} \left(1 - \alpha^{-4/3} \right)^{-1/2} 2^{-2N/3} \left(2^{4N/3} - 1 \right)^{1/2} \widehat{\mathbf{u}}_h, \tag{147}$$

see [121]. In (147), C_{sgs} is a constant, the parameter α comes from the definition of the large scales $u^{\alpha h}$, i.e., $\alpha = 3$ in (143), and

$$N = \log_2\left(\frac{h_K}{\lambda_v}\right) \tag{148}$$

is the number of cascades, which depends on the local mesh width h_K and the viscous scale length λ_v . Model (147) is inserted in (144).

In [121], the value $C_{\rm sgs} = 0.25$ was used. The viscous scale length is about six times larger than the Kolmogorov scale, [121]. The following approximations were proposed in [121] [119, Section 4.2.5]

$$\frac{h_K}{\lambda_v} = C_v \left(\operatorname{Re}_K^h \right)^{3/4}$$

with $C_v = 1/12.3$ or $C_v = 1/11.2$ and

$$\operatorname{Re}_{K}^{h} = \frac{\|\mathbb{D}(\boldsymbol{u}_{h})\|_{F}h_{K}^{2}}{v}$$
 or $\operatorname{Re}_{K}^{h} = \frac{\|\boldsymbol{u}_{h}\|_{2}h_{K}}{v}$.

Thus, the value obtained on the right-hand side of (148) is generally not a natural number. In practice, the non-natural numbers which are computed with the right-hand side of (148) are used for N, which can be seen, e.g., in [121, Figure 11] or [119, Figure 4.7].

The multifractal modeling can be adapted to wall-bounded turbulent flows and it allows backscatter, see [119, 121] for details. To enhance numerical stability, it is proposed in [119, 121] to extend the multifractal model with residual-based stabilization terms, namely the SUPG term, the grad-div term, and the PSPG term. The arising method is called algebraic variational multiscale-multigrid-multifractal method, AVM⁴, in [119].

9.3 Relations to Other Methods

Since the algebraic VMS methods and the three-scale projection-based VMS method presented in Sect. 8 have the same principal goal, to apply a turbulent viscosity term directly only to some small resolved scales, their final



equations look similar, compare (146) and (113). The additional PSPG-type stabilization in (146) was only introduced because an equal-order pair of finite element spaces was used in [63].

9.4 Experience in Numerical Simulations

The algebraic VMS method AVM³ was compared in [63] with the two-scale residual-based VMS method from [10] presented in Sect. 4. A turbulent channel flow problem and a turbulent lid driven cavity problem were considered. The simulations were performed for Q_1/Q_1 finite elements. It was observed that the results with AVM³ were more accurate in several aspects and the simulations were somewhat more efficient. Only small differences in accuracy and efficiency between both VMS methods were observed in [65] for the simulation of a turbulent flow around a cylinder. Both VMS methods turned out to be clearly more efficient than the dynamic Smagorinsky model.

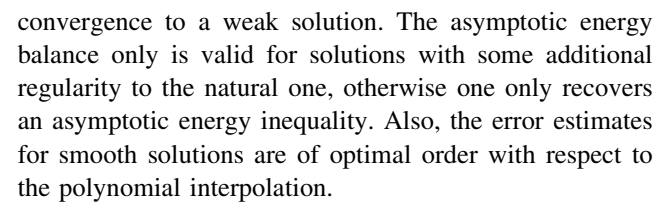
AVM⁴ was compared in [119] also with the two-scale residual-based VMS method from Sect. 4 and the dynamic Smagorinsky model. Again, the simulations were performed with the Q_1/Q_1 pair of finite element spaces. It turned out that the adaption of the method at the wall which is described in [119] is of great importance for computing accurate results. For turbulent channel flows substantial better solutions were obtained with AVM⁴ compared with the other methods. Also for the turbulent flow around a cylinder, AVM⁴ provided the best results near the cylinder. The computing times of AVM⁴ and the residual-based VMS method were similar.

The methods AVM³ and AVM⁴ were applied successfully also for the simulation of variable-density flows at low Mach numbers, see [66, 120].

10 An Unsteady Three-Scale Projection-Based VMS Method

This section studies the thee-scales projection-based VMS turbulence model for unsteady flows (34) with the turbulence modeling given by (38). It has a simplified structure with respect to residual-based VMS models, and equally applies to laminar and turbulent flows without further adaptation. Globally, it provides a good compromise between accuracy and computational complexity. Finally, it allows a thorough numerical analysis, parallel to that of Navier–Stokes equations, parallel to the analysis for the velocity deformation projection-based VMS model presented in Sect. 8.

Stability in the natural $L^2 \left(0,T; \boldsymbol{H}^1(\Omega)\right)$ and $L^\infty \left(0,T; \boldsymbol{L}^2(\Omega)\right)$ norms will be proved, so as weak



The analysis of more complex VMS methods, in particular of residual-based methods requires further adaptations of the analysis that is presented here. The subgrid terms have a very complex structure that includes convective interactions between large and small scales, thus setting serious technical problems just to prove stability. This field of numerical analysis is nowadays in progress.

10.1 Model Statement

The model stated in Sect. 6.4 is considered in its unsteady version. However, for simplicity of notation, a stable mixed method will be studied (see [35] for the analysis of the unsteady stabilized approximation with wall-laws), actually the Taylor–Hood pair of spaces: $X_h = [V_h^l(\Omega)]^d$, $Y_h = V_h^{l-1}(\Omega)$, $l \ge 2$, are considered, where it is assumed that the domain Ω is bounded and polygonal (when d=2) or polyhedral (when d=3). The family of couples of spaces (X_h, Y_h) satisfies the discrete inf-sup condition (9). Two kinds of spaces of small resolved scales are considered: the space \widehat{X}_h may be formed either by polynomials of degree smaller than those of X_h :

$$\widehat{X}_h = \left[V_h^k(\Omega) \right]^d, \quad \text{with} \quad 1 \le k < l, \tag{149}$$

or by polynomials of the same degree constructed on a coarser grid:

$$\widehat{X}_h = \left[V_H^l(\Omega) \right]^d, \tag{150}$$

where typically H = q h for some $q \ge 2$. A stable restriction operator $\rho_h : X \mapsto \widehat{X}_h$ satisfying optimal error estimates is associated to the method.

The following projection-based VMS model with Smagorinsky projection-based eddy viscosity model is considered: Find $(u_h, p_h) \in X_h \times Y_h$ such that

$$\frac{d}{dt}(\boldsymbol{u}_{h}, \boldsymbol{u}_{h}) + b_{s}(\boldsymbol{u}_{h}, \boldsymbol{u}_{h}, \boldsymbol{u}_{h}) + a(\boldsymbol{u}_{h}, \boldsymbol{u}_{h}) - (\nabla \cdot \boldsymbol{u}_{h}, p_{h})
+ c(\boldsymbol{u}_{h}; \boldsymbol{u}_{h}, \boldsymbol{u}_{h}) = \langle \boldsymbol{f}, \boldsymbol{u}_{h} \rangle,
(\nabla \cdot \boldsymbol{u}_{h}, q_{h}) = 0,
\boldsymbol{u}_{h}(0) = \boldsymbol{u}_{0,h},$$
(151)

for all $(u_h, q_h) \in X_h \times Y_h$, where $u_{0,h}$ is the Stokes projection of $u_h(0)$ on X_h and the form c is again given by (99)

$$c(\mathbf{u}_h; \mathbf{u}_h, \mathbf{v}_h) = (2\mathbf{v}_{\mathsf{T}}(\mathbf{u}_h) \, \mathbb{D}(\widehat{\mathbf{u}}_h), \, \mathbb{D}(\widehat{\mathbf{v}}_h)),$$



with

$$\widehat{\boldsymbol{u}}_h = (\boldsymbol{I} - \boldsymbol{\rho}_h)\boldsymbol{u}_h, \quad \widehat{\boldsymbol{v}}_h = (\boldsymbol{I} - \boldsymbol{\rho}_h)\boldsymbol{v}_h,$$

where I is the identity operator, and the eddy diffusion v_T is defined by the small-small (36) VMS-Smagorinsky modeling.

The role of the small scale (or high frequency) components $\hat{u}_h = (I - \rho_h)u_h$ that appear in the eddy diffusion term c is to absorb the energy consumed in the formation of small eddies in the inertial range (the unresolved scales). So the basic grid to build the space X_h should be fine enough to ensure that this space covers the large scales and an initial segment of the inertial range. Only the large scales are expected to be solved accurately.

In practice, a full space-time discretized model should be used. For the sake of simplicity, as a model problem the semi-implicit Euler discretization of (151) will be considered:

- *Initialization*. $\mathbf{u}_h^0 = \mathbf{u}_{0,h}$.
- *Iteration*. For n = 0, 1, ..., N 1: Assume that $\boldsymbol{u}_h^n \in \boldsymbol{X}_h$ is known. Compute $\boldsymbol{u}_h^{n+1} \in \boldsymbol{X}_h$, $p_h^{n+1} \in \boldsymbol{Y}_h$ such that for all $\boldsymbol{u}_h \in \boldsymbol{X}_h$, $q_h \in \boldsymbol{Y}_h$

$$\left(\frac{\boldsymbol{u}_{h}^{n+1} - \boldsymbol{u}_{h}^{n}}{\Delta t}, \boldsymbol{u}_{h}\right) + b_{s}(\boldsymbol{u}_{h}^{n}, \boldsymbol{u}_{h}^{n+1}, \boldsymbol{u}_{h}) + a(\boldsymbol{u}_{h}^{n+1}, \boldsymbol{u}_{h})
+ c(\boldsymbol{u}_{h}^{n+1}; \boldsymbol{u}_{h}^{n+1}, \boldsymbol{u}_{h}) - (p_{h}^{n+1}, \nabla \cdot \boldsymbol{u}_{h}) = \langle \boldsymbol{f}^{n+1}, \boldsymbol{u}_{h} \rangle,
(\nabla \cdot \boldsymbol{u}_{h}^{n+1}, q_{h}) = 0,$$
(152)

where $\Delta t = T/N$ for some integer number $N \ge 1$, and f^{n+1} is the average value of f in (t_n, t_{n+1}) .

The main hints for the analysis of model (152), following [38], are stated next. The main point is to prove the weak convergence of the solution provided by this model to a weak solution of the Navier–Stokes equations.

10.2 Stability and Convergence Analysis

To perform the numerical analysis of model (152) assume that the family of triangulations $\{T_h\}_{h>0}$ is regular.

Important properties of the form c defined by (99) are summarized in the following lemma.

Lemma 5

- (i) The form c is non-negative, in the sense that $c(\mathbf{w}; \mathbf{u}, \mathbf{u}) \ge 0$, for all $\mathbf{w}, \mathbf{u} \in H^1(\Omega)$.
- (ii) For any u_h , $w_h \in X_h$, $|c(u_h; u_h, w_h)| \le C_1 h^{2-d/2} \|\mathbb{D}(\widehat{u}_h)\|_0^2 \|\mathbb{D}(\widehat{w}_h)\|_0.$ (153)

(iii) For all
$$\mathbf{w}$$
, $\mathbf{u} \in \mathbf{W}^{1,3}(\Omega)$,

$$c(\mathbf{w}; \mathbf{w}, \mathbf{w} - \mathbf{u}) - c(\mathbf{u}; \mathbf{u}, \mathbf{w} - \mathbf{u}) \ge C_2 \underline{h}^2$$

$$\|\mathbb{D}(\widehat{\mathbf{w}} - \widehat{\mathbf{u}})\|_{0.3 \Omega}^3.$$
(154)

(iv) For all
$$u_h$$
, w_h , $z_h \in X_h$,
 $|c(w_h; w_h, z_h) - c(u_h; u_h, z_h)|$
 $\leq C_3 h^{2-d/2} (\|\mathbb{D}(w_h)\|_0 + \|\mathbb{D}(u_h)\|_0) \|\mathbb{D}(z_h)\|_0$
 $\|\mathbb{D}(w_h - u_h)\|_0$, (155)

where the constants C_1 , C_2 and C_3 only depend on d, Ω , and the aspect ratio of the family of triangulations.

Let *B* be a Banach space. Consider the following semidiscrete norms,

$$\|\boldsymbol{u}_h\|_{l^p(B)} = \left(\sum_{n=0}^N \Delta t \|\boldsymbol{u}_h^n\|_B^p\right)^{1/p}, \|\boldsymbol{u}_h\|_{l^\infty(B)} = \max_{n=0,\dots,N} \|\boldsymbol{u}_h^n\|_B,$$

where $\mathbf{u}_h = (\mathbf{u}_h^0, \mathbf{u}_h^1, \dots, \mathbf{u}_h^N) \in B^{N+1}$. Also, consider the piecewise in time function $\tilde{p}_h : (0,T) \to Y_h$ that takes the value p_h^n in the time interval (t_n, t_{n+1}) , and its primitive in time P_h ,

$$P_h(t) := \int_0^t \tilde{p}_h(s) \, ds.$$

To pass to the limit in the discrete formulation to a solution of the Navier–Stokes equations, it is sufficient to obtain an estimate of P_h instead of \tilde{p}_h , which is much simpler from the analytical point of view. Consider also the time increment of the velocity, $\tau_{\delta} u_h(t) = u_h(t+\delta) - u_h(t)$.

The stability of method (152) is given in the following theorem.

Theorem 6 Assume that the family of grids $\{T_h\}_{h>0}$ is regular, $f \in [H^{-1}(\Omega)]^d$, and $\mathbf{u}_0 \in L^2(\Omega)$. Then model (152) admits a unique solution, which satisfies the following estimates:

$$\|\boldsymbol{u}_{h}\|_{l^{\infty}(\boldsymbol{L}^{2}(\Omega))} + \sqrt{\nu} \|\boldsymbol{u}_{h}\|_{l^{2}(\boldsymbol{H}^{1}(\Omega))} + \underline{h} \|\mathbb{D}(\widehat{\boldsymbol{u}}_{h})\|_{l^{3}(\boldsymbol{L}^{3}(\Omega))}^{3/2}$$

$$\leq C_{1} \left(\|\boldsymbol{u}(0)\|_{0} + \frac{1}{\sqrt{\nu}} \|\boldsymbol{f}\|_{l^{2}(\boldsymbol{H}^{-1}(\Omega))} \right), \tag{156}$$

$$\|\tau_{\delta} \boldsymbol{u}_{h}(t)\|_{L^{2}(0,T-\delta;L^{2}(\Omega))}^{2} \le C_{2} \delta^{1/2}$$
, for $0 < \delta < T$, (157)

and

$$||P_h||_{l^{\infty}(L^2(\Omega))} \le C_2,$$
 (158)



for some constant $C_1 > 0$ independent of h, Δt and v, and some constant $C_2 > 0$ independent of h and Δt , where $\underline{h} = \min_{K \in \mathcal{T}_h} h_K$.

Proof The proof is performed in several steps.

Existence and uniqueness of solutions of discrete problem. Problem (152) can be written as

Find $u_h^{n+1} \in X_h$, $p_h^{n+1} \in Y_h$ such that for all $w_h \in X_h$, $q_h \in Y_h$,

$$\tilde{a}(\boldsymbol{u}_{h}^{n+1}, \boldsymbol{w}_{h}) + b_{s}(\boldsymbol{u}_{h}^{n}, \boldsymbol{u}_{h}^{n+1}, \boldsymbol{w}_{h}) + c(\boldsymbol{u}_{h}^{n+1}; \boldsymbol{u}_{h}^{n+1}, \boldsymbol{w}_{h})
- (\nabla \cdot \boldsymbol{w}_{h}, p_{h}^{n+1}) = \langle \tilde{\boldsymbol{f}}^{n+1}, \boldsymbol{w}_{h} \rangle,
(\nabla \cdot \boldsymbol{u}_{h}^{n+1}, q_{h}) = 0,$$

where $\tilde{a}(\boldsymbol{u}, \boldsymbol{w}) = \frac{1}{\Delta t}(\boldsymbol{u}, \boldsymbol{w}) + a(\boldsymbol{u}, \boldsymbol{w})$ and $\tilde{f}^{n+1} = f^{n+1} + \frac{\boldsymbol{u}_h^n}{\Delta t}$. The form \tilde{a} is an inner product on the space $\boldsymbol{H}_0^1(\Omega)$ that generates a norm equivalent to the \boldsymbol{H}^1 norm. The existence of a solution follows from Brouwer's fixed point theorem that uses the positiveness of form c and the inf-sup condition (9). The uniqueness of solutions is a consequence of the well-posedness of the discrete problem (see [38, Chapter 9]).

Velocity estimates. Setting $w_h = u_h^{n+1}$ and $q_h = p_h^{n+1}$ in (152) yields

$$\frac{1}{2} \|\boldsymbol{u}_{h}^{n+1}\|_{0}^{2} + \frac{1}{2} \|\boldsymbol{u}_{h}^{n+1} - \boldsymbol{u}_{h}^{n}\|_{0}^{2} + \Delta t \, v \|\mathbb{D}(\boldsymbol{u}_{h}^{n+1})\|_{0}^{2} + C_{S}^{2} \, \underline{h}^{2} \, \Delta t \\
\|\mathbb{D}(\widehat{\boldsymbol{u}}_{h}^{n+1})\|_{0,3,\Omega}^{3} \leq \frac{1}{2} \|\boldsymbol{u}_{h}^{n}\|_{0}^{2} + \Delta t \, \langle \boldsymbol{f}^{n+1}, \boldsymbol{u}_{h}^{n+1} \rangle .$$
(159)

Using Young's inequality one obtains

$$\|\boldsymbol{u}_{h}^{n+1}\|_{0}^{2} + \|\boldsymbol{u}_{h}^{n+1} - \boldsymbol{u}_{h}^{n}\|_{0}^{2} + \Delta t \, v\|\mathbb{D}(\boldsymbol{u}_{h}^{n+1})\|_{0}^{2} + 2 \, C_{S}^{2} \, \underline{h}^{2} \, \Delta t$$

$$\|\mathbb{D}(\widehat{\boldsymbol{u}}_{h}^{n+1})\|_{0,3,\Omega}^{3} \leq \|\boldsymbol{u}_{h}^{n}\|_{0}^{2} + 4\Delta t v^{-1} \|\boldsymbol{f}^{n+1}\|_{\boldsymbol{H}^{-1}}^{2}.$$
(160)

Then, if $k \le N - 1$, it follows that

$$\|\boldsymbol{u}_{h}^{k+1}\|_{0}^{2} + \sum_{n=0}^{k} \|\boldsymbol{u}_{h}^{n+1} - \boldsymbol{u}_{h}^{n}\|_{0}^{2} + v \, \Delta t \sum_{n=0}^{k} \|\mathbb{D}(\boldsymbol{u}_{h}^{k+1})\|_{0}^{2} + 2 \, C_{S}^{2} \, \underline{h}^{2} \, \Delta t \sum_{n=0}^{k} \|\mathbb{D}(\boldsymbol{u}_{h}^{k+1})\|_{0,3,\Omega}^{3} \leq \|\boldsymbol{u}_{h}^{0}\|_{0}^{2} + 4 \, \Delta t \, v^{-1}$$

$$\times \sum_{n=0}^{k} \|\boldsymbol{f}^{n+1}\|_{\boldsymbol{H}^{-1}}^{2}.$$

$$(161)$$

Estimate (156) follows, because $\|\boldsymbol{u}_{0,h}\|_0 \le \|\boldsymbol{u}(0)\|_0$.

Velocity time increment estimates. Problem (152) is restated in the form

$$(\hat{o}_{t}\boldsymbol{u}_{h}(t),\boldsymbol{w}_{h}) + b_{s}(\tilde{\boldsymbol{u}}_{h}(t-\Delta t),\tilde{\boldsymbol{u}}_{h}(t),\boldsymbol{w}_{h}) + a(\tilde{\boldsymbol{u}}_{h}(t),\boldsymbol{w}_{h}) + c(\tilde{\boldsymbol{u}}_{h}(t);\tilde{\boldsymbol{u}}_{h},\boldsymbol{w}_{h}) - (\tilde{p}_{h}(t),\nabla\cdot\boldsymbol{w}_{h}) = \langle \tilde{\boldsymbol{f}}_{h}(t),\boldsymbol{w}_{h}\rangle (\nabla\cdot\tilde{\boldsymbol{u}}_{h}(t),q_{h}) = 0,$$

$$(162)$$

a.e. in [0,T], where $\boldsymbol{u}_h:[0,T]\to\boldsymbol{X}_h$ is the piecewise linear-in-time function that takes the value \boldsymbol{u}_h^n at $t=t_n=n\Delta t;\; \tilde{\boldsymbol{u}}_h:(-\Delta t,T)\to\boldsymbol{X}_h$ is the piecewise constant function that takes the value \boldsymbol{u}_h^{n+1} on (t_n,t_{n+1}) , and $\tilde{\boldsymbol{u}}_h(t)=\boldsymbol{u}_h^0$ in $(-\Delta t,0);$ and $\tilde{p}_h,\tilde{\boldsymbol{f}}_h:(0,T)\to\boldsymbol{Y}_h$ respectively are the piecewise constant-in-time functions that take the value p_h^n and \boldsymbol{f}^{n+1} in the time interval (t_n,t_{n+1}) . Integrating (162) in $(t,t+\delta)$ for $t\in[0,T-\delta]$ gives

$$(\tau_{\delta} \boldsymbol{u}_{h}(t), \boldsymbol{w}_{h}) = \int_{t}^{t+\delta} \langle \mathcal{F}_{h}(s), \boldsymbol{w}_{h} \rangle ds + \int_{t}^{t+\delta} (\tilde{p}_{h}(s), \nabla \cdot \boldsymbol{w}_{h}) dt,$$

$$(163)$$

where

$$\langle \mathcal{F}_h(s), \mathbf{w} \rangle = -b_s(\tilde{\mathbf{u}}_h(s - \Delta t), \tilde{\mathbf{u}}_h(s), \mathbf{w}) - a(\tilde{\mathbf{u}}_h(s), \mathbf{w}) - c(\tilde{\mathbf{u}}_h(s); \tilde{\mathbf{u}}_h(s), \mathbf{w}) + \langle \tilde{\mathbf{f}}_h(s), \mathbf{w} \rangle, \text{ for all } \mathbf{w} \in \mathbf{H}_0^1(\Omega).$$

Using $(\nabla \cdot \tau_{\delta} \boldsymbol{u}_h(t), \tilde{p}_h(s)) = 0$ yields

$$\int_0^{T-\delta} \|\tau_{\delta} \boldsymbol{u}_h(t)\|_0^2 dt = \int_0^{T-\delta} \int_t^{t+\delta} \langle \mathcal{F}_h(s), \tau_{\delta} \boldsymbol{u}_h(t) \rangle ds dt,$$
(164)

From estimate (153), it follows that

$$\|\mathcal{F}_{h}(s)\|_{\boldsymbol{H}^{-1}} \leq C \Big[1 + \|\tilde{\boldsymbol{u}}_{h}(s - \Delta t)\|_{1}^{2} + (1 + Ch^{2}) \|\mathbb{D}(\tilde{\boldsymbol{u}}_{h}(s))\|_{0}^{2} + \|\mathbb{D}(\tilde{\boldsymbol{u}}_{h}(s))\|_{0} + \|\tilde{\boldsymbol{f}}_{h}(s)\|_{\boldsymbol{H}^{-1}} \Big].$$

Thanks to the stability estimate (156), one deduces that $\mathcal{F}_h \in L^1(\mathbf{H}^{-1})$, and $\|\mathcal{F}_h\|_{L^1(\mathbf{H}^{-1})} \leq C$ for some constant C > 0 independent of h and Δt . By Fubini's theorem, the right-hand side of (164) is estimated by

$$\int_{0}^{T-\delta} \|\tau_{\delta} \boldsymbol{u}_{h}(t)\|_{0}^{2} dt = \left| \int_{0}^{T} \int_{s-\delta}^{s} \langle \mathcal{F}_{h}(s), \widetilde{\tau_{\delta} \boldsymbol{u}_{h}}(t) \rangle dt ds \right|$$

$$\leq \delta^{1/2} \|\mathcal{F}_{h}\|_{L^{1}(\boldsymbol{H}^{-1})} \|\mathbb{D}(\tau_{\delta} \boldsymbol{u}_{h})\|_{L^{2}(\boldsymbol{H}^{1})}$$

$$\leq C\delta^{1/2} \|\boldsymbol{u}_{h}\|_{L^{2}(\boldsymbol{H}^{1})} \leq C\delta^{1/2},$$

where \tilde{v} denotes the extension by zero outside $[0, T - \delta]$ of a function v. Then (157) follows.

Estimate of the primitive of the pressure. Let $w_h \in X_h$. Equation (162) yields



$$(P_h(t), \mathbf{w}_h) = (\mathbf{u}_h(t) - \mathbf{u}_h^0, \mathbf{w}_h) - \int_0^t \langle \mathcal{F}_h(s), \mathbf{w}_h \rangle \, ds$$

$$\leq C \left(\|\mathbf{u}_h\|_{l^{\infty}(L^2)} + \|\mathbf{u}_h^0\|_0 + \|\mathcal{F}\|_{L^1(\mathbf{H}^{-1})} \right)$$

$$\|\mathbf{w}_h\|_1 \leq C \|\mathbf{w}_h\|_1.$$

Estimate (158) follows from the inf-sup condition (9). \square

The convergence of model (152) to the Navier–Stokes equations is based upon the stability estimates from Theorem 6, combined with some compactness properties of injections between parabolic spaces. To state them, let consider the Nikolskii spaces

$$N^{r,p}(0,T;B) = \{ f \in L^p(0,T;B) \text{ such that }$$
$$\|f\|_{\tilde{N}^{r,p}} < +\infty \},$$

for $r \in [0, 1], p \in [0, \infty]$ with

$$||f||_{\tilde{N}^{r,p}} = \sup_{\delta > 0} \frac{1}{\delta^r} ||\tau_{\delta}f||_{L^p(0,T-\delta;B)}.$$

The space $N^{r,p}(0,T;B)$ is a Banach space if it is endowed with the norm

$$||f||_{N^{r,p}(0,T;B)} = ||f||_{L^p(0,T;B)} + ||f||_{\tilde{N}^{r,p}}.$$

The following Simon's compactness theorem holds (cf. [132]).

Lemma 6 Let X, B, Y be Banach spaces such that $X \hookrightarrow B \hookrightarrow Y$ where the injection $X \hookrightarrow B$ is compact. Then the injection

$$L^{p}(0,T;X) \cap N^{r,p}(0,T;Y) \hookrightarrow L^{p}(0,T;B)$$
 with $0 < r < 1, 1 \le p \le +\infty$

is compact.

Observe that by estimates (156) and (157) the functions u_h are uniformly bounded in $N^{1/4,2}(L^2)$. Now, the convergence theorem can be stated.

Theorem 7 Assume that the family of triangulations $\{T_h\}_{h>0}$ is regular, $f \in L^2(\mathbf{H}^{-1})$ and $\mathbf{u}_0 \in \mathbf{L}^2(\Omega)$. Then the sequence $\{(\mathbf{u}_h, p_h)\}_{h>0}$ provided by method (152) contains a subsequence that is weakly convergent in $L^2(\mathbf{H}^1) \times H^{-1}(\mathbf{L}^2)$ to a weak solution (\mathbf{u}, p) of the unsteady Navier–Stokes equations.

Proof The proof is performed in several steps.

Extraction of convergent subsequences. By estimates (156) and (157), the functions u_h are uniformly bounded in $L^2(0,T;\boldsymbol{H}^1)$, in $L^\infty(0,T;\boldsymbol{L}^2)$, and in $N^{1/4,2}(0,T;\boldsymbol{L}^2)$. As the injection $H^1(\Omega) \hookrightarrow L^r(\Omega)$ is compact for $1 \le r < 2d/(d-2)$, by Lemma 6 with $X = \boldsymbol{H}^1(\Omega)$, $B = L^r$, and $Y = \boldsymbol{L}^2(\Omega)$, one deduces that the sequence $\{u_h\}_{h>0}$ is compact in

 $L^2(0,T;\boldsymbol{L}^r)$. Then the sequence $\{\boldsymbol{u}_h\}_{h>0}$ contains a subsequence (that is denoted in the same way) which is strongly convergent in $L^2(0,T;\boldsymbol{L}^r)$, weakly in $L^2(0,T;\boldsymbol{H}^1)$, and weakly-* in $L^\infty(0,T;\boldsymbol{L}^2)$ to some \boldsymbol{u} . Also, by estimate (158), the sequence $\{P_h\}_{h>0}$ is uniformly bounded in $L^\infty(0,T;L^2)$. Then it contains a subsequence (that can be assumed to be a subsequence of the preceding one) which is weakly-* convergent in $L^\infty(0,T;L^2)$ to some P. It will be proved in the sequel that the pair $(\boldsymbol{u},\partial_t P)$ is a weak solution of Navier–Stokes equations.

Limit of the momentum conservation equation. The momentum conservation equation in (162) may be rewritten as

$$-\int_{0}^{T} (\boldsymbol{u}_{h}(t), \boldsymbol{w}_{h}) \varphi'(t) dt - (\boldsymbol{u}_{h0}, \boldsymbol{w}_{h}) \varphi(0)$$

$$+\int_{0}^{T} b_{s}(\tilde{\boldsymbol{u}}_{h}^{-}(t), \tilde{\boldsymbol{u}}_{h}(t), \boldsymbol{w}_{h}) \varphi(t) dt$$

$$+\int_{0}^{T} a(\tilde{\boldsymbol{u}}_{h}(t), \boldsymbol{w}_{h}) \varphi(t) dt$$

$$+\int_{0}^{T} c(\tilde{\boldsymbol{u}}_{h}(t); \tilde{\boldsymbol{u}}_{h}(t), \boldsymbol{w}_{h}) \varphi(t) dt$$

$$+\int_{0}^{T} (P_{h}(t), \nabla \cdot \boldsymbol{w}_{h}) \varphi'(t) dt$$

$$=\int_{0}^{T} \langle \tilde{\boldsymbol{f}}_{h}(t), \boldsymbol{w}_{h} \rangle \varphi(t) dt, \quad \text{for all } \boldsymbol{w} \in \boldsymbol{X}_{h},$$

for any function $\varphi \in \mathcal{D}([0,T])$ such that $\varphi(T) = 0$, where $\tilde{\boldsymbol{u}}_h^-: (0,T) \to \boldsymbol{X}_h$ is the piecewise constant in time function that takes the value \boldsymbol{u}_h^n on (t_n,t_{n+1}) .

By estimate (156) the sequences $\tilde{\boldsymbol{u}}_h$ and $\tilde{\boldsymbol{u}}_h^-$ are also uniformly bounded in $L^2(0,T;\boldsymbol{H}^1)$ and in $L^\infty(0,T;\boldsymbol{L}^2)$. Then, each one of them contains a subsequence weakly convergent in $L^2(0,T;\boldsymbol{H}^1)$ and weakly-* convergent in $L^\infty(0,T;\boldsymbol{L}^2)$ to some limits. But both limits should be equal to \boldsymbol{u} since

$$\max\{\|\boldsymbol{u}_{h} - \tilde{\boldsymbol{u}}_{h}\|_{L^{2}(0,T;\boldsymbol{L}^{2})}^{2}, \|\boldsymbol{u}_{h} - \tilde{\boldsymbol{u}}_{h}^{-}\|_{L^{2}(0,T;\boldsymbol{L}^{2})}^{2}\}$$

$$\leq \Delta t \|\boldsymbol{u}_{0}\|_{1,2,\Omega} + \frac{\Delta t}{2\nu} \|\boldsymbol{f}\|_{L^{2}(0,T;\boldsymbol{H}^{-1})}^{2}.$$

Time derivative term. Let $\mathbf{w} \in \mathbf{H}_0^1(\Omega)$. Due to the approximation properties of Lagrange finite element spaces, there exists a sequence $\{\mathbf{w}_h\}_{h>0}$ such that $\mathbf{w}_h \in \mathbf{X}_h$ that converges to \mathbf{w} in \mathbf{X}_h in $\mathbf{H}_0^1(\Omega)$. Observe that if $\mathbf{z} \in L^{\infty}(0,T;\mathbf{L}^2) \cap L^2(0,T;\mathbf{L}^4)$, then by Hölder's inequality

$$||z||_{L^3(0,T;\boldsymbol{L}^3)} \le ||z||_{L^\infty(0,T;\boldsymbol{L}^2)}^{1/3} ||z||_{L^2(0,T;\boldsymbol{L}^4)}^{2/3}.$$

Then, the sequences $\tilde{\pmb{u}}_h^-$ and $\tilde{\pmb{u}}_h$ strongly converge to \pmb{u} in $L^3(0,T;\pmb{L}^3)$ and



$$\lim_{(h,\Delta t)\to 0} \int_0^T (\boldsymbol{u}_h(t), \boldsymbol{w}_h) \varphi'(t) dt = \int_0^T (\boldsymbol{u}(t), \boldsymbol{w}) \varphi'(t) dt.$$

Convection term. Integration by parts yield

$$b_s(\tilde{\boldsymbol{u}}_h^-(t), \tilde{\boldsymbol{u}}_h(t), \boldsymbol{w}_h) = (\tilde{\boldsymbol{u}}_h^-(t) \cdot \nabla \tilde{\boldsymbol{u}}_h(t), \boldsymbol{w}_h) \\ -\frac{1}{2} \left(\nabla \cdot \tilde{\boldsymbol{u}}_h^-(t), \boldsymbol{w}_h \cdot \tilde{\boldsymbol{u}}_h(t) \right) \text{ a.e. in } (0, T).$$

As $\tilde{\boldsymbol{u}}_h^-$ and $\tilde{\boldsymbol{u}}_h$ strongly converge to \boldsymbol{u} in $L^3(0,T;\boldsymbol{L}^3)$, and weakly in $L^2(0,T;\boldsymbol{H}^1)$, both terms pass to the limit and

$$\lim_{(h,\Delta t)\to 0} \int_0^T b_s(\tilde{\boldsymbol{u}}_h^-(t), \tilde{\boldsymbol{u}}_h(t), \boldsymbol{w}_h) \varphi(t) dt$$
$$= \int_0^T b_s(\boldsymbol{u}(t), \boldsymbol{u}(t), \boldsymbol{w}) \varphi(t) dt.$$

Diffusion terms. As $\tilde{u}_h(t)$ is weakly convergent to u in $L^2(0,T; \mathbf{H}^1)$, it holds

$$\lim_{(h,\Delta t)\to 0} \int_0^T a(\tilde{\boldsymbol{u}}_h(t),\boldsymbol{w}_h) \, \varphi(t) \, dt = \int_0^T a(\boldsymbol{u}(t),\boldsymbol{w}) \, \varphi(t) \, dt.$$

Also, $\lim_{(h,\Delta t)\to 0} \int_0^T c(\tilde{\boldsymbol{u}}_h(t); \tilde{\boldsymbol{u}}_h(t), \boldsymbol{w}_h) \, \varphi(t) \, dt = 0$. This statement follows from (153), that yields

$$\begin{split} & \left| \int_{0}^{T} c(\tilde{\boldsymbol{u}}_{h}(t); \tilde{\boldsymbol{u}}_{h}(t), \boldsymbol{w}_{h}) \, \varphi(t) \, dt \right| \\ & \leq C \, h^{2-d/2} \, \int_{0}^{T} \| \mathbb{D}(\boldsymbol{u}_{h}(t)) \|_{0}^{2} \| \mathbb{D}(\boldsymbol{w}_{h}) \|_{0} \, |\varphi(t)| \, dt \\ & \leq C \, h^{2-d/2} \, \| \mathbb{D}(\boldsymbol{u}_{h}) \|_{L^{2}(0,T;L^{2})}^{2} \, \| \mathbb{D}(\boldsymbol{w}_{h}) \|_{0} \, \| \varphi \|_{L^{\infty}(0,T)}. \end{split}$$

Pressure term. As $\nabla \cdot \mathbf{w}_h(\mathbf{x}) \varphi'(t)$ is strongly convergent in $L^2(0,T;L^2)$ to $\nabla \cdot \mathbf{w}(\mathbf{x}) \varphi'(t)$ and $(P_h)_{h>0}$ is weakly-* convergent in $L^{\infty}(0,T;L^2)$ to P, it follows that

$$\lim_{(h,\Delta t)\to 0} \int_0^T (P_h, \nabla \cdot \boldsymbol{w}_h(\boldsymbol{x})) \, \varphi'(t) \, dt$$
$$= \int_0^T (P, \nabla \cdot \boldsymbol{w}(\boldsymbol{x})) \, \varphi'(t) \, dt.$$

Limit of the continuity equation. Consider some function $q \in L_0^2(\Omega)$, and some interpolate $q_h \in Y_h$, strongly convergent in $L_0^2(\Omega)$ to q. As u_h is weakly convergent to u in $H^1(\Omega)$, it follows that

$$\int_0^T (\nabla \cdot \boldsymbol{u}(t), q) \, \varphi(t) \, dt$$

$$= \lim_{(h,\Delta t) \to 0} \int_0^T (\nabla \cdot \boldsymbol{u}_h(t), q_h) \, \varphi(t) \, dt = 0.$$

Conclusion. As a consequence of the preceding analysis, \boldsymbol{u} belongs to $L^2(0,T;\boldsymbol{H}_0^1)\cap L^\infty(0,T;\boldsymbol{L}^2)$, P belongs to $L^\infty(0,T;\boldsymbol{L}^2)$, and the pair (\boldsymbol{u},P) satisfies

$$-\int_{0}^{T} (\boldsymbol{u}(t), \boldsymbol{w}) \varphi'(t) dt - (\boldsymbol{u}_{0}, \boldsymbol{w}) \varphi(0)$$

$$+ \int_{0}^{T} [b_{s}(\boldsymbol{u}(t), \boldsymbol{u}(t), \boldsymbol{w}) dt + a(\boldsymbol{u}(t), \boldsymbol{w})] \varphi(t) dt$$

$$+ \int_{0}^{T} (P(t), \nabla \cdot \boldsymbol{w}) \varphi'(t) dt = \int_{0}^{T} \langle \boldsymbol{f}(t), \boldsymbol{w} \rangle \varphi(t) dt.$$
(166)

for all $\mathbf{w} \in H_0^1(\Omega)$, $\varphi \in \mathcal{D}([0,T])$. Thus, the pair $(\mathbf{u}, \partial_t P)$ is a weak solution of the Navier–Stokes equations. As P_h weakly converges to P in $L^2(0,T;L^2)$, then $p_h = \partial_t P_h$ weakly converges to $p = \partial_t P$ in $H^{-1}(0,T;L^2)$.

The above proof shows that the eddy diffusion terms vanish in the weak limit, and a standard weak solution of Navier–Stokes equations is recovered. No eddy diffusion concentration effects take place in the weak limit.

10.3 Error Estimates

Let B_h be a sub-space of a Banach space B. Given $u \in C^0([0,T],B)$, denote

$$d_{l^{p}(B)}(\boldsymbol{u}, B_{h}) = \left[\Delta t \sum_{n=0}^{N} d_{B}(\boldsymbol{u}(t_{n}), B_{h})^{p} \right]^{1/p},$$

$$d_{l^{\infty}(B)}(\boldsymbol{u}, B_{h}) = \max_{n=0,\dots,N} d_{B}(\boldsymbol{u}(t_{n}), B_{h}).$$

Theorem 8 Assume that the family of grids $\{T_h\}_{h>0}$ is regular, that the data satisfy $\mathbf{f} \in C^0(0,T;L^2)$, $\partial_t \mathbf{f} \in L^2(0,T;\mathbf{H}^{-1})$, $\mathbf{u}_0 \in \mathbf{W}^{1,3}(\Omega)$ and that the unsteady Navier–Stokes equations (166) admit a solution $(\mathbf{u},p) \in C^0(0,T;\mathbf{W}^{1,3}) \times C^0(0,T;L^2)$ such that $\partial_t^2 \mathbf{u} \in L^2(0,T;L^2)$. Then the sequence $\{(\mathbf{u}_h,p_h)\}_{h>0}$ given by the discrete projection-based VMS model (152) satisfies the error estimates

$$\|\boldsymbol{u} - \boldsymbol{u}_h\|_{l^{\infty}(\boldsymbol{L}^2)} + \|\boldsymbol{u} - \boldsymbol{u}_h\|_{l^2(\boldsymbol{H}^1)} \leq M(h, \Delta t) + Cd_{l^{\infty}(\boldsymbol{L}^2)}(\boldsymbol{u}, \boldsymbol{X}_h),$$
(167)

$$||P - P_h||_{l^{\infty}(L^2)} \le M(h, \Delta t) + C d_{l^{\infty}(L^2)}(P, Y_h),$$
 (168)

where

$$M(h, \Delta t) = C \left[\Delta t + d_0(\mathbf{u}(0), \mathbf{X}_h) + \frac{1}{\Delta t} d_{l^2(L^2)}(\mathbf{u}, \mathbf{X}_h) + d_{l^2(H^1)}(\mathbf{u}, \mathbf{X}_h) + d_{l^2(L^2)}(p, Y_h) + h^{2-d/2} \left(d_{l^4(H^1)}(\mathbf{u}, \mathbf{X}_h)^2 + d_{l^4(H^1)}(\mathbf{u}, \widehat{\mathbf{X}}_h)^2 \right) \right],$$
(169)

and C is a constant independent of h and Δt , increasing with T.



Proof As $\boldsymbol{u}(t_n)$ is divergence-free, its Stokes projection, defined by (15), satisfies the estimate $\|\mathbb{D}(\boldsymbol{u}(t_n) - \overline{\boldsymbol{v}}_h^n)\|_0 \le C \, d_{H^1}(\boldsymbol{u}(t_n), \boldsymbol{X}_h)$. Let \overline{p}_h^n also denote the $L^2(\Omega)$ orthogonal projection of $p(t_n)$ on Y_h . Define the errors in velocity and pressure by $\boldsymbol{e}_h^n = \boldsymbol{u}_h^n - \overline{\boldsymbol{v}}_h^n$, $\lambda_h^n = p_h^n - \overline{p}_h^n$. Due to the regularity of data and solution, the unsteady Navier–Stokes equations (166) yield

$$(\partial_{t}\mathbf{u}(t),\mathbf{w}) + a(\mathbf{u}(t),\mathbf{w}) + b_{s}(\mathbf{u}(t),\mathbf{u}(t),\mathbf{w}) - (\nabla \cdot \mathbf{w}, p(t))$$

$$= \langle \mathbf{f}(t), \mathbf{w} \rangle (\nabla \cdot \mathbf{u}(t), q) = 0, \mathbf{u}(0) = \mathbf{u}_{0},$$
(170)

for all $\mathbf{w} \in \mathbf{H}_0^1(\Omega)$, $q \in L_0^2(\Omega)$, for all $t \in [0, T]$. Subtracting term by term (152) from (170) at $t = t_{n+1}$ one obtains the error equation: for all $\mathbf{w}_h \in \mathbf{X}_h$, $q_h \in \mathbf{Y}_h$,

$$\left(\frac{\boldsymbol{e}_{h}^{n+1} - \boldsymbol{e}_{h}^{n}}{\Delta t}, \boldsymbol{w}_{h}\right) + a(\boldsymbol{e}_{h}^{n+1}, \boldsymbol{w}_{h}) + b_{s}(\boldsymbol{u}_{h}^{n}, \boldsymbol{u}_{h}^{n+1}, \boldsymbol{w}_{h})
- b_{s}(\overline{\boldsymbol{v}}_{h}^{n}, \overline{\boldsymbol{u}}_{h}^{n+1}, \boldsymbol{w}_{h}) - (\nabla \cdot \boldsymbol{w}_{h}, \lambda_{h}^{n+1}) + c(\boldsymbol{u}_{h}^{n+1}; \boldsymbol{u}_{h}^{n+1}, \boldsymbol{w}_{h})
- c(\overline{\boldsymbol{u}}_{h}^{n+1}; \overline{\boldsymbol{u}}_{h}^{n+1}, \boldsymbol{w}_{h}) = \langle \boldsymbol{\varepsilon}_{h}^{n+1}, \boldsymbol{w}_{h} \rangle, (\nabla \cdot \boldsymbol{e}_{h}^{n+1}, q_{h}) = 0,$$
(171)

where $\boldsymbol{\varepsilon}_h^{n+1} \in \boldsymbol{H}^{-1}$ is the consistency error, defined by

$$\langle \boldsymbol{\varepsilon}_{h}^{n+1}, \boldsymbol{w} \rangle = \left(\widehat{o}_{t} \boldsymbol{u}(t_{n+1}) - \frac{\overline{\boldsymbol{u}}_{h}^{n+1} - \overline{\boldsymbol{v}}_{h}^{n}}{\Delta t}, \boldsymbol{w} \right)$$

$$+ b_{s}(\boldsymbol{u}(t_{n+1}), \boldsymbol{u}(t_{n+1}), \boldsymbol{w}) - b_{s}(\overline{\boldsymbol{v}}_{h}^{n}, \overline{\boldsymbol{u}}_{h}^{n+1}, \boldsymbol{w})$$

$$+ a(\boldsymbol{u}(t_{n+1}) - \overline{\boldsymbol{u}}_{h}^{n+1}, \boldsymbol{w}) - c(\overline{\boldsymbol{u}}_{h}^{n+1}; \overline{\boldsymbol{u}}_{h}^{n+1}, \boldsymbol{w})$$

$$- (p(t_{n+1}) - \overline{\boldsymbol{p}}_{h}^{n+1}, \nabla \cdot \boldsymbol{w}) + \langle \boldsymbol{f}^{n+1} - \boldsymbol{f}(t_{n+1}), \boldsymbol{w} \rangle.$$

$$(172)$$

Due to the monotonicity of the form c (Lemma 5 iii)), it holds

$$c(\boldsymbol{u}_h^{n+1}; \boldsymbol{u}_h^{n+1}, \boldsymbol{w}_h) - c(\overline{\boldsymbol{u}}_h^{n+1}; \overline{\boldsymbol{u}}_h^{n+1}, \boldsymbol{w}_h) \ge C \underline{h}^2$$
$$\|\mathbb{D}(\boldsymbol{u}_h^{n+1} - \overline{\boldsymbol{u}}_h^{n+1})\|_{0,3,Q}^3 \ge 0.$$

Then the stability estimate (156) holds when \boldsymbol{u}_h^n is replaced by the error \boldsymbol{e}_h^n , $\tilde{\boldsymbol{f}}_h^{n+1}$ is replaced by $\boldsymbol{\varepsilon}_h^{n+1}$ and $\boldsymbol{u}_{0,h}$ is replaced by \boldsymbol{e}_h^0 . Obtaining error estimates for the velocity is then reduced to estimate the $l^2(\boldsymbol{H}^{-1})$ norm of the consistency error $\boldsymbol{\varepsilon}_h^{n+1}$. In particular, the penalty term $\eta^{n+1}(\boldsymbol{w}) = c(\overline{\boldsymbol{u}}_h^{n+1}; \overline{\boldsymbol{u}}_h^{n+1}, \boldsymbol{w})$ that appears in the expression of $\boldsymbol{\varepsilon}_h^{n+1}$ has to be bounded. Denoting $\hat{\boldsymbol{\varepsilon}}_h^{n+1} = (\boldsymbol{I} - \boldsymbol{\rho}_h) \overline{\boldsymbol{e}}_h^{n+1}$ and $\hat{\boldsymbol{u}}(t_{n+1}) = (\boldsymbol{I} - \boldsymbol{\rho}_h) \boldsymbol{u}(t_{n+1})$ gives

$$\begin{split} \|\mathbb{D}(\widehat{\mathbf{u}}_{h}^{n+1})\|_{0} &\leq \|\mathbb{D}(\widehat{\mathbf{e}}_{h}^{n+1})\|_{0} + \|\mathbb{D}(\widehat{\boldsymbol{u}}(t_{n+1}))\|_{0} \\ &\leq C \|\mathbb{D}(\overline{\boldsymbol{e}}_{h}^{n+1})\|_{0} + \|\mathbb{D}(\widehat{\boldsymbol{u}}(t_{n+1}))\|_{0}. \end{split}$$

Combining this estimate with (153) one deduces

$$\begin{aligned} |\eta^{n+1}(\boldsymbol{w})| &\leq C \, h^{2-d/2} \, \|\mathbb{D}(\widehat{\boldsymbol{u}}_h^{n+1})\|_0^2 \, \|\mathbb{D}(\widehat{\boldsymbol{w}})\|_0 \\ &\leq C \, h^{2-d/2} \, \Big(\|\mathbb{D}(\overline{\boldsymbol{e}}_h^{n+1})\|_0^2 + \|\mathbb{D}(\widehat{\boldsymbol{u}}(t_{n+1}))\|_0^2 \Big) \\ &\|\mathbb{D}(\widehat{\boldsymbol{w}})\|_0. \end{aligned}$$

It follows that

$$\sum_{n=0}^{N-1} \Delta t \| \eta^{n+1} \|_{\boldsymbol{H}^{-1}}^2 \le C h^{2(2-d/2)}$$

$$\times \left(\| \mathbb{D}(\overline{\boldsymbol{e}}_h^{n+1}) \|_0^4 + \| \mathbb{D}(\widehat{\boldsymbol{u}}(t_{n+1})) \|_0^4 \right)$$

$$\le C h^{2(2-d/2)} \left(d_{l^4(H^1)}(\boldsymbol{u}, \boldsymbol{X}_h)^4 + d_{l^4(H^1)}(\boldsymbol{u}, \widehat{\boldsymbol{X}}_h)^4 \right).$$

This yields the last term in the error estimate (169). The estimates of the remaining terms in the expression (172) of ε_h^{n+1} are obtained by means of a discrete version of the Gronwall Lemma used in the proof of Theorem 5, to conclude the error estimates (167) and (168).

The error estimates (167) and (168) would be of optimal order in space if the term $h^{2-d/2}\left(d_{l^4(H^1)}(\boldsymbol{u},\boldsymbol{X}_h)^2+d_{l^4(H^1)}(\boldsymbol{u},\boldsymbol{X}_h)^2+d_{l^4(H^1)}(\boldsymbol{u},\boldsymbol{X}_h)^2\right)$ is at least of the same order as the term $d_{l^2(H^1)}(\boldsymbol{u},\boldsymbol{X}_h)$ for sufficiently smooth \boldsymbol{u} . If the spaces \boldsymbol{X}_h and $\widehat{\boldsymbol{X}}_h$ are given by (149), this happens if $k \geq l/2 + d/4 - 1$. If spaces \boldsymbol{X}_h and $\widehat{\boldsymbol{X}}_h$ are given by (150), then this property directly holds.

10.4 Asymptotic Energy Balance

In the steady case, the subgrid eddy dissipation energy is given by

$$E_{S}(\boldsymbol{u}_{h}) = C_{S}^{2} \sum_{K \in \mathcal{T}_{h}} h_{K}^{2} \int_{K} |\mathbb{D}(\widehat{\boldsymbol{u}}_{h})(\boldsymbol{x})|^{3} d\boldsymbol{x},$$

see (106). Then, E_S asymptotically vanishes as $h \to 0$ and, using the notation of Section 6.4, it holds

$$\lim_{h\to 0}[E_D(\boldsymbol{u}_h)+E_S(\boldsymbol{u}_h)]=E_D(\boldsymbol{u}).$$

In the unsteady case, the inverse estimates

$$\|\mathbb{D}(\widehat{\boldsymbol{u}}_h(t))\|_{0,3,K} \leq C h_K^{-1-d/r+d/3} \|\widehat{\boldsymbol{u}}_h(t)\|_{0,r,K}, \text{ for } 1 \leq r \leq 3,$$

$$\|\mathbb{D}(\widehat{\boldsymbol{u}}_h(t))\|_{0,3,K} \leq C h_K^{-d/6} \|\mathbb{D}(\widehat{\boldsymbol{u}}_h(t))\|_{0,2,K},$$

vield

$$h_K^2 \| \mathbb{D}(\widehat{\boldsymbol{u}}_h(t)) \|_{0,3,K} \le C h_K^{1-d/r} \| \widehat{\boldsymbol{u}}_h(t) \|_{0,r,K} \| \mathbb{D}(\widehat{\boldsymbol{u}}_h(t)) \|_{0,2,K}^2.$$



Consequently, it follows that

$$E_{S}(\boldsymbol{u}_{h}) \leq C \underline{h}^{1-d/r} \|\widehat{\boldsymbol{u}}_{h}\|_{L^{\infty}(0,T;\boldsymbol{L}^{r})} \|\widehat{\boldsymbol{u}}_{h}\|_{L^{2}(0,T;\boldsymbol{H}^{1})}^{2}.$$

Then, the subgrid energy $E_S(u_h)$ asymptotically vanishes if \hat{u}_h is bounded in $L^{\infty}(L^r)$ for some r > d. However the standard stability estimates yield uniformly bounds in $L^{\infty}(L^2)$ and then one cannot ensure that the subgrid energy asymptotically vanishes.

10.5 Experience in Numerical Simulations

Some experience in numerical simulations of models (98) and (152) with LPS stabilization will be reported here, respectively for steady and unsteady flows. In [36] the results of simulations of the steady three-dimensional turbulent channel flow at $Re_{\tau} = 180$ with several VMS methods on relatively coarse grids were compared:

- SMA model: The Smagorinsky LES model, given by $c(\mathbf{u}_h; \mathbf{u}_h, \mathbf{v}_h) = 2(v_T(\mathbf{u}_h)D(\mathbf{u}_h), D(\mathbf{v}_h));$
- VMS-S model: The small-small VMS-LPS setting, given by (36), i.e.,

$$c(\mathbf{u}_h; \mathbf{u}_h, \mathbf{v}_h) = 2(v_{\mathrm{T}}(\widehat{\mathbf{u}}_h)D(\widehat{\mathbf{u}}_h), D(\widehat{\mathbf{v}}_h));$$

 VMS-B model: The Berselli–Iliescu–Layton setting [18], in which:

$$c(\mathbf{u}_h; \mathbf{u}_h, \mathbf{v}_h) = 2\Big(v_{\mathrm{T}}(\widetilde{\boldsymbol{\Pi}}_h^* D(\mathbf{u}_h)) \widetilde{\boldsymbol{\Pi}}_h^* D(\mathbf{u}_h), \widetilde{\boldsymbol{\Pi}}_h^* D(\mathbf{v}_h)\Big),$$

where $\widetilde{\Pi}_h^* = I - \widetilde{\Pi}_h$, and $\widetilde{\Pi}_h$ is an interpolation operator on a coarser P_0 finite element space;

• STAB: The purely stabilized method, i e., (98), with c = 0

Two versions of the VMS-S and the STAB methods were tested, one with wall laws and the other with no-slip boundary conditions.

Equal-order interpolation P_2 for velocity and pressure were used. Also, a Crank–Nicolson scheme for the temporal discretization was used, combined with a linearization of convective and subgrid eddy viscosity terms. This approach provides a good compromise between accuracy and computational complexity.

Table 1 displays a comparison of the L^2 errors in the stream-wise direction, with respect to the DNS results from [116] with a grid four times finer in each space direction. One can observe that the errors range between 11% and 24%, the best ones correspond to the VMS-S method with no-slip boundary conditions. The accuracy provided by the methods with wall laws is acceptable for this stream-wise direction, although reaching too high error levels for the

Table 1 L^2 norm of the deviation from the DNS profiles for the stream-wise velocity

Methods	$e_0^{\langle u_1 \rangle} \ (y^+ \in [0, 180])$		
VMS-S (NO-SLIP BC)	0.1141		
VMS-S (WALL-LAW BC)	0.1734		
VMS-B (NO-SLIP BC)	0.1786		
SMA (NO-SLIP BC)	0.1260		
STAB (NO-SLIP BC)	0.1791		
STAB (WALL-LAW BC)	0.2373		

Table 2 L^2 norm of the deviation from the DNS profiles for the second-order statistics

Methods	$e_0^{\sqrt{\langle ilde{u}_1^2 angle}}$	$e_0^{\sqrt{\langle ilde{u}_2^2 angle}}$	$e_0^{\sqrt{\langle ilde{u}_3^2 angle}}$	$e_0^{\langle ilde{u}_1 ilde{u}_2 angle}$
VMS-S (NO-SLIP BC)	0.2252	0.1652	0.1108	0.1162
VMS-B (NO-SLIP BC)	0.2281	0.2018	0.1246	0.1706
SMA (NO-SLIP BC)	0.3002	0.2236	0.1597	0.1249
STAB (NO-SLIP BC)	0.3781	0.2536	0.1955	0.1708

homogeneous (cross-flow) directions. The use of wall laws provides a reduction of the computing time of about 35%.

Also, Table 2 displays the normalized (by the computed u_{τ}) root mean square (r.m.s.) values of velocity fluctuations $\sqrt{\langle \tilde{u}_{i}^{2} \rangle} = \|\langle u_{i}^{2} \rangle - \langle u_{i} \rangle^{2} \|^{1/2}$ (i=1,2,3) in wall coordinates y^{+} at the upper half-width of the channel, as a measure of the error in turbulence intensities. Only the no-slip boundary conditions were considered, as the errors with wall-laws were much larger. For those second-order statistics the errors are larger than for the first order ones, ranging around 30%. Again, the VMS-S method is in general in good agreement with the DNS data.

Only limited numerical experience with the solution of evolution turbulent flows with (152) is available. In [1] method (152) with LPS stabilization of convection, divergence and pressure gradient is applied to the simulation of a high Reynolds number ($Re = 10^4$) plane mixing layer flow, with accurate results for relatively coarse grids. Equal-order interpolation P_2 for velocity and pressure is used. Space and time accurate simulation of the pairing of primary and secondary vortex is achieved. Quite accurate time evolution of the vorticity thickness is computed with grids of 160×160 nodes. Also, model (152) with LPS stabilization has been extended to buoyant flows. Some recent yet unpublished results obtained by the authors show that a similar accuracy for the natural convection of high Rayleigh numbers (Ra) airflows in a differentially heated



plane cavity (up to $Ra = 10^7$) is achieved with relatively coarse grids.

11 Summary and Conclusions

The purpose of this article has been to present a state-ofthe-art review of VMS methods for the simulation of turbulent incompressible flows. These methods are widely used nowadays as one of the most promising and successful approaches that seeks to simulate large scale structures in turbulent flows, also in combination with advanced techniques such as, e.g., isogeometric analysis [10, 11].

The common feature of these methods is the use of multiple scales in modeling the turbulence, where the scales are defined by variational projections into appropriate function spaces. Apart from this common feature, the realization of VMS methods differs considerably, and a "jungle" of several types of VMS methods is present in the scientific literature. So, even if there exist much research work published on VMS turbulence models, the different VMS methods are mainly used in the groups that proposed them, and there is no structured presentation of them. The present review aimed at giving such a presentation with the emphasis on derivation, numerical analysis in the framework of the finite element method, and experience in numerical studies. In this way, the common features of VMS methods should become clear as well as their main differences.

Starting point was the presentation of the basic concepts of VMS methods: The basis of all VMS methods is the separation of the flow field into resolved and unresolved scales. VMS methods which use just resolved and unresolved scales belong to the class of two-scale VMS methods.

Within two-scale VMS methods, the residual-based VMS method, the OSS method, and LPS methods were presented.

The first two methods are residual-based models, since the basic procedure consists in keeping all terms in the residual-driven structure of the resolved flow equations and to perform an approximated analytical solution of the small scale flow through a diagonalization procedure, where a proper definition of stabilization coefficients is crucial. This procedure does not make use of the statistical theory of equilibrium turbulence (eddy viscosity models). The main difference between the two approaches consists in the fact that in the OSS only the orthogonal projection of the residual on the large scale space is used. One of its relevant features is that it introduces a numerical diffusion on the large scales which is asymptotically equivalent, as the Reynolds number increases, to the eddy viscosity

dissipated by the unresolved scales, for sufficiently fine grids. These methods are consistent.

In contrast, LPS methods can be considered as simplified methods that provide specific stabilization of any single term that could be a source of instability for the numerical discretization. Their structure could be achieved by retaining in the OSS method the specific diffusive interactions that stabilize convection, divergence, and pressure gradient, and by changing the global L^2 projection by local L^2 projections. This approach leads to a family of methods, associated to the choice of the actual local L^2 projection. The main difference with residual-based models is that they are not fully consistent, but of optimal order with respect to the finite element interpolation. The fact that the stabilization enjoys the right asymptotic behavior without full consistency allows to decouple the stabilization of the pressure and the velocity. This feature could be considered an important advantage with respect to the more complex residual-based methods in view of practical implementations such as to perform the numerical analysis, since it leads to a simpler and less expensive structure.

Nevertheless, the VMS framework allows various other arrangements, going beyond a two-scale decomposition, so that other classes of VMS methods can be distinguished. The most common approach allows a further decomposition of the resolved scales into large resolved scales (or large scales) and small resolved scales, leading finally to a so-called three-scale VMS method. Within three-scale VMS methods, a bubble VMS method, velocity deformation tensor projection-based VMS methods, and algebraic VMS-multigrid methods were discussed. All these methods include eddy viscosity modeling in the small resolved scale equations to model the dissipative effects of the unresolved scales. The eddy diffusion only affects the small resolved scales, thus reducing or even avoiding over-diffusive effects.

There are several realizations of bubble VMS methods which differ in some details: The derivation presented in this work corresponds to the three-level finite element method based on residual-free bubbles (RFB). The computation and storage of the RFB functions is computationally quite consuming and several simplifications to solve the resolved small scale equation can be performed. The resolved small scale pressure is not solved, but modeled as in the residual-based VMS methods. On the one hand, the diffusive grad-div stabilization appears in the large scale equation. On the other hand, this step allows to eliminate the incompressibility restriction for the resolved small scale velocity. Thus, the resolved small scale equations are approximated by a system of convection-diffusion equations, where a subgrid eddy viscosity term is added to model the effect of the unresolved scales on the small



resolved scales. However, these equations are strongly convection-dominated, which results in the necessity to use large values in the coefficient of the eddy viscosity term. From the computational point of view, the use of RFB-based VMS methods is quite involved.

A different way of realizing a three-scale VMS method consists in adding to the standard Galerkin formulation an eddy viscosity term that only affects directly the small resolved scales. These scales might be defined as the L^2 projection of the velocity deformation tensor into an appropriate large scale space, which leads to the so-called velocity deformation tensor projection-based VMS method. The large scale space can be defined on the same grid as the finite element space, enabling an efficient implementation of the method. The structure of the method allows a thorough numerical analysis, along the same lines as that of the Navier–Stokes equations.

Algebraic VMS-multigrid methods apply a different definition of the large scales. In these methods, the scale separation is performed for the velocity (and not for the deformation tensor). This separation uses components of an AMG method thus avoiding to introduce another finite element space or another grid, just matrix restriction/prolongation operators have to be defined, thus creating a multilevel structure starting from a coarse level.

The numerical analysis has been developed to a different degree for the individual VMS methods. Most results are known for LPS methods and the velocity deformation tensor projection-based VMS method. For some other VMS methods, at least results are available for simpler equations or for simplifications in the formulation of the method. Analytical results concerning the well-posedness of the discrete problems to guarantee the existence and uniqueness of a solution, stability results to obtain a priori bounds on the solution, or energy estimates are certainly of importance for practical purposes. The situation is somewhat different for error estimates of the form (20) or (136) because the constants in the error bounds become unrealistic huge even for small times. However, current mathematical tools do not allow to prove error estimates of a different kind. In summary, even if there are many results concerning the numerical analysis of VMS methods, in comparison with other approaches for turbulence modeling, there are still many open questions.

VMS methods were compared in numerical studies usually with LES methods, like the Smagorinsky LES method or the dynamic Smagorinsky LES method. Generally, the results obtained with the VMS methods were not worse, often even better than those of the LES methods. Excellent results using for instance residual-based VMS models were first presented in [10], applying isogeometric analysis for the space approximation [82]. In the recent

vears, residual-based VMS methods have demonstrated to be able to simulate (the large scales of) transient and steady turbulent flows with high accuracy. However, there are relatively few comparisons of different VMS methods, see [63, 98] for some examples. In our opinion, comparisons of different numerical methods should be performed with the same code. Besides using different codes for comparisons of different VMS methods, other aspects like the choice of the finite element spaces (inf-sup stable or equal-order, degree of the polynomials), the concrete grid, the explicit or semi-implicit treatment of certain terms, the time stepping scheme, the stopping criterion for solving the nonlinear problem, the choice of the local mesh width for anisotropic mesh cells, the concrete choice of parameters in the models, etc. might have an unknown influence on the results. Since comprehensive studies of several VMS methods within one code are not available, there will be no recommendation of VMS methods to use. If one wishes to apply a VMS method for the simulation of turbulent incompressible flow problems, the decision which concrete VMS method should be used will be guided from subjective preference and from the structure and the features of the used code.

Acknowledgments The research of Tomás Chacón Rebollo and Samuele Rubino has been partially supported by the Spanish Government Project MTM2012-36124-C02-01. Samuele Rubino would also gratefully acknowledge the financial support received from VPPI-US (V Plan Propio de Investigación-Universidad de Sevilla) and FSMP (Fondation Sciences Mathématiques de Paris) during his postdoctoral research involved in this article.

References

- Ahmed N, Chacón Rebollo T, John V, Rubino S (2015) Analysis of a full space-time discretization of the Navier-Stokes equations by a local projection stabilization method. IMA J Numer Anal (Submitted)
- Apel T, Knopp T, Lube G (2008) Stabilized finite element methods with anisotropic mesh refinement for the Oseen problem. Appl Numer Math 58(12):1830–1843
- Arndt D, Dallmann H (2015) Error estimates for the fully discretized incompressible Navier–Stokes problem with LPS stabilization. Preprint 08, Institut für Numerische und Angewandte Mathematik, Göttingen
- Arndt D, Dallmann H, Lube G (2015) Local projection FEM stabilization for the time-dependent incompressible Navier–Stokes problem. Numer Methods Partial Diff. Equ 31(4):1224–1250
- Arndt D, Dallmann H, Lube G (2015) Quasi-optimal error estimates for the stabilized incompressible Navier–Stokes problem discretized by finite element methods and pressurecorrection projection. Math Model Numer Anal (Submitted)
- Arnold DN, Brezzi F, Fortin M (1985) A stable finite element for the Stokes equations. Calcolo 21(4):337–344 1984
- Asensio MI, Russo A, Sangalli G (2004) The residual-free bubble numerical method with quadratic elements. Math Models Methods Appl Sci 14(5):641–661



- Babuška I (1970/1971) Error-bounds for finite element method. Numer Math 16:322–333
- Bazilevs Y, Akkerman I (2010) Large eddy simulation of turbulent Taylor–Couette flow using isogeometric analysis and the residual-based variational multiscale method. J Comput Phys 229(9):3402–3414
- Bazilevs Y, Calo VM, Cottrell JA, Hughes TJR, Reali A, Scovazzi G (2007) Variational multiscale residual-based turbulence modeling for large eddy simulation of incompressible flows. Comput Methods Appl Mech Engrg 197(1–4):173–201
- Bazilevs Y, Michler C, Calo VM, Hughes TJR (2010) Isogeometric variational multiscale modeling of wall-bounded turbulent flows with weakly enforced boundary conditions on unstretched meshes. Comput Methods Appl Mech Engrg 199(13–16):780–790
- Becker R, Braack M (2001) A finite element pressure gradient stabilization for the Stokes equations based on local projections. Calcolo 38(4):173–199
- Becker R, Braack M (2004) A two-level stabilization scheme for the Navier–Stokes equations. In: Feistauer M (ed) Numerical mathematics and advanced applications. Springer, Berlin, pp 123–130
- Bensow RE, Larson MG (2010) Residual based VMS subgrid modeling for vortex flows. Comput Methods Appl Mech Engrg 199(13–16):802–809
- Bensow RE, Larson MG, Vesterlund P (2007) Vorticity-strain residual-based turbulence modelling of the Taylor–Green vortex. Int J Numer Methods Fluids 54(6–8):745–756
- Bernardi C, Maday Y, Rapetti F (2004) Discrétisations variationnelles de problèmes aux limites elliptiques, Mathématiques & Applications (Berlin) [Mathematics & Applications], vol 45. Springer, Berlin
- 17. Bernardi C, Raugel G (1985) Analysis of some finite elements for the Stokes problem. Math Comp 44(169):71–79
- Berselli LC, Iliescu T, Layton WJ (2006) Mathematics of large eddy simulation of turbulent flows. Scientific computation. Springer, Berlin
- Bordás R, John V, Schmeyer E, Thévenin D (2012) Measurement and simulation of a droplet population in a turbulent flow field. Comput Fluids 66:52–62
- Bordás R, John V, Schmeyer E, Thévenin D (2013) Numerical methods for the simulation of a coalescence-driven droplet size distribution. Theoret Comput Fluid Dyn 27(3–4):253–271
- 21. Boris JP, Grinstein FF, Oran ES, Kolbe RL (1992) New insights into large eddy simulation. Fluid Dyn Res 10(4–6):199–228
- Braack M, Burman E, John V, Lube G (2007) Stabilized finite element methods for the generalized Oseen problem. Comput Methods Appl Mech Engrg 196(4–6):853–866
- Brachet ME, Meiron D, Orszag S, Nickel B, Morf R, Frisch U (1984) The Taylor–Green vortex and fully developed turbulence. J Statist Phys 34(5–6):1049–1063
- 24. Brezzi F (1974) On the existence, uniqueness and approximation of saddle-point problems arising from Lagrangian multipliers. Rev Française Automat Informat Recherche Opérationnelle Sér Rouge 8(R-2):129-151
- Brezzi F, Hughes TJR, Marini LD, Russo A, Süli E (1999) A priori error analysis of residual-free bubbles for advection-diffusion problems. SIAM J Numer Anal 36(6):1933–1948
- Brezzi F, Marini D, Süli E (2000) Residual-free bubbles for advection-diffusion problems: the general error analysis. Numer Math 85(1):31–47
- Brezzi F, Russo A (1994) Choosing bubbles for advection-diffusion problems. Math Models Methods Appl Sci 4(4):571–587
- 28. Brooks AN, Hughes TJR (1982) Streamline upwind/Petrov– Galerkin formulations for convection dominated flows with particular emphasis on the incompressible Navier–Stokes

- equations. Comput Methods Appl Mech Engrg 32(1–3):199–259 (FENOMECH '81, Part I (Stuttgart, 1981))
- Burton GC, Dahm WJA (2005) Multifractal subgrid-scale modeling for large-eddy simulation. I. Model development and a priori testing. Phys Fluids 17(7):075111–075116
- Burton GC, Dahm WJA (2005) Multifractal subgrid-scale modeling for large-Eddy simulation. II. Backscatter limiting and a posteriori evaluation. Phys Fluids 17(7):075112–075119
- Calderer R, Masud A (2013) Residual-based variational multiscale turbulence models for unstructured tetrahedral meshes. Comput Methods Appl Mech Engrg 254:238–253
- 32. Chacón Rebollo T (1998) A term by term stabilization algorithm for finite element solution of incompressible flow problems. Numer Math 79(2):283–319
- Chacón Rebollo T (2001) An analysis technique for stabilized finite element solution of incompressible flows. Math Model Numer Anal 35(1):57–89
- Chacón Rebollo T, Gómez Mármol M, Girault V, Sánchez Muñoz I (2013) A high order term-by-term stabilization solver for incompressible flow problems. IMA J Numer Anal 33(3):974–1007
- 35. Chacón Rebollo T, Gómez Mármol M, Rubino S (2015) Finite element approximation of an unsteady projection-based VMS turbulence model with wall laws. To appear in BAIL 2014 Proc.: Springer Series Lecture Notes in Computational Science and Engineering
- 36. Chacón Rebollo T, Gómez Mármol M, Rubino S (2015) Numerical analysis of a finite element projection-based VMS turbulence model with wall laws. Comput Methods Appl Mech Engrg 285:379–405
- Chacón Rebollo T, Gómez Mármol M, Sánchez Muñoz I (2012)
 Numerical solution of the primitive equations of the ocean by the orthogonal sub-scales VMS method. Appl Numer Math 62(4):342–359
- 38. Chacón Rebollo T, Lewandowski R (2014) Mathematical and numerical foundations of turbulence models and applications. Birkhäuser, Boston
- Chacón Rebollo T, Dia BM (2015) A variational multi-scale method with spectral approximation of the sub-scales: application to the 1D advection-diffusion equations. Comput Methods Appl Mech Engrg 285:406–426
- Ciarlet PG (1978) The finite element method for elliptic problems. Studies in mathematics and its applications, vol 4. North-Holland, Amsterdam
- 41. Codina R (1998) Comparison of some finite element methods for solving the diffusion–convection–reaction equation. Comput Methods Appl Mech Engrg 156(1–4):185–210
- Codina R (2000) Stabilization of incompressibility and convection through orthogonal sub-scales in finite element methods.
 Comput Methods Appl Mech Engrg 190(13–14):1579–1599
- Codina R (2001) A stabilized finite element method for generalized stationary incompressible flows. Comput Methods Appl Mech Engrg 190(20–21):2681–2706
- 44. Codina R (2002) Stabilized finite element approximation of transient incompressible flows using orthogonal subscales. Comput Methods Appl Mech Engrg 191(39–40):4295–4321
- Codina R (2008) Analysis of a stabilized finite element approximation of the Oseen equations using orthogonal subscales. Appl Numer Math 58(3):264–283
- Codina R, Blasco J (2002) Analysis of a stabilized finite element approximation of the transient convection–diffusion–reaction equation using orthogonal subscales. Comput Vis Sci 4(3):167–174
- 47. Codina R, Principe J, Badia S (2011) Dissipative structure and long term behavior a finite element approximation of incompressible flows with numerical subgrid scalemodeling. In:



Multiscale methods in computational mechanics, volume 55 of Lect. Notes Appl Comput Mech. Springer, pp 75-93

- Codina R, Principe J, Guasch O, Badia S (2007) Time dependent subscales in the stabilized finite element approximation of incompressible flow problems. Comput Methods Appl Mech Engrg 196(21–24):2413–2430
- Colomés O, Badia S, Codina R, Principe J (2015) Assessment of variational multiscale models for the large Eddy simulation of turbulent incompressible flows. Comput Methods Appl Mech Engrg 285:32–63
- de Frutos J, García Archilla B, John V, Novo J (2015) Grad-div stabilization for the evolutionary oseen problem with inf-sup stable finite elements. J Sci Comput 1–34. doi:10.1007/s10915-015-0052-1
- Dunca A, John V, Layton WJ (2004) The commutation error of the space averaged Navier–Stokes equations on a bounded domain. In: Contributions to current challenges in mathematical fluid mechanics. Adv Math Fluid Mech. Birkhäuser, Basel, pp 53–78
- Fauconnier D, De Langhe C, Dick E (2009) Construction of explicit and implicit dynamic finite difference schemes and application to the large-eddy simulation of the Taylor–Green vortex. J Comput Phys 228(21):8053–8084
- Franca LP, Frey SL (1992) Stabilized finite element methods. II.
 The incompressible Navier–Stokes equations. Comput Methods Appl Mech Engrg 99(2–3):209–233
- Franca LP, Hughes TJR (1988) Two classes of mixed finite element methods. Comput Methods Appl Mech Engrg 69(1): 89–129
- Franca LP, John V, Matthies G, Tobiska L (2007) An inf-sup stable and residual-free bubble element for the Oseen equations. SIAM J Numer Anal 45(6):2392–2407 (electronic)
- Franca LP, Valentin F (2000) On an improved unusual stabilized finite element method for the advective–reactive–diffusive equation. Comput Methods Appl Mech Engrg 190(13–14):1785–1800
- Franca LP, Nesliturk A (2001) On a two-level finite element method for the incompressible Navier–Stokes equations. Int J Numer Methods Eng 52(4):433–453
- Galdi GP (2000) An introduction to the Navier–Stokes initialboundary value problem. In: Fundamental directions in mathematical fluid mechanics. Adv Math Fluid Mech. Birkhäuser, Basel, pp 1–70
- Gamnitzer P, Gravemeier V, Wall WA (2010) Time-dependent subgrid scales in residual-based large eddy simulation of turbulent channel flow. Comput Methods Appl Mech Engrg 199(13–16):819–827
- Germano M, Piomelli U, Moin P, Cabot WH (1991) A dynamic subgridscale eddy viscosity model. Phys Fluids A 3(7):1760– 1765
- Girault V, Lions J-L (2001) Two-grid finite-element schemes for the transient Navier–Stokes problem. Math Model Numer Anal 35(5):945–980
- Gravemeier V (2006) The variational multiscale method for laminar and turbulent flow. Arch Comput Methods Engrg 13(2): 249–324
- Gravemeier V, Gee MW, Kronbichler M, Wall WA (2010) An algebraic variational multiscale-multigrid method for large eddy simulation of turbulent flow. Comput Methods Appl Mech Engrg 199(13–16):853–864
- 64. Gravemeier V, Gee MW, Wall WA (2009) An algebraic variational multiscale-multigrid method based on plain aggregation for convection-diffusion problems. Comput Methods Appl Mech Engrg 198(47–48):3821–3835
- 65. Gravemeier V, Kronbichler M, Gee MW, Wall WA (2011) An algebraic variational multiscale–multigrid method for large-eddy simulation: generalized-α time integration, Fourier analysis

- and application to turbulent flow past a square-section cylinder. Comput Mech 47(2):217–233
- 66. Gravemeier V, Wall WA (2010) An algebraic variational multiscale-multigrid method for large-eddy simulation of turbulent variable-density flow at low Mach number. J Comput Phys 229(17):6047–6070
- 67. Gravemeier V, Wall WA (2011) Residual-based variational multiscale methods for laminar, transitional and turbulent variable-density flow at low Mach number. Int J Numer Methods Fluids 65(10):1260–1278
- Gravemeier V, Wall WA, Ramm E (2004) A three-level finite element method for the instationary incompressible Navier–Stokes equations. Comput Methods Appl Mech Engrg 193(15–16): 1323–1366
- Gravemeier V, Wall WA, Ramm E (2005) Large eddy simulation of turbulent incompressible flows by a three-level finite element method. Int J Numer Methods Fluids 48(10):1067–1099
- Guasch O, Codina R (2013) Statistical behavior of the orthogonal subgrid scale stabilization terms in the finite element large eddy simulation of turbulent flows. Comput Methods Appl Mech Engrg 261(262):154–166
- Guermond J-L (1999) Stabilization of Galerkin approximations of transport equations by subgrid modeling. Math Model Numer Anal 33(6):1293–1316
- Hansbo P, Szepessy A (1990) A velocity–pressure streamline diffusion finite element method for the incompressible Navier–Stokes equations. Comput Methods Appl Mech Engrg 84(2):175–192
- He L, Tobiska L (2012) The two-level local projection stabilization as an enriched one-level approach. Adv Comput Math 36(4):503–523
- Heywood JG, Rannacher R (1982) Finite element approximation of the nonstationary Navier–Stokes problem. I. Regularity of solutions and second-order error estimates for spatial discretization. SIAM J Numer Anal 19(2):275–311
- Heywood JG, Rannacher R (1988) Finite element approximation of the nonstationary Navier–Stokes problem. III. Smoothing property and higher order error estimates for spatial discretization. SIAM J Numer Anal 25(3):489–512
- Hickel S, Adams NA, Domaradzki JA (2006) An adaptive local deconvolution method for implicit LES. J Comput Phys 213(1): 413–436
- Hood P, Taylor C (1974) Navier–Stokes equations using mixed interpolation. In: Oden JT, Gallagher RH, Zienkiewicz OC, Taylor C (eds) Finite element methods in flow problems. University of Alabama, Huntsville Press, Huntsville, pp 121– 132
- 78. Hopf E (1951) Über die Anfangswertaufgabe für die hydrodynamischen Grundgleichungen. Math Nachr 4:213–231
- Hsu M-C, Bazilevs Y, Calo VM, Tezduyar TE, Hughes TJR (2010) Improving stability of stabilized and multiscale formulations in flow simulations at small time steps. Comput Methods Appl Mech Engrg 199(13–16):828–840
- Hughes TJR (1995) Multiscale phenomena: Green's functions, the Dirichlet-to-Neumann formulation, subgrid scale models, bubbles and the origins of stabilized methods. Comput Methods Appl Mech Engrg 127(1–4):387–401
- 81. Hughes TJR, Brooks A (1979) A multidimensional upwind scheme with no crosswind diffusion. In: Finite element methods for convection dominated flows (Papers, Winter Ann. Meeting Amer. Soc. Mech. Engrs., New York, 1979), volume 34 of AMD, pages 19–35. Amer. Soc. Mech. Engrs. (ASME), New York
- 82. Hughes TJR, Cottrell JA, Bazilevs Y (2005) Isogeometric analysis: CAD, finite elements, NURBS, exact geometry and mesh refinement. Comput Methods Appl Mech Engrg 194(39–41): 4135–4195



- Hughes TJR, Feijóo GR, Mazzei L, Quincy J-B (1998) The variational multiscale method—a paradigm for computational mechanics. Comput Methods Appl Mech Engrg 166(1–2):3–24
- 84. Hughes TJR, Franca LP, Balestra M (1986) A new finite element formulation for computational fluid dynamics. V. Circumventing the Babuška-Brezzi condition: a stable Petrov-Galerkin formulation of the Stokes problem accommodating equal-order interpolations. Comput Methods Appl Mech Engrg 59(1):85–99
- Hughes TJR, Mazzei L, Jansen KE (2000) Large eddy simulation and the variational multiscale method. Comput Vis Sci 3(1–2):47–59
- Hughes TJR, Mazzei L, Oberai AA, Wray AA (2001) The multiscale formulation of large eddy simulation: decay of homogeneous isotropic turbulence. Phys Fluids 13(2):505–512
- 87. Hughes TJR, Oberai AA, Mazzei L (2001) Large eddy simulation of turbulent channel flows by the variational multiscale method. Phys Fluids 13(6):1784–1799
- Hughes TJR, Sangalli G (2007) Variational multiscale analysis: the fine-scale Green's function, projection, optimization, localization, and stabilized methods. SIAM J Numer Anal 45(2):539–557
- 89. Hughes TJR, Scovazzi G, Franca LP (2004) Multiscale and stabilized methods, chap 2. Wiley, London
- Jenkins EW, John V, Linke A, Rebholz LG (2014) On the parameter choice in grad-div stabilization for the Stokes equations. Adv Comput Math 40(2):491–516
- John V (2004) Large eddy simulation of turbulent incompressible flows, volume 34 of lecture notes in computational science and engineering. Analytical and numerical results for a class of LES models. Springer, Berlin
- John V (2006) On large eddy simulation and variational multiscale methods in the numerical simulation of turbulent incompressible flows. Appl Math 51(4):321–353
- 93. John V, Kaya S (2005) A finite element variational multiscale method for the Navier–Stokes equations. SIAM J Sci Comput 26(5):1485–1503 (electronic)
- John V, Kaya S (2008) Finite element error analysis of a variational multiscale method for the Navier–Stokes equations. Adv Comput Math 28(1):43–61
- John V, Kaya S, Kindl A (2008) Finite element error analysis for a projection-based variational multiscale method with nonlinear eddy viscosity. J Math Anal Appl 344(2):627–641
- John V, Kaya S, Layton W (2006) A two-level variational multiscale method for convection-dominated convection-diffusion equations. Comput Methods Appl Mech Engrg 195(33–36):4594–4603
- John V, Kindl A (2008) Variants of projection-based finite element variational multiscale methods for the simulation of turbulent flows. Int J Numer Methods Fluids 56(8):1321–1328
- John V, Kindl A (2010) Numerical studies of finite element variational multiscale methods for turbulent flow simulations. Comput Methods Appl Mech Engrg 199(13–16):841–852
- John V, Kindl A (2010) A variational multiscale method for turbulent flow simulation with adaptive large scale space. J Comput Phys 229(2):301–312
- 100. John V, Kindl A, Suciu C (2010) Finite element LES and VMS methods on tetrahedral meshes. J Comput Appl Math 233(12): 3095–3102
- John V, Layton WJ (2002) Analysis of numerical errors in large eddy simulation. SIAM J Numer Anal 40(3):995–1020
- 102. John V, Linke A, Merdon C, Neilan M, Rebholz LG (2015) On the divergence constraint in mixed finite element methods for incompressible flows. Preprint 2177, WIAS, Berlin
- 103. John V, Novo J (2011) Error analysis of the SUPG finite element discretization of evolutionary convection–diffusion-reaction equations. SIAM J Numer Anal 49(3):1149–1176
- 104. John V, Roland M (2007) Simulations of the turbulent channel flow at $Re_{\tau} = 180$ with projection-based finite element

- variational multiscale methods. Int J Numer Methods Fluids 55(5):407-429
- Layton W (2002) A connection between subgrid scale eddy viscosity and mixed methods. Appl Math Comput 133(1):147–157
- 106. Layton W, Röhe L, Tran H (2011) Explicitly uncoupled VMS stabilization of fluid flow. Comput Methods Appl Mech Engrg 200(45–46):3183–3199
- 107. Leray J (1934) Sur le mouvement d'un liquide visqueux emplissant l'espace. Acta Math 63(1):193–248
- Lilly DK (1992) A proposed modification of the Germano subgrid-scale closure method. Phys Fluids A 4(3):633–635
- 109. Löwe J, Lube G (2012) A projection-based variational multiscale method for large-eddy simulation with application to nonisothermal free convection problems. Math Models Methods Appl Sci 22(2):1150011–1150031
- Lube G, Rapin G (2006) Residual-based stabilized higher-order FEM for a generalized Oseen problem. Math Models Methods Appl Sci 16(7):949–966
- 111. Lube G, Tobiska L (1990) A nonconforming finite element method of streamline diffusion type for the incompressible Navier–Stokes equations. J Comput Math 8(2):147–158
- 112. Masud A, Calderer R (2009) A variational multiscale stabilized formulation for the incompressible Navier–Stokes equations. Comput Mech 44(2):145–160
- 113. Masud A, Calderer R (2011) A variational multiscale method for incompressible turbulent flows: bubble functions and fine scale fields. Comput Methods Appl Mech Engrg 200(33–36):2577–2593
- 114. Matthies G, Lube G, Röhe L (2009) Some remarks on residualbased stabilisation of inf-sup stable discretisations of the generalised Oseen problem. Comput Methods Appl Math 9(4):368–390
- 115. Matthies G, Skrzypacz P, Tobiska L (2007) A unified convergence analysis for local projection stabilisations applied to the Oseen problem. Math Model Numer Anal 41(4):713–742
- 116. Moser R, Kim J, Mansour NN (1999) Direct numerical simulation of turbulent channel flow up to $Re_{\tau} = 590$. Phys Fluids 11(4):943-945
- 117. Olshanskii MA, Reusken A (2004) Grad-div stabilization for Stokes equations. Math Comp 73(248):1699–1718
- 118. Principe J, Codina R, Henke F (2010) The dissipative structure of variational multiscale methods for incompressible flows. Comput Methods Appl Mech Engrg 199(13–16):791–801
- 119. Rasthofer U (2015) Computational multiscale methods for turbulent single and two-phase flows. Bericht 27, Lehrstuhl für Numerische Mechanik, Technische Universität München. PhD thesis
- 120. Rasthofer U, Burton GC, Wall WA, Gravemeier V (2014) An algebraic variational multiscale–multigrid–multifractal method (AVM⁴) for large-eddy simulation of turbulent variable-density flow at low Mach number. Int J Numer Methods Fluids 76(7): 416–449
- Rasthofer U, Gravemeier V (2013) Multifractal subgrid-scale modeling within a variational multiscale method for large-eddy simulation of turbulent flow. J Comput Phys 234:79–107
- Risch U (2001) Convergence analysis of the residual free bubble method for bilinear elements. SIAM J Numer Anal 39(4): 1366–1379 (electronic)
- 123. Röhe L, Lube G (2010) Analysis of a variational multiscale method for large-eddy simulation and its application to homogeneous isotropic turbulence. Comput Methods Appl Mech Engrg 199(37–40):2331–2342
- 124. Roos HG, Stynes M, Tobiska L (2008) Robust numerical methods for singularly perturbed differential equations, volume 24 of Springer series in computational mathematics. Convection-diffusion-reaction and flow problems, 2nd edn. Springer, Berlin



 Rubino S (2014) Numerical modeling of turbulence by Richardson number-based and VMS models. PhD thesis, University of Seville

- Sagaut P (2006) Large eddy simulation for incompressible flows.
 Scientific computation, 3rd edn. Springer, Berlin An introduction
- 127. Sala M, Tuminaro RS (2008) A new Petrov–Galerkin smoothed aggregation preconditioner for nonsymmetric linear systems. SIAM J Sci Comput 31(1):143–166
- Schmeyer E, Bordás R, Thévenin D, John V (2014) Numerical simulations and measurements of a droplet size distribution in a turbulent vortex street. Meteorol Z 23(4):387–396
- Scott LR, Zhang S (1990) Finite element interpolation of nonsmooth functions satisfying boundary conditions. Math Comput 54(190):483–493
- 130. Serrin J (1963) The initial value problem for the Navier–Stokes equations. In: Nonlinear problems (proceedings of symposium, Madison, WI, 1962). University of Wisconsin Press, Madison, pp 69–98
- 131. Shakib F, Hughes TJR, Johan Z (1991) A new finite element formulation for computational fluid dynamics. X. The compressible Euler and Navier–Stokes equations. Comput Methods Appl Mech Engrg 89(1–3):141–219 (second world congress on computational mechanics, part I (Stuttgart, 1990))
- 132. Simon J (1987) Compact sets in the space $L^p(0, T; B)$. Ann Mat Pura Appl 4(146):65–96

- Sohr H (1983) Zur Regularitätstheorie der instationären Gleichungen von Navier-Stokes. Math Z 184(3):359–375
- 134. Sohr H (2001) The Navier–Stokes equations. Birkhäuser advanced texts: Basler Lehrbücher. [Birkhäuser advanced texts: Basel Textbooks]. An elementary functional analytic approach. Birkhäuser Verlag, Basel
- 135. Stüben K (2001) A review of algebraic multigrid. J Comput Appl Math 128(1–2):281–309 (Numerical analysis 2000, vol VII, partial differential equations)
- 136. Tobiska L, Lube G (1991) A modified streamline diffusion method for solving the stationary Navier–Stokes equation. Numer Math 59(1):13–29
- 137. Tobiska L, Verfürth R (1996) Analysis of a streamline diffusion finite element method for the Stokes and Navier–Stokes equations. SIAM J Numer Anal 33(1):107–127
- 138. Vaněk P, Mandel J, Brezina M (1996) Algebraic multigrid by smoothed aggregation for second and fourth order elliptic problems. Computing 56(3):179–196 International GAMM-Workshop on Multi-level Methods (Meisdorf, 1994)
- Verfürth R (1984) Error estimates for a mixed finite element approximation of the Stokes equations. RAIRO Anal Numér 18(2):175–182

